Quaternary Science Reviews 30 (2011) 528–554

Contents lists available at ScienceDirect

Quaternary Science Reviews

journal homepage: www.elsevier.com/locate/quascirev

Constraints on the late Quaternary glaciations in Tibet from cosmogenic exposure ages of moraine surfaces

Marie-Luce Chevalier[a,b,*], George Hilley[b], Paul Tapponnier[c], Jérôme Van Der Woerd[d], Jing Liu-Zeng[e], Robert C. Finkel[f], Frederick J. Ryerson[g], Haibing Li[a], Xiaohan Liu[e]

[a] Key laboratory for Continental Dynamics, Institute of Geology, CAGS, 26, Baiwanzhuang Road, Beijing 100037, China
[b] Department of Geological and Environmental Sciences, 450 Serra Mall, Braun Hall, Stanford University, Stanford, CA 94305, USA
[c] Earth Observatory of Singapore, 50 Nanyang Ave, N2-01a-09, Singapore 639798
[d] Institut de Physique du Globe de Strasbourg, UMR 7516 CNRS/ Université de Strasbourg, 5 rue Descartes, 67084 Strasbourg, France
[e] Institute of Tibetan Plateau Research, Chinese Academy of Sciences, P.O. Box 2871, 18 Shuang Qing Road, 100085 Beijing, China
[f] Earth and Planetary Science Department, University of California, Berkeley, 371 McCone Hall, Berkeley, CA 94720-4767, USA
[g] L-231, Atmospheric Earth and Energy Division, Physical and Life Sciences directorate, Lawrence Livermore National Laboratory, Livermore, CA 94550, USA

A R T I C L E I N F O

Article history:
Received 26 June 2010
Received in revised form
2 November 2010
Accepted 9 November 2010
Available online 20 January 2011

A B S T R A C T

This contribution provides new constraints on the timing of Tibetan glacial recessions recorded by the abandonment of moraines. We present cosmogenic radionuclide ^{10}Be inventories at 17 sites in southern and western Tibet (32 crests, 249 samples) and infer the range of permissible emplacement ages based on these analyses. Individual large embedded rock and boulder samples were collected from the crests of moraine surfaces and analyzed for ^{10}Be abundance. We consider two scenarios to interpret the age of glacial recession leading to the moraine surface formation from these sample exposure ages: 1) Erosion of the moraine surface is insignificant and so the emplacement age of the moraines is reflected by the mean sample age; and 2) Erosion progressively exposes large boulders with little prior exposure, and so the oldest sample age records the minimum moraine emplacement age. We found that depending on the scenario chosen, the moraine emplacement age can vary by > 50% for ~100 ka-old samples. We consider two scaling models for estimating the production rates of ^{10}Be in Tibet, which has an important, although lesser, effect on inferred moraine ages. While the data presented herein effectively increase the database of sample exposure ages from Tibet by ~20%, we find that uncertainties related to the interpretation of the ^{10}Be abundance within individual samples in terms of moraine emplacement ages are sufficient to accommodate either a view in which glacial advances are associated with temperature minima or precipitation maxima that are recorded by independent paleoclimate proxies. A reanalysis of published data from moraines throughout Tibet shows that the variation we observe is not unique to our dataset but rather is a robust feature of the Tibetan moraine age database. Thus, when viewed in a similar way with other samples collected from this area, uncertainties within moraine exposure ages obscure attribution of Tibetan glacial advances to temperature minima or precipitation maxima. Our work suggests that more reliable chronologies of Tibetan glaciations will come from improvements in production rate models for this portion of the world, as well as a better understanding of the processes that form and modify these geomorphic surfaces.

1. Introduction

Mountain glaciers are sensitive climatic markers that usually advance or withdraw rapidly with changes in temperature and/or precipitation. In Tibetan and Himalayan glacial valleys in particular, successions of multiple moraines that record glacial recessions are common, providing a potential opportunity to investigate the nature of climate changes in mid-latitude continental regions where climate proxies are far more sparse than in ocean basins or polar ice-caps. Preserved embedded boulders on moraine crests

* Corresponding author. Key Laboratory for Continental Dynamics, Institute of Geology, CAGS, 26, Baiwanzhuang Rd, Beijing 100037, China.
E-mail addresses: mlchevalier@hotmail.com (M.-L. Chevalier), hilley@stanford.edu (G. Hilley), tappon@ntu.edu.sg (P. Tapponnier), jeromev@eost.u-strasbg.fr (J. Van Der Woerd), liu-zeng@itpcas.ac.cn (J. Liu-Zeng), rfinkel@berkeley.edu (R.C. Finkel), Ryerson1@llnl.gov (F.J. Ryerson), lihaibing06@yahoo.com.cn (H. Li), liuxh@itpcas.ac.cn (X. Liu).

0277-3791/$ – see front matter
doi:10.1016/j.quascirev.2010.11.005

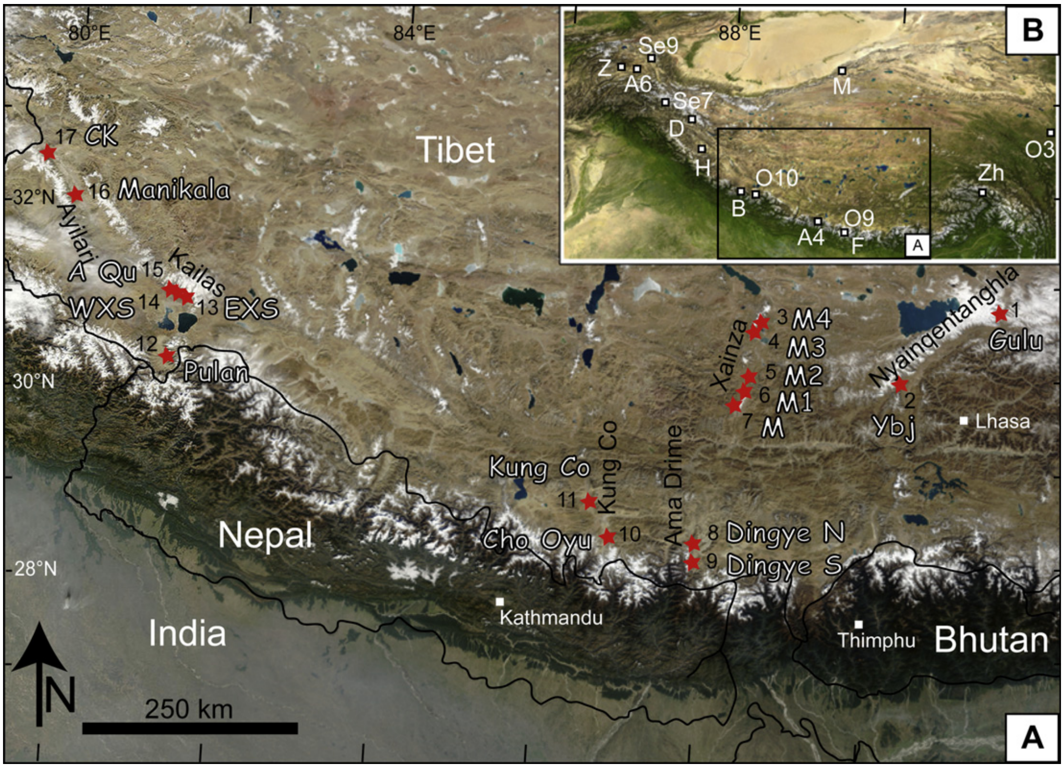

Fig. 1. A) Location of the 17 new sampled moraine sites of this study (red stars), 32 crests (with >2 samples), on a Landsat satellite image of the southern and western Tibetan Plateau, a region of about 1100 × 500 km. Numbers refer to Fig. 14 and Tables 1, 2 and S1. B) Location of the studies used in the compilation: A4 = Abramowski (2004), A6 = Abramowski et al. (2006), B=Barnard et al. (2004b), D = Dortch et al. (2010), F=Finkel et al. (2003), H=Hedrick et al. (in press), M = Meriaux et al. (2004), O3 = Owen et al. (2003a), O9 = Owen et al. (2009), O10 = Owen et al. (2010), Se7 = Seong et al. (2007), Se9 = Seong et al. (2009), Z = Zech et al. (2005a), Zh = Zhou et al. (2007).

provide ideal targets for cosmogenic radionuclide surface-exposure dating (Gosse and Phillips, 2001), which allows dating of features devoid of datable organic material or features too old to be dated using radiocarbon.

A number of studies have recently been carried out to assess the timing of past glaciations in Tibet and to infer the relative influence that precipitation and temperature play in triggering glacial advances here (e.g. Gillespie and Molnar, 1995; Benn and Owen, 1998; Owen et al., 2001, 2002, 2009; Brown et al., 2002; Schaefer et al., 2002, 2008; Van der Woerd et al., 2002; Finkel et al., 2003; Zech et al., 2005a, 2009; Abramowski et al., 2006; Gayer et al., 2006; Seong et al., 2007, 2009; Zhou et al., 2007). Such a chronology could help to inform how the high elevation and large area of the Tibetan Plateau influences global climatic patterns, as there is some uncertainty as to whether the winter Westerlies in the west and the summer South Asian Monsoon in the east change their relative importance in response to long-period climate changes. Most studies posit that Quaternary glaciations in Tibet and the Himalayas were asynchronous with those of the Northern Hemisphere (e.g. Gillespie and Molnar, 1995; Benn and Owen, 1998; Phillips et al., 2000; Richards et al., 2000; Owen et al., 2008b, 2009), suggesting that increased precipitation during warm periods may be primarily responsible for glacial advances.

While cosmogenic exposure age studies have provided important insights into the potential controls on the timing of glacial advances, there is some question as to whether the inferred ages of surface samples represent the moraine emplacement age in a straightforward way. Typically, rock samples collected from the crest of a moraine are analyzed for ^{10}Be concentrations (hereafter [^{10}Be]), which are used to infer the exposure age of each of the surface samples. The age distribution of samples on the moraine crest is then used to infer the emplacement age of the moraine (i.e. the transition between glaciation and deglaciation, i.e. when the moraine starts to be exposed to cosmic-rays). To this end, there are two main sources of uncertainty in moraine surface emplacement ages that could be better characterized by a comprehensive dataset from across the Tibetan Plateau. First, production rates of ^{10}Be vary strongly with atmospheric depth and geomagnetic latitude—models of these effects are particularly poorly calibrated for the Tibetan Plateau (e.g. Dunai, 2000; Stone, 2000; Gosse and Phillips, 2001; Balco et al., 2008). Second, only a handful of samples are typically collected from a given moraine surface/crest, and so the limited number of samples may introduce significant uncertainty when interpreting a moraine emplacement age in terms of the rocks that are presently mantling its surface. Also, while many studies assume that the mean age of surface-mantling boulders represents the emplacement age of the moraine (e.g. Gosse et al., 1995; Briner et al., 2001; Finkel et al., 2003; Meriaux et al., 2004; Chevalier et al., 2005a; Owen et al., 2005; Barrows et al., 2007; Schaefer et al., 2009; Hedrick et al., in press), others indicate that such boulders are progressively exhumed to the surface as erosion winnows the fines from the moraine (e.g. Hallet and Putkonen, 1994; Lasserre et al., 2002; Putkonen and Swanson, 2003; Abramowski, 2004, 2006; Zech et al., 2005a, 2008, 2009; Applegate et al., 2010; Heyman et al., in press) and erosion transports material away from the crest. Thus, uncertainties in the way in which the moraine surface is modified over time can alter the manner in which we relate the moraine emplacement age to the exposure ages of the boulders mantling its surface.

In this contribution, we present new ^{10}Be surface exposure ages of 249 samples (Table S1 in the Supplementary Information) collected in 2000-2007, on 32 lateral (and one frontal) moraine crests (17 sites, red stars on Fig. 1) located over a region of ∼1100 km by ∼500 km in southern and western Tibet. This new dataset increases the size of the Tibetan exposure age database by ~ 20% (compared to Heyman et al., 2010) and contains enough data to allow a better understanding of the influence of the uncertainties in moraine emplacement ages that result from the number and interpretation of samples collected from the moraine surface. We found that when considering the quantifiable uncertainties cited above, it is difficult to compellingly associate the timing of Tibetan glacial advances with either temperature minima or precipitation maxima (assuming that glacial advances during temperature maxima are driven by increased precipitation). Indeed, the $\delta^{18}O$ of ice varies with temperature; therefore it may be used to assess the correlation between temperature minima and glacial expansion using this geochemical proxy (Yao et al., 1996; Thompson et al., 1997). A precipitation-related glacial advance is more difficult to constrain, but we know that an increase of precipitation (during both warm and cold climate) brings snowfall at high elevation and allows glaciers to advance. Our study suggests that the development of such chronologies would foremost benefit from a better understanding of how these surfaces are denuded over time, and secondarily from the construction of better constrained models that describe the distribution of cosmogenic production rates in this area.

2. Methods

2.1. Sample processing and dating

Moraine crests were sampled by collecting fragments from the top surface of discrete large embedded granite boulders (up to 4 m in diameter) on the crest (highest point) of the moraine, or well-rooted cobbles (20-30 cm in diameter) in cases where boulders were not present (see Table S1 for a complete description of each of the samples collected). We sampled at least 5 different surface boulders/clasts from each moraine crest, and up to 15 samples for large-size moraines with many available boulders.

Each rock sample was crushed, sieved, and cleaned to isolate quartz from the sample, which is the mineral that we use to analyze the *in situ*-produced [^{10}Be]. The *in-situ* produced ^{10}Be was isolated by progressive HF/HNO_3 leaches to etch the exterior portion of the quartz crystals that may contain garden-variety ^{10}Be that was sorbed on the mineral surface (e.g. Brown et al., 1991; Kohl and Nishiizumi, 1992; Gosse and Phillips, 2001). The purified quartz was then digested, a ^{9}Be carrier of known concentration was added, and $Be(OH)_2$ was chemically isolated using ion exchange columns. The $Be(OH)_2$ was ignited to BeO, and the ^{10}Be/^{9}Be ratios were measured at Lawrence Livermore National Laboratory's Center for Accelerator Mass Spectrometry (LLNL-CAMS, USA) and the Aster Accelerator Mass Spectrometer at LN2C-Cerege, France. These ratios were finally converted to [^{10}Be] using the measured total Be concentrations prior to chemical separation.

The production rate of ^{10}Be scales with the atmospheric depth, geomagnetic latitude, and geomagnetic field intensity. Thus, the history of the production rate must be calculated at each sample location and integrated in time to find the exposure age that most closely reproduces the measured ^{10}Be abundance. We used the CRONUS 2.2 calculator with the constant file 2.2.1 (Balco et al., 2008, http://hess.ess.washington.edu) to infer each sample's exposure age from its [^{10}Be].

2.2. Moraine dating

In this analysis, we assessed uncertainties in the measured [^{10}Be] of each rock sample, the systematic uncertainties in the age of each sample that arise from uncertainties in the appropriate ^{10}Be scaling model, and the systematic uncertainties associated with the transformation of the exposure age of individual rock samples into the emplacement age of the moraine surface. Analytical precision related to the Accelerator Mass Spectrometer (AMS) measurement are reported in Table S1, and are typically on the order of ~2-4% of the measured [^{10}Be]. These uncertainties are quite small relative to the uncertainties associated with converting [^{10}Be] into sample exposure age and moraine emplacement age. Therefore, we focus our attention on the uncertainties that arise from (1) production rate scaling models and (2) the manner in which moraine emplacement ages are inferred from the distribution of ages of rock samples collected from its crest.

There are a number of sites throughout the world where the ^{10}Be production rate has been calibrated (e.g. Nishiizumi et al., 1989, 2007; Phillips et al., 2000); however, a number of models have been developed to interpolate these point measurements to areas where such measurements do not exist. The Tibetan Plateau in particular, lacks direct calibration of production rates, and so we consider five different production rate scaling models that span the range of likely production rates when inferring the exposure ages of rocks (Balco et al., 2008). We regard the range in production rates spanned by these five models (Lal (1991)/Stone (2000) time-dependent and Lal (1991)/Stone (2000) time-independent; Dunai, 2001; Desilets and Zreda, 2003, 2006; and Lifton et al., 2005 models) as capturing the uncertainties associated with our lack of direct calibration of production rates in this area.

To assimilate systematic biases that exist between the production rate models into the covariance of the sample ages, we would need to know the likelihood of the different model scenarios, which is currently unavailable for samples collected from Tibet because of a lack of direct measurement of cosmogenic sample ages that have been dated by independent means. Thus, to provide some measure of uncertainty in moraine ages that arises due to our lack of knowledge of the appropriate production rate model, we simply report the range spanned by all model choices as encapsulating the range of possible ages that arise due to variation between production rate models. We acknowledge that these uncertainties are systematic and so will only subtly affect sample ages relative to one another; nonetheless, this range provides a useful metric to evaluate the importance of different sources of uncertainty in estimating the variations in a particular moraine's absolute age when considering different production rate model scenarios.

Inferring the timing of glacial recession, which is recorded by the age of abandonment of the moraine, requires a model that associates exposure ages of individual samples on the surface of the moraine crest to an effective abandonment age (e.g. Phillips et al., 1990). In the simplest model, clasts that are quarried by glacial erosion experience little exposure to cosmogenic radiation prior to their transport and deposition, and the surface of the moraine remains unmodified over time (assuming no post-glacial shielding). Statistical analyses of published clast exposure ages suggest that the percentage of surface boulders that experience exposure prior to glacial erosion may be quite small (<3%, Putkonen and Swanson, 2003), although this estimate may be biased by a lack of reporting of exposure ages that appear unreasonably old relative to other ages collected on the same surface (Putkonen and Swanson, 2003). In the case that the surface remains stable over time, the mean age of boulders collected on the surface of the moraine may reflect the emplacement age of the moraine surface, assuming that prior exposure is as important as incomplete exposure due to post-glacial shielding (e.g. Zreda et al., 1994; Gosse et al., 1995; Zreda and Phillips, 1995; Briner et al., 2001; Finkel et al., 2003; Meriaux et al., 2004; Chevalier et al., 2005a; Owen et al., 2005; Barrows et al., 2007; Gillespie et al., 2008; Schaefer et al., 2009; Hedrick et al., in press). The small fraction of rocks that may have experienced prior exposure to cosmogenic radiation before being eroded, transported, and deposited by glacial processes may be revealed by outlying boulder ages that are far older than the majority of the sample ages. In this case, such outliers should be identified and discarded prior to computing the mean sample age (e.g. Putkonen and Swanson, 2003; Meriaux et al., 2004; Chevalier et al., 2005a). However, Applegate et al. (2010) recently argued that the mean is a poor estimator of moraine age for data sets drawn from skewed parent distributions, and even excluding outliers before calculating the mean does not improve this mismatch.

Alternatively, a second scenario can be envisioned in which the moraine surface does not remain stable after its initial exposure. In this case, large boulders interspersed throughout the deposit may be exhumed to the surface as erosion transports the fine, and eventually, coarse material away (e.g. Hallet and Putkonen, 1994; Zreda et al., 1994; Zreda and Phillips, 1995; Phillips et al., 1997; Lasserre et al., 2002; Putkonen and Swanson, 2003; Abramowski, 2004, 2006; Briner et al., 2005; Zech et al., 2005a, 2008, 2009; Putkonen and O'Neal, 2006; Schaefer et al., 2008; Applegate et al., 2010; Heyman et al., in press). In this model, the exposure ages of boulders that gradually accumulate on the surface of the moraine represent various stages of boulder exhumation as the surface lowers around them and/or cryoturbation selectively brings boulders near the surface. Should the prior exposure rate indeed be low (Putkonen and Swanson, 2003), then the oldest age found on the surface should more closely represent the exposure age of the moraine surface, although it is still considered a minimum exposure age (e.g. Hallet and Putkonen, 1994; Zreda et al., 1994; Zreda and Phillips, 1995; Putkonen and Swanson, 2003; Briner et al., 2005; Zech et al., 2008; Applegate et al., 2010; Heyman et al., in press).

It is not altogether clear which of these scenarios may be appropriate when inferring the moraine surface emplacement age from sample exposure ages of boulders on its surface. It is still an open question as to what conceptual model applies to moraine degradation in a general sense, and to the majority of Tibetan moraines in particular. In addition, especially for pre-Holocene moraines, the boulders themselves may begin to suffer some attrition as smaller fragments are spalled from larger boulders. Processes such as spallation, erosion, weathering, rolling and snow cover can all lead to apparent young ages. The older the moraine, the more important these processes likely become. Given the unknown rates of each of these processes that may be acting to modify the Tibetan moraines, we consider both scenarios to represent the possible moraine emplacement ages that may be inferred from the ages of clasts collected from their surfaces. As with the different production rate models, this source of uncertainty, hereafter referred to as that associated with the interpretive framework that relates sample ages to moraine emplacement ages, produces a systematic variation. Because we do not have prior information that sheds light on which of these two scenarios may be more likely (and direct field observations to date do not inform the appropriateness of either of these models as applied to Tibetan moraines), we report the possible moraine emplacement ages that span these models of the interpretive framework. Finally, to provide an estimate of the range of possible moraine ages that arises due to both variation between production rate models and the interpretive framework, we use the production rate scaling model of Lifton et al. (2005) with the mean age interpretive framework to provide a minimum bound on moraine surface age, and the time-dependent production rate scaling model of Lal (1991)/Stone (2000) with the oldest age interpretive framework to provide an upper bound on moraine surface ages (which is nonetheless, still a minimum age). Importantly, this range represents the quiver of end-member production rate scaling scenarios that are adjusted for temporal changes in the geomagnetic intensity, all of which produce ages that vary systematically with the model used.

The discussion about the correct interpretative model of moraine ages derives in part from moraine age distributions obtained on individual moraine crests, which may represent instantaneous temporal events of glacier retreat. This is particularly true when a large number of samples, i.e. more than 5, are dated on a single moraine (e.g. Zreda and Phillips, 1995; Lasserre et al., 2002; Meriaux et al., 2004; Chevalier et al., 2005a; Owen et al., 2009). However, in most paleoclimatic studies involving cosmogenic dating of Tibetan moraines, the tendency is to sample very few boulders (<5). For instance, if one considers the large moraine ages database of Tibet (Owen et al., 2008b; Heyman et al., 2010, and Heyman et al., in press) of about ~1300 boulders collected on ~320 individual moraine crests, only ~29% of these moraines have at least 5 boulders dated per moraine and only ~2% have at least 10 boulders dated per moraine. In comparison, our study, with 249 samples on 32 individual moraine crests (with >2 samples), has 88% moraines (28 crests) with at least 5 samples, and 16% moraines (5 crests) with 10 or more samples.

Following Abramowski (2004) who distinguishes between the shape of different age distributions when plotted from youngest to oldest on each moraine, we discuss below the distribution of ages obtained on the 32 moraine crests after a presentation of their geomorphic setting. Each moraine age distribution is shown with the results from the two end-member production rate scaling scenarios that are adjusted for temporal changes in the geomagnetic intensity (i.e. Lifton et al. (2005) and Lal (1991)/Stone (2000) time-dependent). As advocated by Putkonen and Swanson (2003), we identified clasts that contained prior exposure as samples whose exposure age was more than twice that of the next oldest sample. These samples were not considered in calculating either the mean or identifying the maximum rock sample exposure age for each moraine (it is the case for two of our moraines: sample KC2-78 on #15 AQu and sample T7C-62 on #7 Xainza M, Table S1).

Finally, in the Discussion of this contribution, we explored scenarios in which possible additional outliers were identified and excluded from the calculation of ages of specific moraine crests at particular sites, by considering the samples whose error bars (1σ) do not overlap with those of the other samples. As a consequence, mean and oldest ages for these moraines are modified. We acknowledge that such outlier rejection is subjective and we will therefore discuss each moraine case by case (Table 1). We then ranked the moraine mean exposure ages into three groups based on their 1σ standard deviation, i.e. group 1, 2 and 3, for 1σ <17%, 17% <1σ<32%, and 1σ >32% of their mean age, respectively (Table 1). Not surprisingly, as more outliers are rejected, more moraines fit into group 1 or 2 (see Table 1). Again, we acknowledge that such quality assessment of the age distribution is not robust, but it provides some insight into the impact of different outlier rejection scenarios on the broader inferences of moraine age distributions across Tibet.

3. Results

3.1. Sampled sites

Samples were collected along the Ayilari Range (Chaxikang CK and Manikala moraines (Chevalier et al., 2005a)), the Kailas Range (AQu, West Xiong Se and East Xiong Se moraines), the Pulan half-graben (Pulan Rongguo moraine), the KungCo half-graben (KungCo and Cho Oyu moraines), the Ama Drime Range (Dingye N and Dingye S moraines), the Xainza graben (M4, M3, M2, M1 and M moraines), and the Nyainqentanghla Range (YanBaJain Ybj, and Gulu moraines) (locations shown in Fig. 1). Below, we describe each moraine site, from east to west. Details about the samples (location, sample thickness, lithology, qualitative size, shielding factor, [^{10}Be], standard

Table 1
Compilation of all our samples (ages with 1σ uncertainties) and separation in groups of confidence[a] before and after rejecting possible outliers.

# in Fig. 14	Sites	group before rejection	Lal/Stone time-dep mean ages (ka)	Lal/Stone time-dep oldest ages (ka)	Lifton mean ages (ka)	Lifton oldest ages (ka)	outliers?	group after rejection	Lal/Stone time-dep mean ages (ka)	Lal/Stone time-dep oldest ages (ka)	Lifton mean ages (ka)	Lifton oldest ages (ka)
1a	Gulu W	1	16.242 ± 0.79	17.464 ± 1.546	14.651 ± 0.672	15.685 ± 1.604	no	1	16.242 ± 0.79	17.464 ± 1.546	14.651 ± 0.672	15.685 ± 1.604
1b	Gulu E	1	17.927 ± 1.476	20.59 ± 1.822	16.164 ± 1.215	18.355 ± 1.877	no	1	17.927 ± 1.476	20.59 ± 1.822	16.164 ± 1.215	18.355 ± 1.877
2a	Ybj outer W	2	28.836 ± 9.442	49.757 ± 4.383	24.802 ± 7.477	40.986 ± 4.178	1 old	2	26.511 ± 6.285	34.66 ± 3.057	23.003 ± 5.149	29.618 ± 3.022
2b	Ybj inner	2	13.803 ± 3.983	20.316 ± 1.759	12.421 ± 3.303	17.82 ± 1.793	1 old	1	12.175 ± 1.868	14.384 ± 1.252	11.071 ± 1.551	12.925 ± 1.305
2c	Ybj outer E	2	39.162 ± 9.714	48.748 ± 4.259	33.653 ± 7.885	40.873 ± 4.142	1 young	1	41.436 ± 6.928	48.748 ± 4.259	35.533 ± 5.496	40.873 ± 4.142
3a	M4#1	3	67.346 ± 32.122	116.367 ± 10.139	55.399 ± 25.853	95.497 ± 9.669	2 old	1	46.133 ± 8.96	55.571 ± 4.796	38.32 ± 5.774	44.081 ± 4.425
4a	M3 main	1	39.011 ± 5.648	50.025 ± 3.671	33.408 ± 5.205	41.488 ± 3.528	1 old	1	36.809 ± 1.868	38.815 ± 3.356	31.793 ± 1.663	33.626 ± 3.382
4b	M3 inner	1	12.711 ± 1.486	15.55 ± 1.334	11.566 ± 1.254	13.963 ± 1.395	no	1	12.711 ± 1.486	15.55 ± 1.334	11.566 ± 1.254	13.963 ± 1.395
4c	M3 old	3	326.525 ± 151.884	561.669 ± 54.831	260.159 ± 120.549	447.554 ± 49.554	1 old	2	267.739 ± 87.863	359.361 ± 33.395	213.31 ± 68.878	282.908 ± 30.095
5	M2	2	30.665 ± 10.167	45.163 ± 3.877	26.379 ± 8.364	38.075 ± 3.809	3 young	1	35.785 ± 5.893	45.163 ± 3.877	30.598 ± 4.826	38.075 ± 3.809
6	M1	1	26.854 ± 2.083	30.945 ± 2.7	23.476 ± 1.744	26.98 ± 2.731	no	1	26.854 ± 2.083	30.945 ± 2.7	23.476 ± 1.744	26.98 ± 2.731
7	M[c]	3	18.662 ± 6.595	30.502 ± 2.614	16.479 ± 5.444	26.214 ± 2.618	1 old	2	16.689 ± 17.854	24.457 ± 2.126	14.857 ± 3.669	21.301 ± 2.15
8	Dingye N	3	88.015 ± 73.022	287.44 ± 26.406	73.259 ± 59.147	234.071 ± 24.718	1 young, 6 old	2	44.013 ± 13.159	62.652 ± 5.607	37.302 ± 8.86	50.458 ± 5.204
9a	Dingye S frontal	1	20.769 ± 2.563	24.509 ± 2.168	18.543 ± 2.159	21.734 ± 2.222	no	1	20.769 ± 2.563	24.509 ± 2.168	18.543 ± 2.159	21.734 ± 2.222
9b	Dingye S main#1	2	17.601 ± 5.895	25.7 ± 2.278	15.686 ± 4.92	22.42 ± 2.296	1 old	2	14.901 ± 2.9	17.111 ± 1.513	13.441 ± 2.467	15.32 ± 1.566
9c	Dingye S main#2	3	21.937 ± 10.14	40.784 ± 3.615	19.36 ± 8.554	35.279 ± 3.614	2 old	1	16.369 ± 2.784	18.824 ± 1.776	14.675 ± 2.359	16.729 ± 1.796
9d	Dingye S main#3	3	25.067 ± 10.099	39.768 ± 3.516	22.06 ± 8.532	34.545 ± 3.532	1 old	2	21.392 ± 6.779	28.716 ± 2.559	18.94 ± 5.668	25.047 ± 2.575
10	Cho oyu	1	28.46 ± 1.798	31.158 ± 2.775	25.084 ± 1.531	27.382 ± 2.814	no	1	28.46 ± 1.798	31.158 ± 2.775	25.084 ± 1.531	27.382 ± 2.814
11	Kungco	3	26.288 ± 16.175	64.545 ± 5.8	23.101 ± 13.07	52.954 ± 5.48	5 old	2	16.625 ± 4.48	21.794 ± 1.919	15.21 ± 3.82	19.66 ± 2.003
12a	Pulan M1W	1	20.641 ± 1.951	22.743 ± 2.087	18.989 ± 1.69	20.817 ± 2.189	no	1	20.641 ± 1.951	22.743 ± 2.087	18.989 ± 1.69	20.817 ± 2.189
12b	Pulan M2	3	60.559 ± 23.354	94.724 ± 8.45	51.872 ± 19.274	80.542 ± 8.3	2 young	2	69.645 ± 17.138	94.724 ± 8.45	59.258 ± 14.454	80.542 ± 8.3
12c	Pulan M1E	2	31.493 ± 9.808	45.499 ± 4.041	28.226 ± 8.318	39.861 ± 4.09	no	2	31.493 ± 9.808	45.499 ± 4.041	28.226 ± 8.318	39.861 ± 4.09
13	EXS	1	15.436 ± 1.521	16.974 ± 1.599	14.275 ± 1.313	15.594 ± 1.672	no	1	15.436 ± 1.521	16.974 ± 1.599	14.275 ± 1.313	15.594 ± 1.672
14	WXS	2	35.5 ± 9.157	48.354 ± 4.212	31.084 ± 7.599	41.026 ± 4.148	3 young	1	39.627 ± 4.463	48.354 ± 4.212	34.535 ± 3.572	41.026 ± 4.148
15	AQu[b]	2	28.351 ± 6.062	36.895 ± 3.207	24.69 ± 5.003	31.764 ± 3.206	no	2	28.351 ± 6.062	36.895 ± 3.207	24.69 ± 5.003	31.764 ± 3.206
16a	Manikala M1	2	33.652 ± 8.095	42.005 ± 3.728	29.575 ± 6.839	36.713 ± 3.765	2 young	1	37.566 ± 2.639	42.005 ± 3.728	32.868 ± 2.328	36.713 ± 3.765
16b	Manikala M2E	2	186.871 ± 59.91	287.017 ± 26.115	154.781 ± 48.461	235.758 ± 24.733	3 old	1	153.287 ± 24.886	191.361 ± 16.99	127.424 ± 19.525	159.837 ± 16.447
16c	Manikala M2W	1	126.74 ± 20.979	163.341 ± 14.53	105.713 ± 16.069	132.302 ± 13.609	no	1	126.74 ± 20.979	163.341 ± 14.53	105.713 ± 16.069	132.302 ± 13.609
16d	Manikala M3	3	114.28 ± 59.873	194.086 ± 17.37	95.749 ± 49.059	163.013 ± 16.877	4 young	1	173.727 ± 22.3	194.086 ± 17.37	144.266 ± 19.539	163.013 ± 16.877
17a	CK M3	1	122.248 ± 21.382	155.882 ± 13.803	103.824 ± 16.542	128.931 ± 13.224	no	1	122.248 ± 21.382	155.882 ± 13.803	103.824 ± 16.542	128.931 ± 13.224
17b	CK M2 inner	3	52.241 ± 33.675	81.387 ± 7.152	44.354 ± 27.573	68.794 ± 7.008	1 young	2	70.673 ± 15.151	81.387 ± 7.152	59.3 ± 13.425	68.794 ± 7.008
17c	CK M2 outer	3	47.24 ± 16.719	67.824 ± 6.103	40.931 ± 13.571	58.091 ± 6.022	3 old	2	36.273 ± 9.244	47.71 ± 4.229	32.087 ± 7.661	41.226 ± 4.224

Note that Ybj outer N, M4 #2 and M4 #3 have < 2 samples and therefore are not presented in this table.

[a] group1: 1σ < 17%, group 2: 17%< 1σ < 32%, group 3: 1σ > 32%.

[b] KC2-78 on AQu is an outlier because twice as old as the next oldest age.

[c] T7C-62 on M is an outlier because twice as old as the next oldest age.

used and model ages using all scaling models) are listed in Table S1 in the Supplementary Information, as well as geomorphic maps and field photos of each site and each sample collected, when available. While in the field, we focused our attention to the particular geomorphic circumstances of our sites and sampled adequately (e.g. samples collected from the crest, presenting minimum weathering, well-rooted cobbles or embedded large boulders, top of boulders to limit shielding, located far from slopes or gullies, etc.).

3.1.1. Nyainqentanghla Range

YanBaJain and Gulu moraines are located on the southeastern side of the Nyainqentanghla Range, the most prominent mountain range on the Tibetan Plateau, at the edge of the monsoon-influenced Tibet region. Previous cosmogenic moraine chronologies along the range, south of our Gulu site, have shown ages that range from 15 to 40 ka, and 50 to 110 ka (Owen et al., 2005). Initial morphotectonic mapping of these sites was first carried out by Armijo et al. (1986) (drawing, Fig. 2).

The YanBaJain (Ybj) moraine is located at 30°N-90.2°E, at an elevation of ~5000-5300 m asl. It is composed of two lateral crests vertically offset by the active normal fault along the range-front, and extends about 2 km southeast of the range-front (Fig. 2, S1 and S2). The present-day glacier terminus is located about 3 km upstream from the range-front. Several inset river terraces are observed along the present-day river outwash (T on Fig. S1 and S2), located several tens of meters downslope from the range-front. The surface of the moraine is covered by a thin veneer of grass-topped turf with emerging large embedded boulders (50 cm to 4 m in diameter, Fig. S2 to S4). We collected 20 granite and quartzite boulders on the crest of the southern lateral moraine (Ybj outer W #2a: T5C-25-34 and Ybj outer E #2c: T5C-35-44 on either side of the fault) and 2 on the crest of the northern lateral moraine (Ybj outer N #2d: T5C-44bis-45). Five additional samples were collected from the crest of an inset moraine, closer to the present-day glacier (Ybj inner #2b: T5C-19-23) (Fig. 2, S3 and S4, Table S1).

Moraine Ybj outer W has ages that range from 15 to 41 ka, with a mean of 25 ± 7 ka (using Lifton) ($1\sigma\sim30\%$, group 2) (Fig. 3, Tables 1 and 2 and S1). If sample T5C-30, which seems different from all other samples at the 1σ level, is considered as an outlier, the mean clusters at 23 ± 5 ka ($1\sigma\sim22\%$, group 2) (Table 1). Moraine Ybj outer E has older ages that range from 17 to 41 ka, with a mean of 34 ± 8 ka ($1\sigma\sim23\%$, group 2) (Fig. 3, Tables 1 and S1). Sample T5C-35 seems different than all others at the 1σ level, and if considered as an outlier, produces a mean age of 36 ± 5 ka ($1\sigma\sim15\%$, group 1) (Table 1). The five boulders of Ybj inner have ages that range from 10 to 18 ka, with a mean of 12 ± 3 ka ($1\sigma\sim26\%$, group 2) (Fig. 3, Tables 1 and S1). Considering sample T5C-22 as an outlier results in a mean age of 11 ± 2 ka ($1\sigma\sim14\%$, group 1) (Table 1).

The Gulu moraine is located at 30.8°N-91.6°E, at an elevation of ~4800-5000 m asl, at the terminus of a 4-km-long U-shaped valley, whose drainage area is headed by Samdain Kangsang Peak (6532 m, Fig. 2, S5 and S6). The lateral moraine crests are vertically offset by a series of normal faults along the range-front (Fig. S5), whose rupture probably dates back to the M ~ 8, 1951 Damxung earthquake (Armijo et al., 1986). The moraine extends about 1 km east of the range-front and the present-day glacier terminus is located about 4 km upstream from it. We collected 15 samples from large embedded boulders located on the crest of the southern lateral moraine (Gulu W #1a: T5C-58-64 and Gulu E #1b: T5C-66-73 on either side of the fault) (Fig. 2, S5 and S7, Table S1). An inset frontal moraine located upstream (Fig. S6) was not sampled in this study. The surface is covered by a thin veneer of grass-topped turf with emerging large embedded granite boulders (up to 3 m in diameter, Fig. S6 and S7).

The ages of Gulu W (ranging from 14 to 16 ka) and Gulu E (from 15 to 18 ka) average at 15 ± 1 and 16 ± 1 ka (using Lifton), respectively (Fig. 3, Tables 2 and S1). No outliers are identified. Both moraines belong to group 1 ($1\sigma\sim4$-7%) (Table 1). While the means are not significantly different, Gulu E is slightly older than Gulu W, as expected for a slowly retreating glacier. These two tectonically separated ridges, while processed as two different sets of samples, clearly belong to the same moraine crest, subsequently offset by active normal faulting, and may be considered to belong to the same glacial advance.

3.1.2. Xainza range

The Xainza Range is located about 200 km west of the Nyainqentanghla Range, south of Gyaring Co (Fig. 4 and S8). The five moraines sampled here are referred to as M4 and M3, which are located on the eastern side of the northern range, in addition to M2, M1 and M, which are located on the western side of the southern range.

The M4 moraine is located at 30.7°N-88.6°E, at an elevation of about 5200 m asl, and consists of two wide lateral crests extending 4 km southeast of the range-front. The present-day glacier terminus is located about 3 km upstream and is very restricted (Fig. 4). We collected 3 samples from large embedded boulders and two samples from well-rooted cobbles (20-30 cm in diameter), all located on the crest of the southern moraine (M4 # 3a (crest #1): T7C-7, 11, 15, 17 and 18), and two samples from large embedded boulders collected on two nearby crests (M4 #3b: T7C-14 and M4 #3c: T7C-12) (Fig. S9 and Table S1). The surface is not as sharp-crested as at Ybj or Gulu. We tried to avoid weathered boulders as much as possible but the available boulders were typically fractured. The surface is mantled by a thin veneer of turf on which only grass is growing, with emerging boulders up to 1 m in diameter (Fig. S9 and S10).

The ages of moraine M4 (crest #1) range from 33 to 95 ka, with a mean of 55 ± 26 ka (using Lifton) ($1\sigma\sim46\%$, group 3) (Fig. 5, Tables 1 and S1). If samples T7C-11 and T7C-17, which seem different from the others at the 1σ level, are considered outliers, the mean samples age is 38 ± 6 ka ($1\sigma\sim15\%$, group 1) (Table 1).

The M3 moraine is located 8 km southwest of M4 (Fig. 4 and S9), at 30.6°N-88.5°E, at an elevation of about 5000-5300 m asl, and is composed of two relatively sharp, lateral crests along the river outwash, 40-50 m lower (Fig. 4 and S11), as well as an older lateral moraine ~1 km to the north that is not as sharp-crested. A smaller inset moraine is present upstream from this location (Fig. S11 and S12). The frontal moraine has been breached by the glacial outwash river, which is feeding a lake to the east. The moraines extend about 3 km southeast of the range-front and were fed by glaciers coming from 4 main valleys. Small ice patches are currently located about 4 km upstream from the range-front. We collected 19 granite samples from large embedded boulders (n = 16) and well-rooted cobbles (20-30 cm in diameter, n = 3) (Fig. S13 and S14) located on the crests of the northern moraines: 5 (Xainza M3-old #4c: T7C-19-24) on the outer smoother crest, 7 (Xainza M3 inner #4b: T7C-32-39) on the inner moraine upstream and 7 (Xainza M3 main #4a: T7C-24-30) on the main crest (Table S1). The main surfaces are vegetation-free (Fig. S12) and are covered by ~1 m diameter boulders (Fig. S12 to S14). The inset moraine is covered by huge 5-10 m fragmented boulders.

The samples on Xainza M3-old belong to the oldest surface samples ever dated in Tibet and range from 132 to 448 ka, with a mean of 260 ± 121 ka (using Lifton) ($1\sigma\sim46\%$, group 3). The oldest sample, T7C-22 seems different from the others at the 1σ level and considering it as an outlier allows to tighten the mean at 213 ± 69 ka ($1\sigma\sim32\%$, group 2) (Tables 1 and S1). The samples on Xainza M3 inner have ages ranging from 10 to 14 ka, with a mean of 12 ± 1 ka ($1\sigma\sim10\%$, group 1) (Fig.5, Tables 1 and 2). No outlier appears present on that surface. The ages on Xainza M3 main range from 29

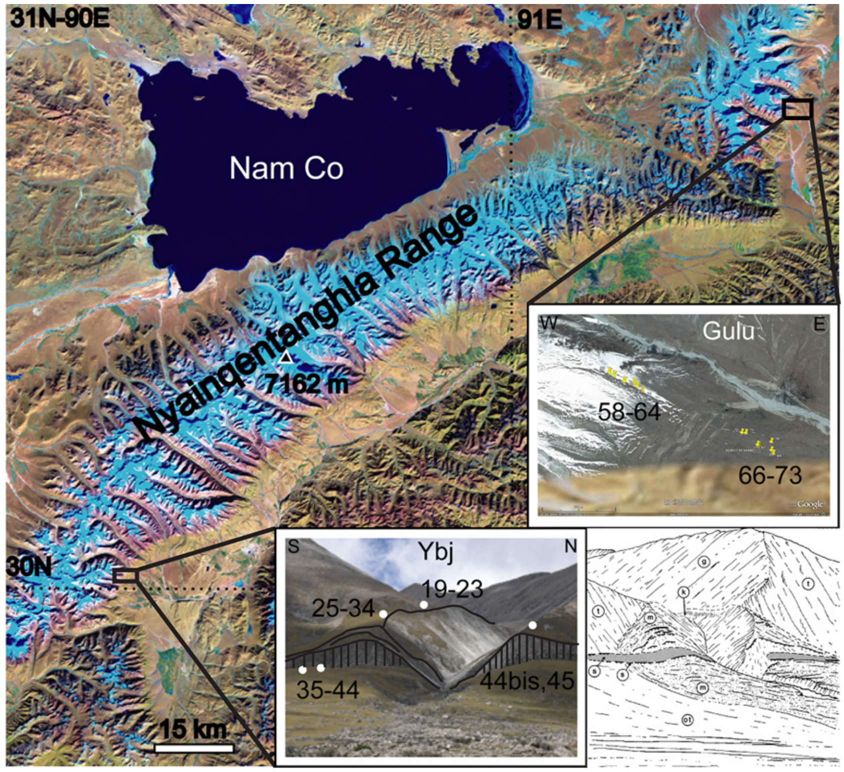

Fig. 2. Landsat satellite image of the Nyainqentanghla area, with location of YanBaJain (Ybj) and Gulu sites. The numbers on each inset photo refer to sample numbers. The drawing represents the Ybj moraine from Armijo et al. (1986).

to 41 ka, with a mean of 33 ± 5 ka ($1\sigma \sim 15\%$, group 1) (Fig.5, Tables 1 and 2). Sample T7C-24-24bis (same collected sample processed separately) may be different from the others at the 1σ level and when considered as outliers, result in a mean age of 32 ± 2 ka ($1\sigma \sim 5\%$, group 1) (Fig. 5, Tables 1 and S1).

The M2 moraine is located about 60 km south of M3 (Fig. 4), at 30°N-88.4°E, at an elevation of about 5300 m asl, and is composed of sharp lateral and frontal crests that extend 3 km west of the range-front (Fig. S16). The U-shaped valley east of the range-front is 4 km-long and is free of ice today. The large embedded boulders are up to 5 m in diameter (Fig. S15 and S17) and show some signs of surficial weathering, although the competence of the rock suggests limited attrition has taken place. We collected 11 granite samples along the crest of the southern lateral moraine (Xainza M2 #5: T7C-40-51). The surface of the moraine is vegetation-free (Fig. S15).

The ages on Xainza M2 range from 13 to 38 ka, with a mean of 26 ± 8 ka (using Lifton) ($1\sigma \sim 31\%$, group 2) (Tables 1 and 2). The three youngest samples do not overlap with other samples at the 1σ level, and when considered outliers, the mean becomes 31 ± 5 ka ($1\sigma \sim 16\%$, group 1) (Fig. 5, Tables 1 and S1).

The M1 moraine is located 20 km south of M2 (Fig. 4), at 29.9°N-88.3°E, at an elevation of about 5100 m asl and is composed of one

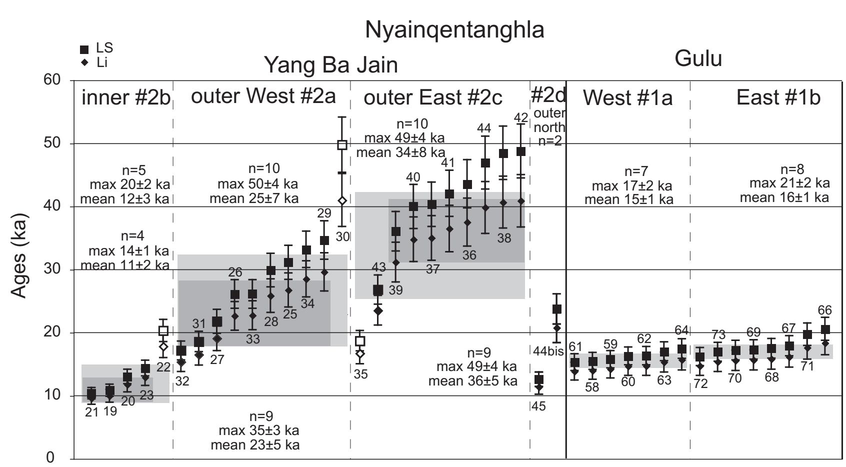

Fig. 3. ^{10}Be surface exposure ages for the YanBaJain and Gulu sites (in the Nyainqentanghla range) plotted from youngest to oldest, with 1 σ error bars. The numbers next to each sample refer to sample numbers in Table S1. Squares show ages calculated using the Lal(1991)/Stone(2000) time-dependent scaling model (LS), diamonds represent ages using the Lifton et al. (2005) model (Li). The oldest age (using Lal/Stone) and the mean age (using Lifton) for each crest are also shown, as well as the number of samples on each crest. Light grey-shaded boxes represent the mean age of all samples (using Lifton) while dark grey-shaded boxes represent the mean age (using Lifton) without the possible outliers (in white, see text for details).

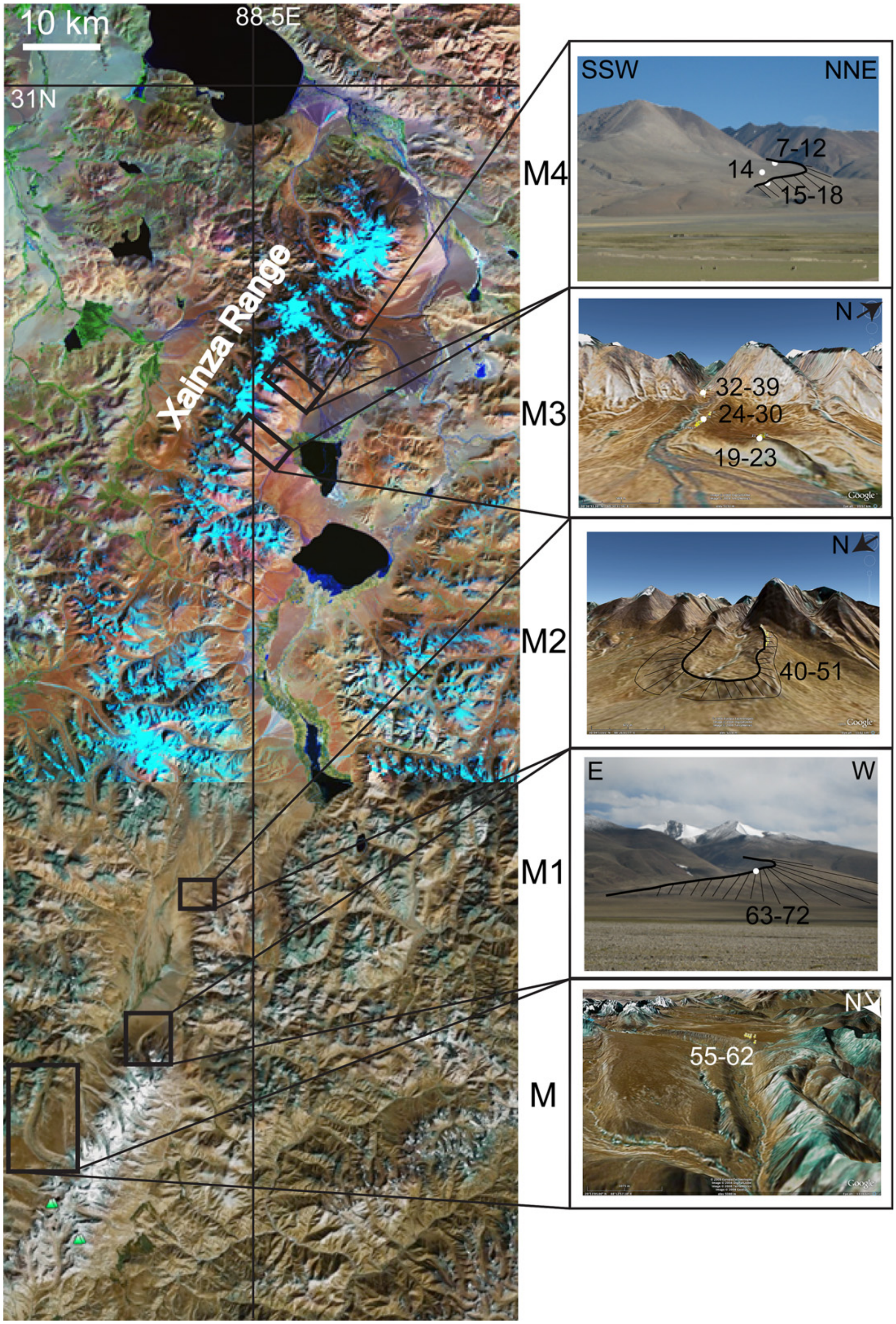

Fig. 4. Landsat satellite image of the Xainza area, where we sampled five sites: M4, M3, M2, M1 and M, from north to south. The numbers on each inset photo refer to sample numbers.

sharp lateral crest on the west side of the range (Fig. S16). The crest is up to 120 m higher than the river outwash (Fig. S15). The present-day glacier terminus is located 6 km from the moraine terminus. We collected samples from 9 large embedded granite boulders (up to 3 m in diameter) on the western crest (Xainza M1 #6: T7C-63-72, Fig. S18, Table S1). The surface is slightly vegetated with very short grass (Fig. S15).

The ages of Xainza M1 range from 21 to 27 ka, with a mean of 23 ± 2 ka (using Lifton) ($1\sigma \sim 7\%$, group 1) (Fig. 5, Tables 1, 2 and S1). No outliers can be identified.

The M moraine is located 15 km southwest of M1 (Fig. 4), at 29.8°N-88.2°E, at an elevation of about 5300 m asl, and is composed of two sharp lateral crests. It extends > 10 km west of the range-front and the present-day glacier terminus is about 4 km upstream from it (Fig. S16). The surface is mantled by a thin veneer of turf on which only grass is growing, with large emerging embedded granite boulders (up to 6 m in diameter) (Fig. S15 and S19). The river outwash has incised ~100 m-deep near the range-front, to 250 m-deep further downstream (Fig. S15). We collected 8 samples from the crest of the southwestern moraine (Xainza M #7: T7C-55-62, Fig. 5 and S19, Table S1).

The ages of Xainza M range from 11 to 26 ka (sample T7C-62 already excluded because it is twice the value of the next oldest sample; Putkonen and Swanson, 2003), with a mean of 16 ± 5 ka (using Lifton) (1σ~33%, group 3) (Tables 1 and 2). Sample T7C-59 seems different than the others at the 1σ level, and when rejected, it allows to calculate a mean of 15 ± 4 ka (1σ~24%, group 2) (Fig. 5, Tables 1 and S1).

3.1.3. Ama Drime Range

The Ama Drime Range is located close to the Himalayan Range, south of the Xainza graben and east of the Phung Chu-Arun river valley, which crosses the Himalaya (Fig. 1). We collected samples from two sites (Dingye N and S) along its eastern front (Fig. 6).

Dingye N moraine is located at 28.3°N-87.7°E, at an elevation of about 4700-5100 m asl and is composed of two lateral crests (Fig. S20) that extend < 2 km from the range-front. The U-shaped valley is about 3 km-long upstream from it and is free of ice today. The surface is somewhat smooth, covered with well-rooted cobbles and lacks a vegetative cover (Fig. S20). The river outwash has incised about 100 m deep. We collected 14 samples (mostly quartzite, 20-30 cm in diameter) on the crest of the northern lateral moraine (Dingye N #8: T5C-141-155, Figs. 6, 7 and S21, Table S1).

The ages of Dingye N range from 16 to 234 ka, with a mean of 73 ± 59 ka (using Lifton) (1σ~80%, group 3) (Tables 1 and 2). We note that the youngest ages are found closer to the range front (samples T5C-141 to 148, with the exception of sample T5C-155) and that they may form a different group between 16 and 50 ka. Rejecting the youngest sample T5C-141 from that younger population (as well as the 6 older samples), because it is different than the others at the 1σ level, allows to calculate a mean of 37 ± 9 ka (1σ~23%, group 2) (Table 1).

The Dingye S moraine is located 20 km south of Dingye N, at 28.1°N-87.6°E, at an elevation of ~5000-5300 m asl, and presents lateral moraine crests and one frontal moraine that extends 3-4 km east of the range-front. The present-day glacier terminus (and glacial lake) is located 3 km upstream. The lateral moraines are characterized by well-rooted cobbles and large embedded boulders up to 4 m in diameter and are devoid of vegetation (Fig. S22 and S23). Large truncated spurs (Fig. S22) are present at the site, attesting the normal faulting activity along the range-front. We collected 7 samples (5 cobbles about 20-30 cm in diameter, and 2 boulders) on the crest of the frontal moraine (Dingye S frontal #9a: T5C-133-140) and 15 samples (8 cobbles about 20-30 cm in diameter, and 7 boulders) on the crest of the southern lateral inset moraine, far from the facets (Dingye S main #9b: T5C-115-119, #9c: T5C-121-126, #9d: T5C-127-132) (Figs. 6 and 7, S24 and S25, Table S1).

The ages of Dingye S main #9b (crest #1) range from 11 to 22 ka with a mean of 16 ± 5 ka (using Lifton) (1σ~31%, group 2). Rejecting the oldest sample T5C-115 allows to compute a mean of 13 ± 2 ka (1σ~18%, group 2) (Table 1). The ages at Dingye S main #9c (crest #2) range from 12 to 35 ka with a mean of 19 ± 9 ka (1σ~44%, group 3) (Tables 1 and 2). Rejecting the two oldest samples brings the mean at 15 ± 2 ka (1σ~16%, group 1) (Table 1). The ages at Dingye S main #9d (crest #3) range from 13 to 35 ka with a mean of 22 ± 9 ka (1σ~38%, group 3). Rejecting the oldest sample T5C-130 brings the mean to 19 ± 6 ka (1σ~30%, group 2) (Table 1). Finally, Dingye S frontal #9a has ages that range from 15 to 22 ka with a mean of 19 ± 2 ka (1σ~11%, group 1) (Tables 1 and 2). No outlier can be identified.

3.1.4. KungCo half-graben

The KungCo half-graben is located ~120 km west of the Ama Drime Range, close to the Himalayan Range. We collected samples from two sites: Cho Oyu and KungCo (Fig. 8).

The Cho Oyu moraine is located at 28.3°N-86.6°E, at an elevation of about 5000 m asl and consists of two sharp, lateral crests with no vegetation cover (Fig. 8 and S26). The samples were embedded boulders of about 50 cm in diameter. We collected 4 samples on the crest of the western moraine (Cho Oyu #10: KC2-A-E, Figs. 8, 10, Table S1).

The ages on Cho Oyu range from 24 to 27 ka, with a mean of 25 ± 2 ka (using Lifton) (1σ~6%, group 1) (Tables 1 and 2). No outliers can be identified.

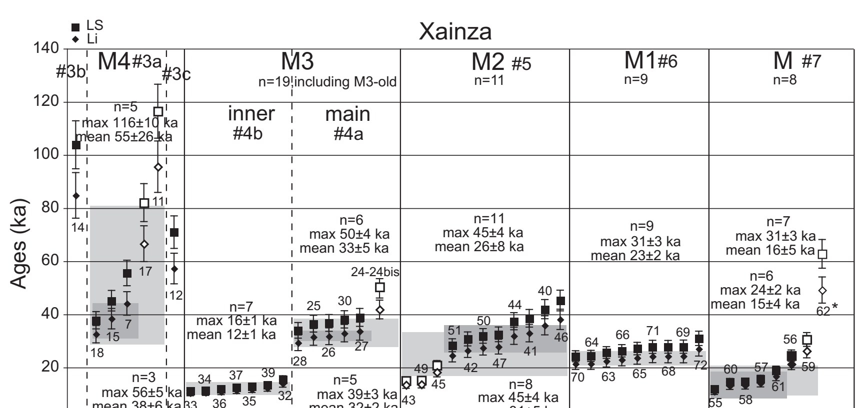

Fig. 5. [10]Be surface exposure ages for the Xainza area, plotted from youngest to oldest, with 1 σ error bars. The numbers next to each sample refer to the sample numbers in Table S1. Sample T7C-62 on M is twice as old as the next oldest sample and is discarded (Putkonen and Swanson, 2003). T7C-24 and 24bis are presented as one uncertainty weighted mean age. M3-old is not plotted on this graph, with ages ranging from ~167 to 562 ka (see Table S1). The oldest age (using Lal/Stone) and the mean age (using Lifton) for each crest are also shown, as well as the number of samples on each crest. Light grey-shaded boxes represent the mean age of all samples (using Lifton) while dark grey-shaded boxes represent the mean age (using Lifton) without the outliers (in white, see text for details).

Table 2
Compilation of moraine ages (<120 ka and with a sufficient number of samples, see text for details) from this study and published studies (total of 71 crests and 524 samples), for each climatic zone. All sample details are in Tables S1 and S2.

	Study	Site	sample #	# of samples per crest	standard used [b]	published ages (ka)	Lifton mean ages (ka)[a, c]	Lal/Stone time-dep oldest ages (ka)[a]
Westernmost Himalayan-Tibetan orogen								
S-Alichur Range (Yashikul)	Zech et al. (2005a)	M2	M2/5	7	S555	46.9 ± 6.1	32.619 ± 16.96	62.278 ± 5.602
		M1	M1/5	7	S555	61.2 ± 8	65.753 ± 2.92	79.845 ± 7.572
S-Alichur Range (Gurumdy)	Abramowski et al. (2006)	GU1	GU19	6	S555	56.8 ± 6.3	31.265 ± 14.986	69.323 ± 6.308
Mustagata and Kongur Shan	Seong et al. (2009)	m3f	MUST-3	6	07KNSTD	8.9 ± 0.3	9.639 ± 0.151	10.083 ± 0.908
		m3f'	MUST-7	8	07KNSTD	8.9 ± 0.3	9.312 ± 0.374	9.981 ± 0.919
		m5a	MUST-21	6	07KNSTD	6.9 ± 0.2	7.381 ± 0.251	7.734 ± 0.682
		m6a	MUST-30	5	07KNSTD	7 ± 0.2	7.35 ± 0.266	7.816 ± 0.690
		m7a	MUST-35	7	07KNSTD	2.1 ± 0.1	2.049 ± 0.193	2.529 ± 0.236
		m6c	MUST-55	5	07KNSTD	0.6 ± 0.1	0.431 ± 0.184	0.684 ± 0.092
		m3c	MUST-61	5	07KNSTD	14.7 ± 0.4	14.08 ± 0.682	16.401 ± 1.441
		m4c	MUST-69	5	07KNSTD	14.2 ± 0.3	14.071 ± 0.301	15.882 ± 1.398
		m4h	KONG_12	6	07KNSTD	7 ± 0.2	7.704 ± 0.094	7.799 ± 0.696
		m5h	KONG_22	5	07KNSTD	4.5 ± 0.1	3.512 ± 1.504	5.174 ± 0.467
		m6h	KONG_26	6	07KNSTD	3.3 ± 0.1	2.71 ± 1.041	3.833 ± 0.351
		m3i	KONG_37	5	07KNSTD	1.5 ± 0.1	1.15 ± 0.501	1.703 ± 0.217
		m2c	MUST-65	6	07KNSTD	75.4 ± 1.4	33.031 ± 18.802	77.666 ± 6.838
		m2b	MUST-90	8	07KNSTD	112.7 ± 1.7	48.025 ± 26.553	113.756 ± 10.016
Transhimalaya and Western Tibet								
Sulamu Tagh	Mériaux et al. (2004)	M1	NNM-9	12	KNSTD	112.7 ± 7.3	39.46 ± 12.695	93.935 ± 8.472
		M2	NNM-11A	12	KNSTD	76.3 ± 4.9	26.289 ± 17.606	70.423 ± 6.209
	Seong et al. (2007)	m2g	K2-65	6	KNSTD	12.6 ± 0.4	7.405 ± 2.864	12.874 ± 1.135
		m1h	K2-93	7	KNSTD	2.1 ± 0.2	1.238 ± 0.64	2.33 ± 0.348
		m1c	K2-13	8	KNSTD	16.7 ± 0.4	16.416 ± 0.608	17.076 ± 1.554
		m1g	K2-59	11	KNSTD	12.3 ± 0.3	11.577 ± 1.095	12.604 ± 1.122
		m1i	K2-76	8	KNSTD	16.5 ± 0.4	12.841 ± 1.157	16.746 ± 1.479
		m2i	K2-81	6	KNSTD	15.3 ± 0.5	13.588 ± 1.434	15.552 ± 1.384
Ladakh	Dortch et al. (2010)	Nubra	NU-24	10	07KNSTD	93.9 ± 6.3	55.512 ± 18.924	99.099 ± 8.93
		Nubra	NU-7	6	KNSTD	51.6 ± 3.4	34.997 ± 10.444	55.411 ± 4.879
	Hedrick et al. (in press)	PM-3	India-47	6	07KNSTD	1.22 ± 0.12	0.61 ± 0.444	1.304 ± 0.122
		PM-2	India-47	7	07KNSTD	7.59 ± 0.77	3.643 ± 2.367	7.49 ± 0.741
		KM-2	TM-9	6	07KNSTD	97.54 ± 9.02	40.71 ± 23.192	85.571 ± 7.674
		KM-1	TM-15	6	07KNSTD	135.13 ± 13.12	39.258 ± 32.584	114.909 ± 10.817
Ayilari Range	Chevalier et al. (2005a)	16a: Manikala M1	WG-15	9	LLNL3000	45.1 ± 3.9	29.575 ± 6.839	42.005 ± 3.728
	This study	17c: CK M2 outer	CK-61	8	KNSTD	/	40.931 ± 13.571	67.824 ± 6.103
Kailas Range	This study	13: EXS	KC2-67	8	LLNL3000	/	14.275 ± 1.313	16.974 ± 1.599
		14: WXS	Zi-88	14	LLNL3000	/	31.084 ± 7.599	48.354 ± 4.212
		15: AQu	KC2-76	7	LLNL3000	/	24.69 ± 5.003	36.895 ± 3.207
Monsoon-influenced Himalaya								
Garhwal (Nanda Devi)	Barnard et al. (2004b)	m2	NDL 30	6	LLNL3000	4.4 ± 0.13	2.804 ± 1.743	4.265 ± 0.381
		m1	NDL 22	5	LLNL3000	16.45 ± 0.4	7.26 ± 5.286	16.285 ± 1.437
Khumbu Himal	Finkel et al. (2003)	Thyangboche I	E84	6	LLNL3000	91.19 ± 1.65	47.5 ± 22.122	85.875 ± 7.562
Nepal	Abramowski (2004)	Macha Khola 4	MK41	5	S555	4.8 ± 0.67	3.916 ± 1.106	5.263 ± 0.643
		Langtang 1	LT16	7	S555	1.71 ± 0.34	0.999 ± 0.46	1.534 ± 0.276
Rongbuk-Everest	Owen et al. (2009)	T5c	Ron-28	9	KNSTD	2.6 ± 0.2	1.856 ± 0.761	2.807 ± 0.266
		T4	Ron-8	12	KNSTD	24.6 ± 2.2	13.666 ± 3.051	23.019 ± 2.028
		T3	Ron-24	11	KNSTD	28.8 ± 2.6	20.231 ± 2.697	26.521 ± 2.299
		T2	Ron-41	8	KNSTD	47.8 ± 4.4	27.074 ± 4.195	40.433 ± 3.646
Pulan graben	Owen et al. (2010)	m4c	Na26	6	07KNSTD	46.1 ± 1.6	32.434 ± 6.158	43.15 ± 3.958
		M4a	Na12	6	07KNSTD	54.5 ± 1.3	26.703 ± 13.333	51.018 ± 4.522
		M3	Na40	6	07KNSTD	64.4 ± 1.3	39.528 ± 11.47	61.521 ± 5.416
		M2	Na42	6	07KNSTD	107.3 ± 2.3	63.563 ± 13.589	100.522 ± 8.957
		M10	Na52	5	07KNSTD	2.7 ± 0.07	1.268 ± 1.441	3.166 ± 0.278
		M4	Na76	6	07KNSTD	54.3 ± 1.3	31.469 ± 15.684	50.867 ± 4.509
		m5a	Na107	7	07KNSTD	15.3 ± 0.4	11.576 ± 2.111	16.374 ± 1.442

(continued on next page)

Table 2 (*continued*)

	Study	Site	sample #	# of samples per crest	standard used [b]	published ages (ka)	Lifton mean ages (ka)[a, c]	Lal/Stone time-dep oldest ages (ka)[a]
Ama Drime Range	This study	9a: Dingye S frontal	T5C-133	7	07KNSTD	/	18.543 ± 2.159	24.509 ± 2.168
		9c: Dingye S main #2	T5C-126	6	07KNSTD	/	19.36 ± 8.554	40.784 ± 3.615
Pulan Graben	This study	12c: Pulan M1E	KC2-45	6	KNSTD	/	28.226 ± 8.318	45.499 ± 4.041
		12b: Pulan M2	KC2-51	9	KNSTD	/	51.872 ± 19.274	94.724 ± 8.45
Monsoon-influenced Tibet								
Nianbaoyeze	Owen et al. (2003a)	Ximencuo	N6	5	LLNL3000	20.89 ± 0.5	17.051 ± 2.082	20.217 ± 1.775
		Jiukehe	N17	10	LLNL3000	42.24 ± 1.09	27.309 ± 6.689	40.258 ± 3.587
		Qiemuqu	A11	5	LLNL3000	17.81 ± 0.38	12.536 ± 2.889	17.844 ± 1.565
Gonga Shan	Zhou et al. (2007)	Baiyu	BYG-9b	9	KNSTD	18.5 ± 2.2	14.189 ± 3.64	18.98 ± 1.723
Nyainqentanghla	This study	1a: Gulu W	T5C-64	7	07KNSTD	/	14.651 ± 0.672	17.464 ± 1.546
		1b: Gulu E	T5C-66	8	07KNSTD	/	16.164 ± 1.215	20.59 ± 1.822
		2c: Ybj outer E	T5C-42	10	07KNSTD	/	33.653 ± 7.885	48.748 ± 4.259
		2a: Ybj outer W	T5C-30	10	07KNSTD	/	24.802 ± 7.477	49.757 ± 4.383
		2b: Ybj inner	T5C-22	5	07KNSTD	/	12.421 ± 3.303	20.316 ± 1.759
Xainza Range	This study	4b: M3 inner	T7C-32	7	07KNSTD	/	11.566 ± 1.254	15.55 ± 1.334
		4a: M3 main	T7C-24-24bis	6	07KNSTD	/	33.408 ± 5.205	50.025 ± 3.671
		5: M2	T7C-46	11	07KNSTD	/	26.379 ± 8.364	45.163 ± 3.877
		6: M1	T7C-72	9	07KNSTD	/	23.476 ± 1.744	30.945 ± 2.7
		7: M	T7C-59	8	07KNSTD	/	16.479 ± 5.444	30.502 ± 2.614
KungCo Graben	This study	11: Kungco	KC2-268	15	KNSTD	/	23.101 ± 13.07	64.545 ± 5.8

See Tables S1 and S2 for more details about each sample.
We used Cronus 2.2 with constant file 2.2.1.
[a] Uncertainties are reported at the 1σ confidence level.
[b] ^{10}Be isotope ratios for KNSTD = 3.11×10^{-12}; for LLNL3000 = 3×10^{-12}; for S555 = 95.5×10^{-12}; for 07KNSTD = 2.85×10^{-12}.
[c] Mean age of the surface.

The KungCo moraine, first described by Armijo et al. (1986) (drawing, Fig. 8), is located at 28.8°N-86.4°E, at an elevation of about 4800 m asl, and consists of two sharp, lateral crests, with sparse grass cover. It is located on the western side of the range, extending ∼ 2 km west of the range-front (Fig. S26). The hanging U-shaped valley is free of ice today. The moraines are vertically offset by the KungCo normal fault (Fig. S26), whose activity has been discussed based on exhumation rate estimates in Maheo et al. (2007). We collected 15 well-rooted quartzite cobbles of about 20-30 cm in diameter on the crest of the northern moraine, far from the triangular facet (KungCo #11: KC2-266-280, Figs. 8, 10, Table S1).

The ages on the KungCo moraine range from 8 to 53 ka with a mean of 23 ± 13 ka (using Lifton) (1σ∼56%, group 3) (Tables 1 and 2). Similarly to Dingye N, it is possible to identify 5 old outliers; their exclusion results in a mean sample age of 15 ± 4 ka (1σ∼25%, group 2) (Table 1).

3.1.5. Rongguo moraine

The Pulan half-graben is located 600 km west of the KungCo half-graben, along the western side of the Gurla Mandhata (7728 m), south of the Manasarovar and Raksas lakes in the Kailas basin.

The Rongguo lateral moraines are located ∼ 10 km north of the town of Pulan, at an elevation of ∼4500 m, at 30.3°N-81.2°E (Fig. 9), on either side of the Rongguo glacial outwash. They form broad till ridges (M, M', Fig. S27) that stand 150-250 m above the outwash and extend ∼ 5 km southwest of the Gurla Mandhata range front (Fig. S27). The three crests we sampled were emplaced NW of the outwash, at the outlet of the deepest and longest (>20 km) U-shaped valley carved by the largest glacier on the south side of Gurla Mandhata's summit. The present terminus of this glacier lies ∼12 km upstream. Smaller glaciers hang from the north cliff of the Rongguo valley (photograph, Fig. S28). The lower moraine M2 (Fig. 9) is broad, relatively flat-topped, and appears to extend continuously downstream to the trunk valley to the Karnali river, which drains the Pulan graben into Nepal's Karnali river. The upper moraines M1E and M1W are much shorter, with M1W extending < 1 km from the range-front. They have narrower sharper crests, with slightly steeper inner edges that stand locally ∼50 m higher than the flat surface of the lower moraine M2, implying M1W was emplaced on top of M2. Between M1E and M1W lies the range-front normal fault zone, whose trace has channeled rills born on the facet, leading to transverse incision (Fig. 9).

All moraine surfaces contain large embedded granite boulders 1-2 m in diameter with smaller well-rooted cobbles (∼20-30 cm-diameter) interspersed (Fig. S28). The surfaces are free of vegetation. The surfaces of M1E and M1W have a rougher, more chaotic micro-topography. Eighteen samples were collected on the crests of the upper and lower moraines, half of them from the top surface of boulders, the other half from cobbles (20-30 cm in diameter, yellow and orange circles on Fig. 9, respectively): 3 samples on the crest of M1W (#12a: KC2-39-44), 6 samples on the crest of M1E (#12c:

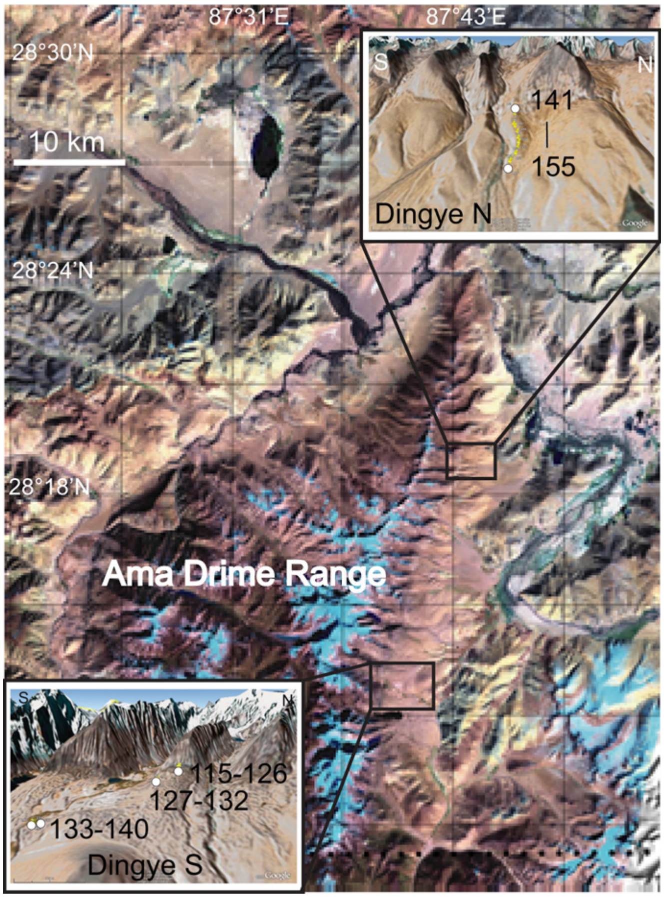

Fig. 6. Landsat satellite image of the Ama Drime area, where we sampled two sites: Dingye north and Dingye south. The numbers on each inset photo refer to sample numbers.

KC2-45-50), and 9 samples on the crest of M2 (#12b: KC2-51-59) (Figs. 9 and 10, Table S1).

On M1W the ages range from 17 to 21 ka with a mean of 19 ± 2 ka (using Lifton) (1σ ~ 9%, group 1). No outlier is identified. On M1E the ages range from 18 to 40 ka with a mean of 28 ± 8 ka (1σ ~ 29%, group 2) (Tables 1 and 2). No outlier is identified. The ages on M2 are widely spread from 26 to 81 ka with a mean at 52 ± 19 ka (1σ ~ 37%, group 3) (Tables 1 and 2). Rejecting the two youngest samples yields a mean age of 59 ± 14 ka (1σ ~ 24%, group 2) (Fig. 10, Tables 1 and S1). Interestingly, while sample ages collected from cobbles show systematically younger cosmogenic exposure ages than boulders at sites along the San Andreas Fault (e.g. Behr et al., 2009), at this particular site, we resolve no difference in exposure ages between these two populations (e.g. Briner, 2009). For this reason, in the following analysis we include both boulder and cobble ages, although the exclusion of these typically less-reliable cobble ages does not substantively affect our results.

We can compare the ages we obtained on our M1W and M2 surfaces with the ages presented in Owen et al. (2010) from M4a and M3, respectively. Our M2 ages ($n = 9$) range from 26 to 81 ka, while the ages from M3 surface ($n = 6$) in Owen et al. (2010) range from 25 to 52 ka (using Lifton). This might reflect that we picked more representative samples from that minimum 80 ka-old surface. Concerning the younger surface, our M1W ($n = 3$) ages range from 17 to 21 ka, while the ages from M4a ($n = 6$) in Owen et al. (2010) range from 10 to 43 ka (using Lifton). Therefore it seems like this surface might be at least twice as old as what we have found, implying that Owen et al. (2010) may have picked more representative samples. One could wonder if our M1W and M1E surfaces might actually be the same surface, that has been right-laterally offset by the Gurla Mandhata fault. Indeed, M1E ages range from 18 to 40 ka, which is very similar to what Owen et al. (2010) have for their M4a surface.

3.1.6. Kailas Range

The Kailas Range is located in western Tibet, north of the Rongguo site (Fig. 9). The highest peak of the range is the Mt. Kailas (6714 m). We sampled three lateral moraines on its southern side: AQu, West Xiong Se and East Xiong Se.

The West Xiong Se and East Xiong Se lateral moraines are located at 31°N – 81.2°E, at an elevation of ~4800 m asl (Fig. 9). They form part of a large, composite, moraine ring complex abandoned by the Xiong Se glacier at the outlet of one of the largest glacial valleys of the range, just west of Mount Kailas. The farthest-reaching lobes of this moraine extend up to ~5 km south of the range-front (Fig. 9). The trunk glacier that formerly covered the wide, flat-floored Xiong Se valley resulted from the confluence of two main glaciers ~10 km north of the range-front. Hanging

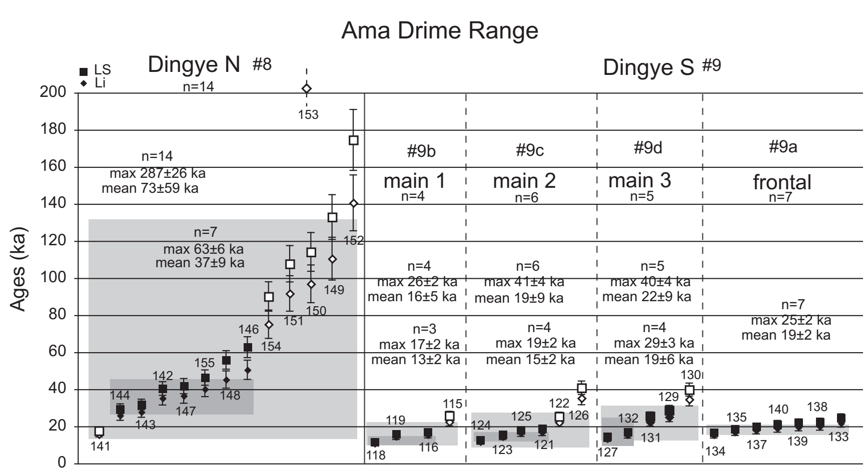

Fig. 7. [10]Be surface exposure ages for the Ama Drime area, plotted from youngest to oldest, with 1 σ error bars. The numbers next to each sample refer to the sample numbers in Table S1. The oldest age (using Lal/Stone) and the mean age (using Lifton) for each crest are also shown, as well as the number of samples on each surface. Light grey-shaded boxes represent the mean age of all samples (using Lifton) while dark grey-shaded boxes represent the mean age (using Lifton) without the outliers (in white, see text for details).

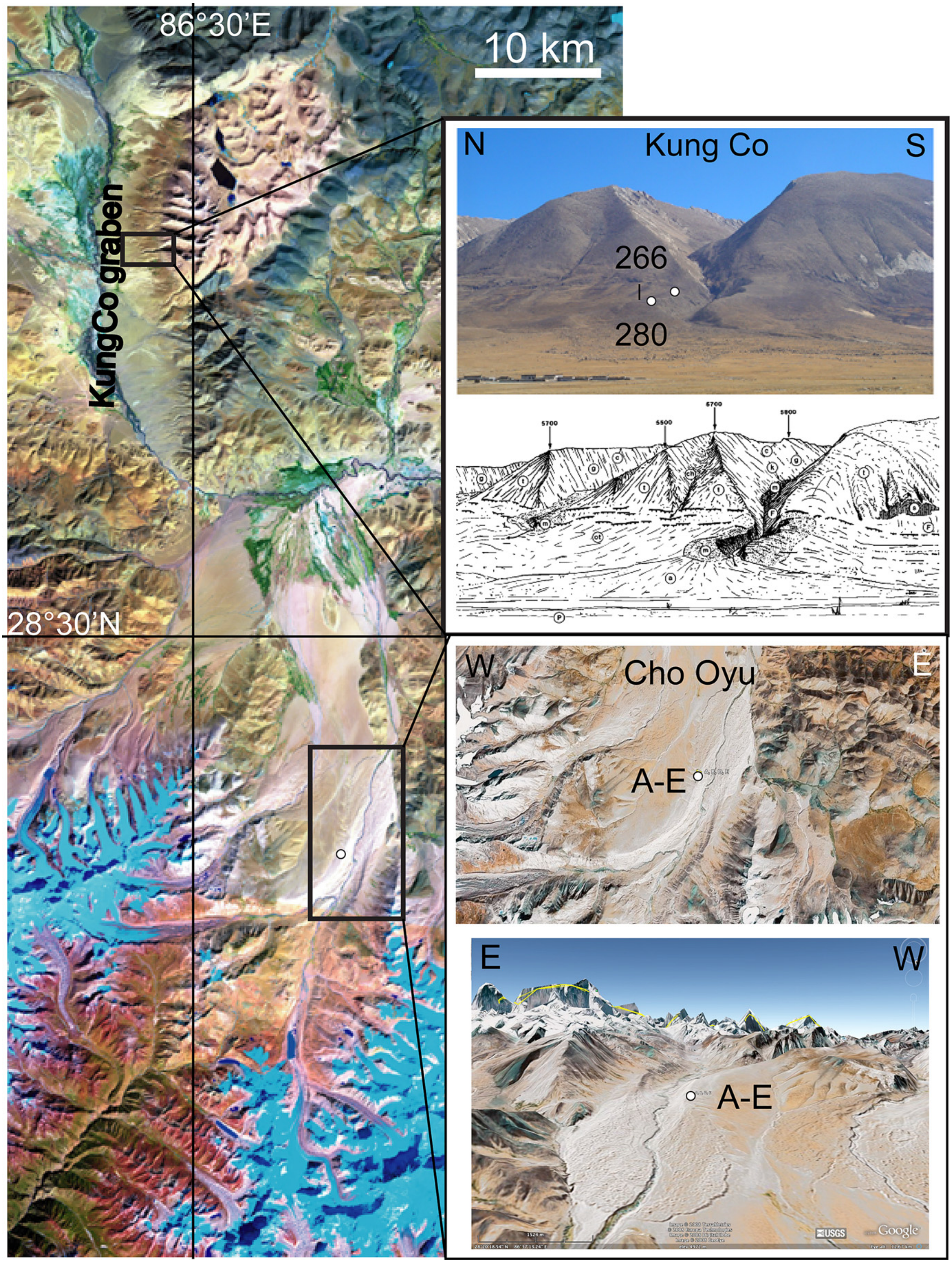

Fig. 8. Landsat satellite image of the KungCo area, where we sampled two sites: KungCo and Cho Oyu. The drawing represents the KungCo moraine from Armijo et al. (1986). The numbers and letters A-E on each inset photo refer to sample numbers.

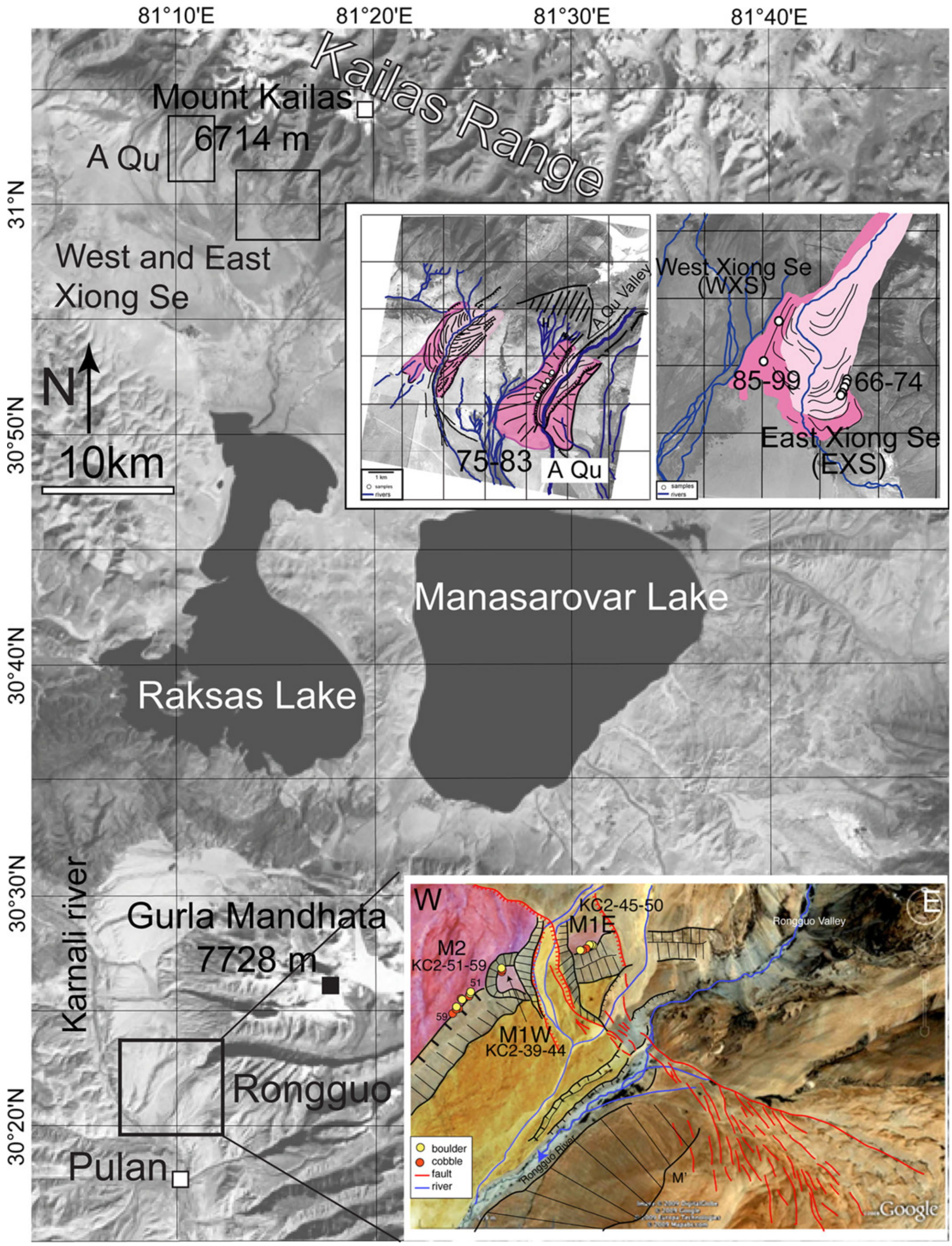

Fig. 9. Landsat satellite image of the Kailas and Pulan areas, where we sampled four sites: AQu, West Xiong Se, East Xiong Se, and Pulan. The numbers on each inset photo refer to sample numbers.

present-day tributary glaciers remain on the north side of Mount Kailas, and much smaller ice patches are perched ~15 km north of the range-front. Within the moraine complex, the Xiong Se outwash river forms a ~90° dogleg bend along one of the innermost moraine rings (Fig. 9 and S30). Large, angular, embedded granite boulders are common along the inner ridge crest of the East Xiong Se moraine (Fig. S30) where some small bushes are present at places. Along the West Xiong Se outer moraine crest, covered by short grass, similarly large embedded boulders, surrounded by smaller well-rooted ones are also found. Eight and fourteen boulders were collected on the crests of the East and West Xiong Se lateral moraines, respectively (EXS #13: KC2-66-74 and WXS #14: ZI-85-99, from south to north, Fig. 11, Table S1).

The ages on EXS range from 12 to 16 ka with a mean of 14 ± 1 ka (using Lifton) ($1\sigma \sim 9\%$, group 1) (Tables 1 and 2). No outlier can be identified. On WXS the ages are more scattered and range from 16 to 41 ka with a mean of 31 ± 8 ka ($1\sigma \sim 24\%$, group 2) (Tables 1 and 2). Separating the 3 youngest samples, which are different from all the others at the 1σ level allows to tighten the mean age at 35 ± 4 ka ($1\sigma \sim 10\%$, group 1) (Fig. 11, Tables 1 and S1).

The AQu lateral moraines are located at about 31°N − 81.2°E, 6 km west of the Xiong Se moraines, at an average elevation of

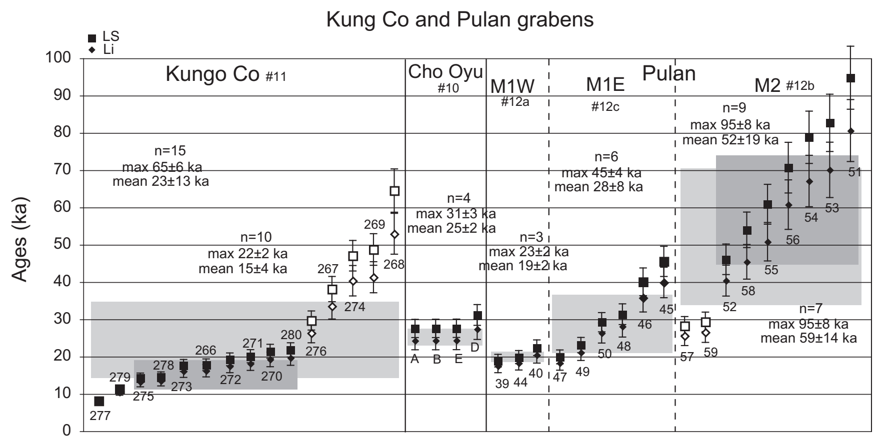

Fig. 10. [10]Be surface exposure ages for the KungCo and Pulan areas, plotted from youngest to oldest, with 1 σ error bars. The numbers next to each sample refer to the sample numbers in Table S1. The oldest age (using Lal/Stone) and the mean age (using Lifton) for each crest are also shown, as well as the number of samples on each surface. Light grey-shaded boxes represent the mean age of all samples (using Lifton) while dark grey-shaded boxes represent the mean age (using Lifton) without the outliers (in white, see text for details).

5100 m. They have well-defined shapes, no vegetation, with sharp crests extending 5 km south of the Kailas range-front (dark pink on Fig. 9; photographs, Fig. S29). The AQu glacial valley was formed by the confluence of two glaciers about ∼3 km north of the Kailas range-front. The present-day termini lie about 6 km north of the front, at 5500 m asl (Fig. 9). A younger moraine complex (light pink on Fig. 9), which probably reflects the penultimate stages of glacial retreat, is inset within and below the highest moraine crests. Seven embedded quartzite boulders, ∼40 cm in diameter (Fig. S29), were collected on the crest of the western AQu lateral moraine (#15: KC2-75-83 from south to north, Figs. 9 and 11, Table S1).

The ages on AQu range from 19 to 32 ka (after sample KC2-78 was rejected as being more than two times older than the next oldest sample on the moraine; Putkonen and Swanson, 2003), with a mean of 25 ± 5 ka (using Lifton) (1σ∼20%, group 2) (Fig. 11, Tables 1, 2 and S1). No other outlier can be identified.

3.1.7. Ayilari Range

The Ayilari Range is located 200 km northwest of the Kailas range in western Tibet, near the disputed border between China and India. We collected samples from two sites located north of the range: Manikala (Chevalier et al., 2005a, 2005b) and Chaxikang CK (Fig. 12).

The Manikala moraine complex lies at the base of the Ayilari range-front, which bounds the west side of the Gar valley, a large basin floored by marshland. It is located at 32°N-80°E and ∼4600 m asl. The moraines lie northeast of the U-shaped Manikala valley, a glacial trough deeply entrenched into the range (Fig. 12). They were emplaced by the Manikala Daer glacier, whose terminus is currently ∼7 km upstream. The relative ages of the moraine groups can be qualitatively assessed from their surface characteristics and from their distance to the upstream source valley (Fig. S2 in Chevalier et al., 2005a). The M1 surface is rough and composed of chaotically distributed embedded blocks as large as 3 m in diameter, which are surrounded by coarse debris, and is devoid of vegetation. The smoother surface of M2 appears older, with well-rooted blocks tens of centimeters to a meter in diameter protruding above a mantle of smaller debris and no vegetation. The surface of M3 is even smoother and is probably the oldest surface of the moraine complex, with relatively smaller well-rooted blocks and still no vegetation. The youngest moraine group, M1 (Fig. 12), is the only one present on both sides of the Manikala outwash valley and displays terminal lobes and sharply defined ridge crests. We collected 9 well-rooted quartzite cobbles (20-30 cm in diameter) on the crest of M1 (#16a: WG-11-19), 18 on the crest of M2 (M2W

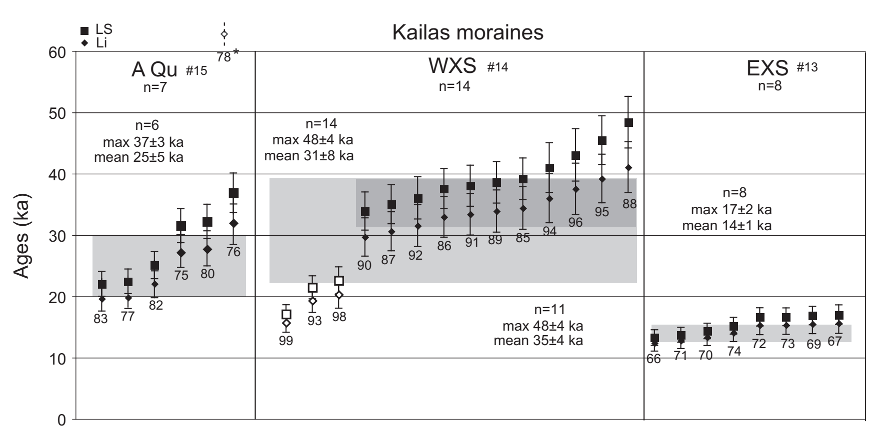

Fig. 11. [10]Be surface exposure ages for the Kailas area, plotted from youngest to oldest, with 1 σ error bars. The numbers next to each sample refer to the sample numbers in Table S1. Sample KC2-78 on AQu is considered as an outlier (∼203 ka). The oldest age (using Lal/Stone) and the mean age (using Lifton) for each crest are also shown, as well as the number of samples on each surface. Light grey-shaded boxes represent the mean age of all samples (using Lifton) while dark grey-shaded boxes represent the mean age (using Lifton) without the outliers (in white, see text for details).

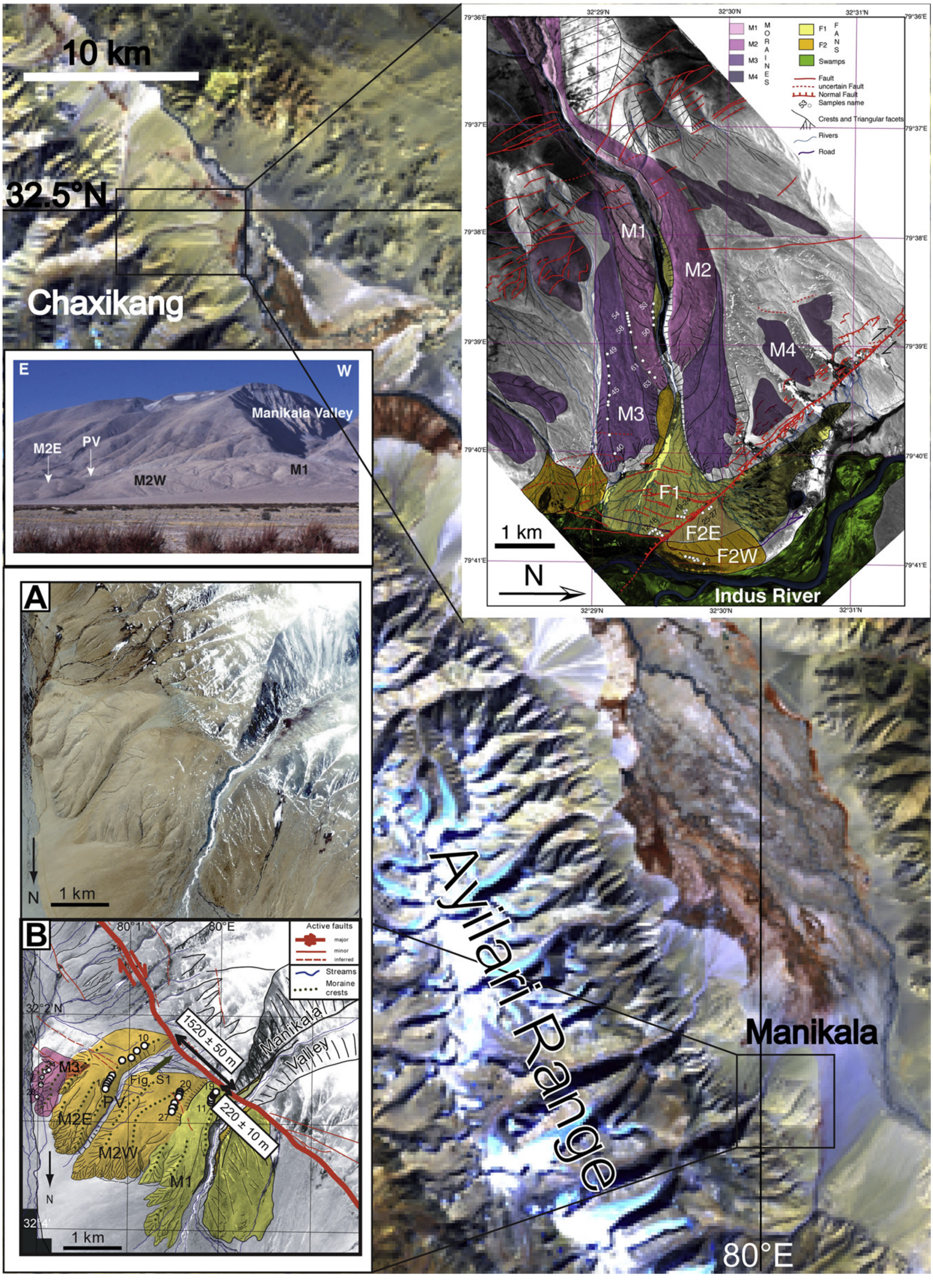

Fig. 12. Landsat satellite image of Manikala (Chevalier et al., 2005a, 2005b) and Chaxikang sites. The numbers on each inset photo refer to sample numbers.

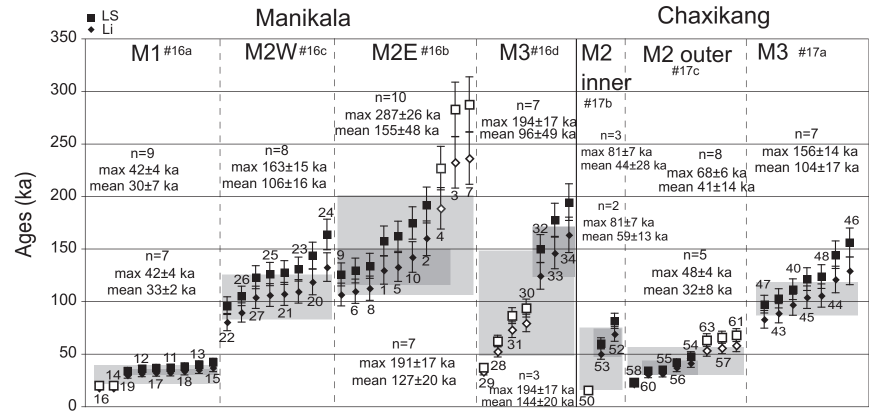

Fig. 13. ^{10}Be surface exposure ages for Manikala and Chaxikang, plotted from youngest to oldest, with 1 σ error bars. The numbers next to each sample refer to the sample numbers in Table S1. The oldest age (using Lal/Stone) and the mean age (using Lifton) for each crest are also shown, as well as the number of samples on each surface. Light grey-shaded boxes represent the mean age of all samples (using Lifton) while dark grey-shaded boxes represent the mean age (using Lifton) without the outliers (in white, see text for details).

#16c: WG-20-27, M2E #16b: WG-1-10) and 7 on the crest of M3 (#16d: WG-28-34) (Figs. 12 and 13, Table S1).

The ages on the crest of Manikala moraine M1 range from 18 to 37 ka with a mean of 30 ± 7 ka (using Lifton) (1σ ~ 23%, group 2) (Tables 1 and 2). Separating the samples in two groups, the two youngest samples of 20 ka on one side and the older ones on the other side, results in a mean sample age of 33 ± 2 ka (1σ ~ 7%, group 1) for the older group (Table 1). The ages on the crest of Manikala M2W range from 80 to 132 ka, with a mean of 106 ± 16 ka (1σ ~ 15%, group 1). No outliers are identified. The ages on the crest of Manikala M2E range from 106 to 236 ka with a mean of 155 ± 48 ka (1σ ~ 31%, group 2). Considering the three oldest samples as outliers results in a mean sample age of 127 ± 20 ka (1σ ~ 15%, group 1) (Table 1). The ages on the crest of Manikala M3 range from 33 to 163 ka with a mean of 96 ± 49 ka (1σ ~ 51%, group 3). Rejecting the 4 youngest samples because they are different from the others at the 1σ level and because geologic relationships require M3 to be older than M2 and M1, revises the mean sample age to 144 ± 20 ka (1σ ~ 13%, group 1) (Fig. 13, Tables 1 and S1).

The Chaxikang moraines (CK M1, M2, M3 and M4) are located 60 km west of Manikala, and lie between the Indus River and the Ayilari range at elevations between 4250 and 4530 m. These moraines are located at the outlet of a large flat-floored glacial valley, the Miren Nongba valley (MRNB, Fig. 12). At times of larger glacial extent, the glacier flowed down from the ice cap topping the westernmost part of the Ayilari Range (5800-5900 m asl), almost all the way to the Indus flood-plain, a distance of ~20 km. Today, only small ice patches are left on top of this part of the range, in contrast to the more extensive ice cover farther south (Fig. 12).

Following the work of Liu (1993), which was mostly based on Spot image interpretation, we have mapped (on Ikonos images and 1/50,000 topographic maps) four main sets of distinct moraines, emplaced downstream from the outlet of the valley (Fig. 12). The youngest moraine (M1, light pink, Fig. 12) extends ~1.6 km north-east of the range-front. This innermost moraine is incised ~20-30 m by the present outwash. Asymmetric patches of only one main, abandoned terrace are visible along the outwash river bed (yellow patches). An older moraine complex (M2, dark pink), at the outlet of which the present-day river has incised a narrow, 50-60 m deep canyon, extends ~3.6 km from the range-front. The oldest moraine complex (M3, light purple) extends 5.2 km from the range-front. The terminus of this complex is not preserved. It has been eroded and breached by the river, as it fanned out of the canyon incised into M2 and M3.

There are other more ancient moraine complexes, whose distinctive shapes indicate that significant surface modification has taken place (for example, M4, dark purple, Fig. 12). Eighteen samples were collected at Chaxikang, along the two distinct vegetation-free moraines on the south side of the Miren Nongba valley: 7 on the crest of CK M3 (#17a: CK-40-48), 8 on the crest of CK M2 outer (#17c: CK-54-63) and 3 on the crest of CK M2 inner (#17b: CK-50-53). All samples were from embedded quartzite boulders 20 to 70 cm in diameter (Fig. S31).

The ages on CK M3 range from 83 to 129 ka with a mean of 104 ± 17 ka (using Lifton) (1σ ~ 16%, group 1). The spread of ages is regular and no outliers can be identified. The ages on CK M2 outer range from 21 to 58 ka with a mean of 41 ± 14 ka (1σ ~ 33%, group 3) (Tables 1 and 2). At the 1σ level, the three oldest samples might be considered outliers, resulting in a mean sample age of 32 ± 8 ka (1σ ~ 24%, group 2) (Table 1). The ages on CK M2 inner range from 14 to 69 ka with a mean of 44 ± 28 ka (1σ ~ 62%, group 3). Considering the youngest sample as an outlier brings the mean to 59 ± 13 ka (1σ ~ 22%, group 2) (Fig. 13, Tables 1 and S1).

3.2. Moraine age distribution

The uncertainties associated with scaling models and with geomorphic interpretation of the moraine emplacement age is illustrated in Fig. 14. The uncertainties in determining moraine exposure age based on the choice of oldest or mean rock sample exposure age on each moraine are shown in Fig. 14A,C versus Fig. 14B,D, respectively. Scaling models advocated by Lifton et al. (2005) (Fig. 14C,D) yield systematically younger rock sample exposure ages than a version of the Lal (1991)/Stone (2000) scaling model that is scaled for temporal variations in geomagnetic field intensities (Fig. 14A,B). On Fig.14A and *D*, we also represented the probability density function (PDF) of all the moraine emplacement ages supposing that each age was normally distributed. The summed PDF was normalized such that the integrated probability density between -∞ and ∞ was unity. We acknowledge that such a summation assumes that we have sampled different moraines without bias as to their ages and location, which is certainly not correct (e.g. Phillips et al., 1997; Putkonen and Swanson, 2003). However, such a PDF illustrates the magnitude of change in the overall age distributions that is incurred when different scenarios are considered. The Gaussian distributions produced by each moraine age were then summed and presented together and according to their group, with group 1 being the most straightforwardly interpreted moraines (due to the tight clustering of individual rock sample ages) and group 3

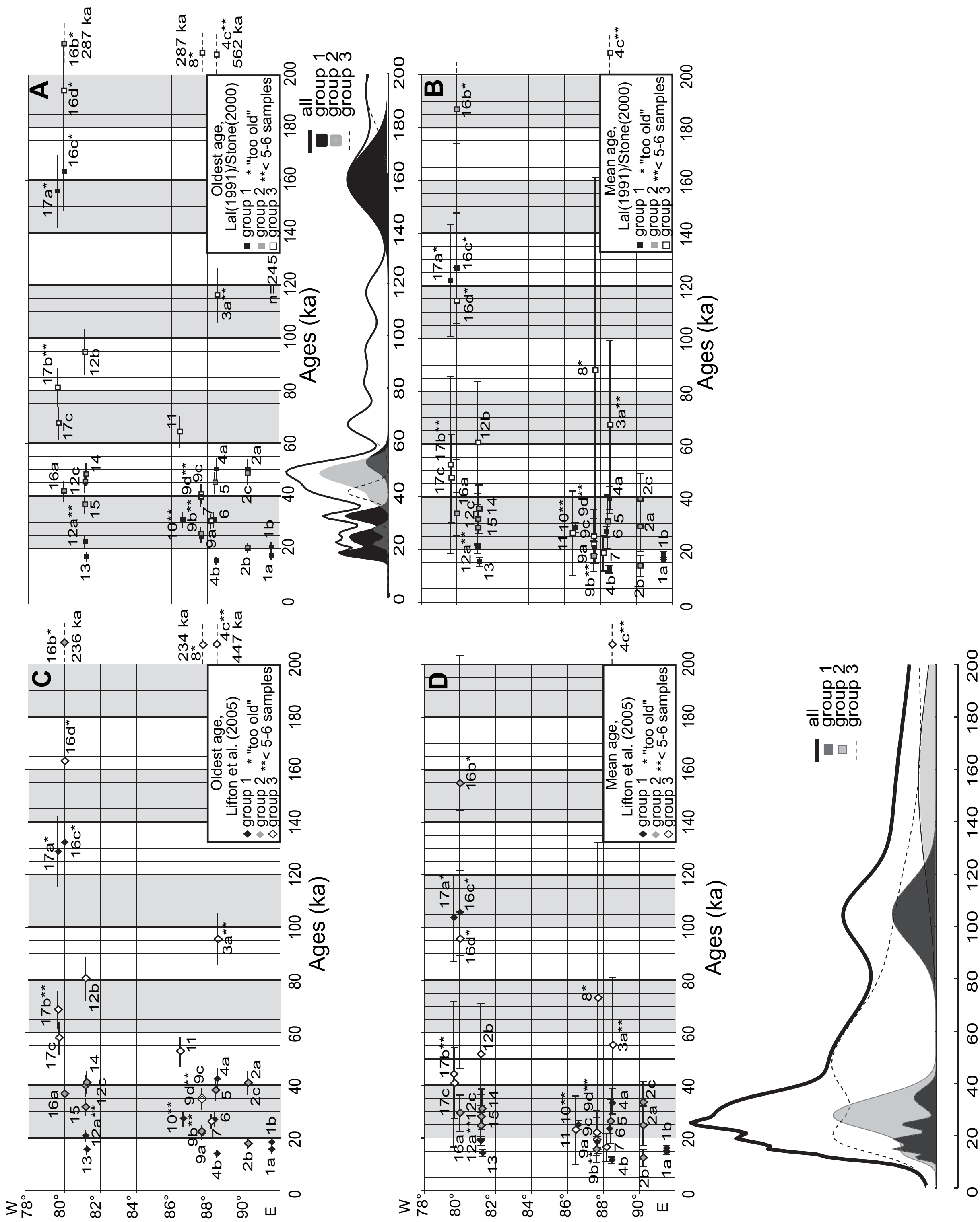

Fig. 14. Compilation of moraine ages from this study, as a function of longitude (Tables 1 and S1). Numeral refers to moraine number as listed in Table 1. $n = 245$ because we do not present crests with <2 samples (Ybj outer N, M4 #2 and M4 #3). A) oldest sample age per moraine crest, calculated using Lal/Stone scaling model, B) mean ages, calculated using Lal/Stone scaling model, C) oldest sample age per moraine crest, calculated using Lifton scaling model and D) mean ages, calculated using Lifton scaling model. In A) and D), probability density function (PDF) of moraine age groups 1 to 3 according to 1σ uncertainties ranking (Table 1).

being the most problematic (due to the wide distribution of sample ages).

As expected, moraine ages derived from the oldest age scenario are systematically older than those derived from using the mean age scenario, regardless of the scaling model used. While the magnitude of this systematic change depends on the specific distribution of rock sample exposure ages on each moraine, it is not unusual for the moraine exposure age to vary >50% between each of these two scenarios. The moraine age distribution shows a large number of moraines between 10 and 50 ka, group 1 moraines

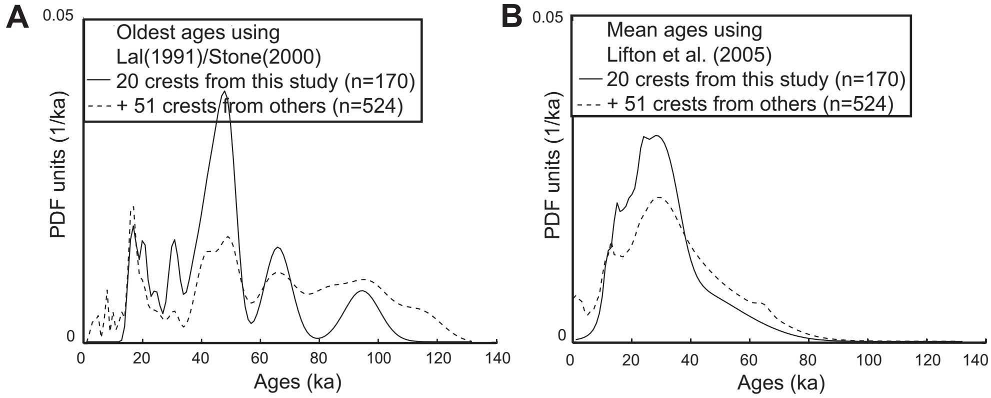

Fig. 15. Probability Density Functions (PDF) of moraine ages (<120 ka and with a sufficient number of samples, see text for details) from this study (20 crests, 170 samples, solid line) and compiled with the published studies (51 crests, 354 samples, dashed line) (Tables 2, S1 and S2). A) oldest ages per moraine crest, calculated using Lal/Stone scaling model and B) mean ages, calculated using Lifton scaling model.

showing distinctive peaks between 10 and 40 ka. The largest number of moraines from all groups is around 25 ka when the mean age is considered, or 50 ka when the oldest age is considered (Fig. 14A and D).

We then grouped our moraines in Tibet (solid line in Fig. 15), or within different sub-regions within the area (solid line in Fig. 16) to assess how the different sources of uncertainty impact regional interpretations of the distribution of moraine exposure ages. This analysis does not include moraines < 20 ka with <5 samples, and moraines > 20 ka with <6 samples per crest (** on Fig. 14 and in Table S1), nor did we include crests > 120 ka (* on Fig. 14 and in Table S1). This represents 20 crests and 170 samples (Table 2), from all groups 1, 2 and 3, i.e. 32 crests minus M4 #1, Dingye S main #1, Dingye S main #3, Cho Oyu, Pulan M1W, CK M2 inner, M3-old, Dingye N, Manikala M2E, Manikala M2E, Manikala M3 and CK M3. In addition to our dataset (solid line in Figs. 15 and 16), we added the results from 51 published moraine crests (or 354 samples) in the same area (dashed line in Figs. 15 and 16) (Fig. 1 inset, Tables 2, S1 and S2 and text below for more details).

When interpreting moraine exposure ages in terms of the mean exposure age of samples collected from its surface for all of Tibet (dashed line, Fig. 15B), the age distribution reaches peaks at 2, 14, 30 and (65) ka, but nonetheless shows relatively poor definition. With just our data, there are peaks at 15 and 24-29 ka (solid line, Fig. 15B). In contrast, viewing the Tibetan moraine exposure ages in terms of the oldest sample exposure age collected from its surface fundamentally changes the age distribution of moraines (Fig. 15A). Instead of a dominant peak at ~30 ka, the maximum age model shows an age distribution that is highly variable with multiple peaks since 120 ka (at 3-5, 8, 10, (13), 17, (24), 31, 43-49, 66, 96 and (114) for the compilation and at 17, 20, 25, 31, 48, 66 and 95 ka for our data alone). In both cases, varying the scaling model both translates and distorts the specific form of each of the PDFs.

Combining our moraine ages throughout our study area may obscure the spatial pattern of the timing of glaciations, and so we divided our dataset into sub-regions of Tibet and the Himalayas as defined by Owen et al. (2008b): Transhimalaya and western Tibet, the monsoon-influenced Himalaya and the monsoon-influenced Tibet (solid line on Fig. 16) and repeated this analysis.

We present the two scenarios for the distribution of moraine ages in the area in Figs. 15 and 16 for expediency and illustration. As before, we acknowledge that the construction of such a PDF assumes that we have sampled both old and young moraines in a representative manner. In Fig. 16A-C-E-G, we show the PDF that is produced by interpreting the moraine exposure age in terms of the oldest exposure age, using the Lal(1991)/Stone(2000) time-varying scaling model. In Fig. 16B-D-F-H, we considered the mean age of the rock samples on each moraine, calculated using the Lifton et al. (2005) scaling model, to represent each moraine surface's emplacement age.

When considering the oldest exposure age of all samples collected from the moraine crest (dashed line on Fig. 16 A, C, E, and G), we find peaks at 2, 5, 8, 10, 16, (66), 77 and 114 ka for the westernmost orogen; peaks at (2), 7, 13, 17, 38-55, 69, 95 and (114) ka for the Transhimalaya and western Tibet (peaks at 17, 38-42, 48 and 68 ka with just our data); peaks at 3, (5), 16, 24, 42, 50, 62 and 95 ka for the monsoon-influenced Himalaya (peaks at 25, 43 and 95 ka with just our data); and peaks at 20, 31, 49 and 65 ka for the monsoon-influenced Tibet (peaks at (16), 20, 31, 49 and 65 ka with just our data). No moraines <10 ka appear from the monsoon-influenced Tibet, most probably due to a sampling bias because our study presents more moraines > 20 ka, those moraines that are < 20 ka-old are produced from the compiled data. Older peaks in moraine ages are observed at 77 and 114 ka only in the westernmost orogen region, while peaks at 95 ka are observed in both the Transhimalayas and Monsoon-influenced Himalayan regions.

As with data from across the region, interpreting moraine exposure ages in terms of the mean rock sample exposure age on each moraine's surface profoundly changes each of the regional moraine-age PDFs. We find peaks (dashed line on Fig. 16 B, *D*, F and H) at 2, (7), (9), 14, 33 and 66 ka for the westernmost orogen; peaks at (6-8), 13 and 32 ka for the Transhimalaya and western Tibet (peaks at 14 and 29 ka with just our data); peaks at 2, 12, 20, 29 and (61) ka for the monsoon-influenced Himalaya (peaks at 19, 26 and 52 ka with just our data); and peaks at (12), 15, 24 and 28 ka for the monsoon-influenced Tibet (peaks at (12), 15, 24 and 28 ka with just our data). In all areas, we observe a broad peak in the moraine age PDF between ~20-60 ka (20-40 ka in the monsoon-influenced Tibet).

4. Discussion

4.1. Effects of data sampling methodology on moraine surface exposure ages

While in the field, we attempted to collect samples from large boulders that were well seated along the moraine crest. Nonetheless, at some sites, these materials were not available, and yet at others, the crest of the moraine was less distinct. Thus, it is important to acknowledge that while we collected samples that we felt had the highest probability of being unaffected by near-surface

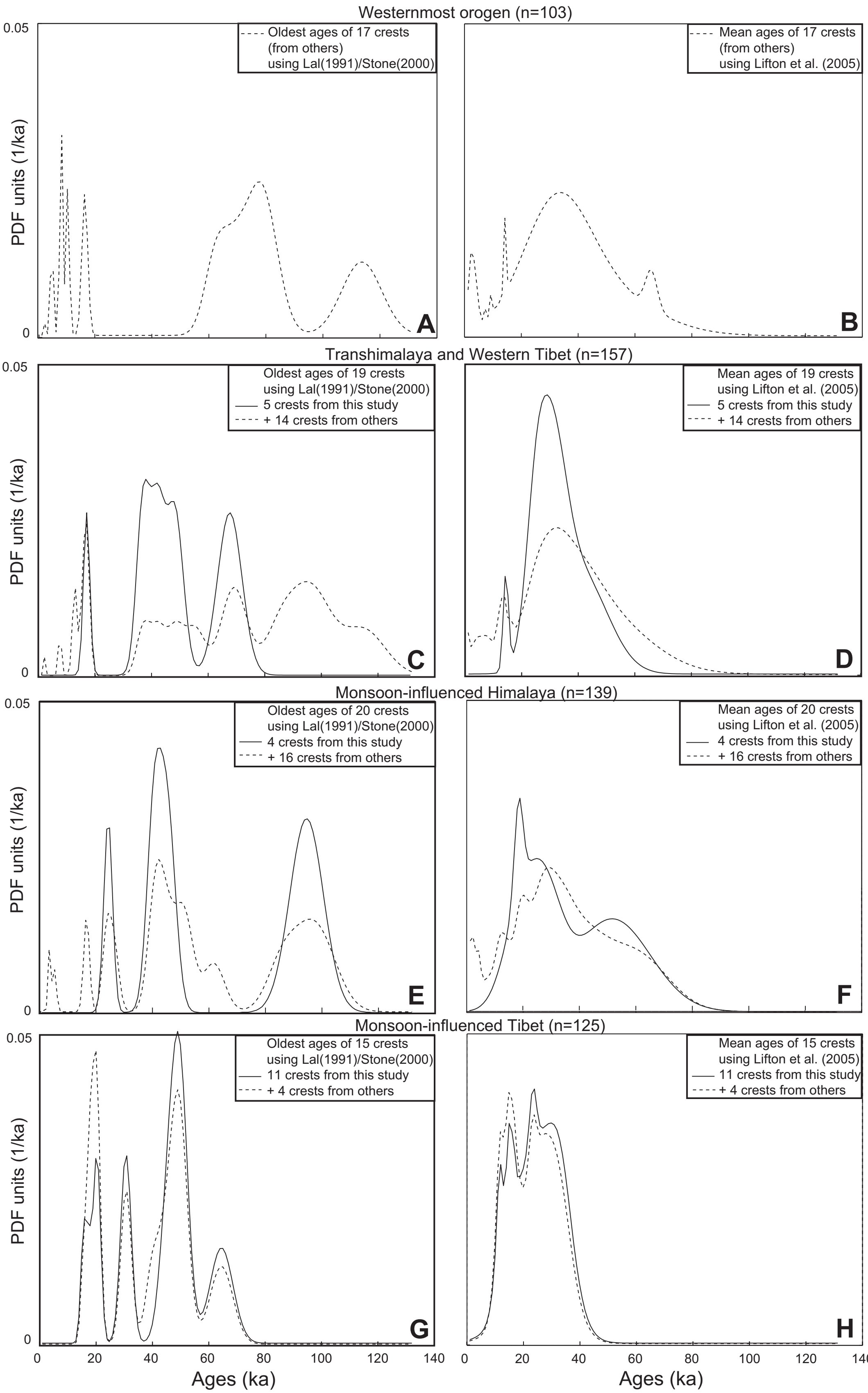

Fig. 16. PDF of moraine ages (<120 ka and with a sufficient number of samples, see text for details) from this study (solid line), and compiled with published studies (dashed line), calculated with the two models. To the left, PDF of oldest ages per moraine crest, using Lal/Stone scaling model, and to the right, PDF of mean ages, using Lifton scaling model. Four different climatic zones are distinguished, as defined in Owen et al. (2008b): Westernmost orogen (panels A and B), Transhimalaya and Western Tibet (panels C and D), monsoon-influenced Himalaya (panels E and F) and monsoon-influenced Tibet (panels G and H).

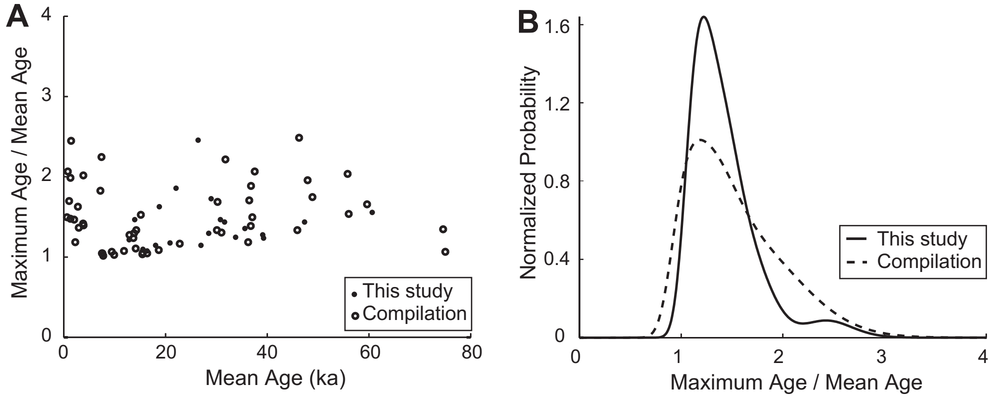

Fig. 17. Compilation of all sample ages reported in Table 2, calculated as for our dataset, using the time-dependent scaling model of Lal/Stone. A) All sampled moraines from Tibet show a comparable range in the ratio of maximum to mean age, regardless of the group that is working there, with our data (closed circles) falling cleanly within this pattern. B) PDF of the maximum to mean age ratio for samples collected by other working groups (dashed line) as well as samples collected as part of this work (solid line). Both visual inspection, as well as a two-sided Student's *T*-test shows that the means of these populations are indistinguishable at the 95% level.

processes, there were certainly sites that were geomorphically more straightforward than others and as such, some of the variation we observe in sample age distributions at individual moraine sites may arise due to local site and sampling conditions. At sites where both cobbles and boulders were analyzed, the ages yielded by these two different populations were indistinguishable (Table S1 and Briner, 2009). This consistency might be interpreted as either an indication that samples from these sites record similar moraine surface processes and/or age of surface establishment, or that our sites were so poorly selected that neither boulder nor cobble ages provide a meaningful estimate of the moraine emplacement age. Below, we provide an assessment of the relative fidelity of our dataset by viewing our results in the context of the larger Tibetan moraine sample age database that spans many working groups across this region to determine if our sampling produced anomalous exposure ages relative to other work reported from this area.

First, we conducted a visual comparison of our sampling sites with those of other working groups in the region (Fig. S32). For most of the moraines analyzed, the visual characteristics of the surfaces we sampled did not appear to be substantively different than those sampled by others. Second, we compiled all sample ages reported for all moraines in this region, and used the CRONUS online calculator to determine sample ages in a manner identical to the methods used for our dataset. We assessed the variation within the sample age distribution by calculating the ratio of the maximum age to the mean age (using the time-dependent scaling model of Lal/Stone) for each moraine sampled by different working groups throughout Tibet (Table 2 and Fig. 17A). Not only does this metric in part quantify the variation in moraine sample ages, but provides a measure of the change in the inferred moraine surface exposure age that is incurred by using the two different interpretive frameworks discussed above. Two important conclusions can be reached by analyzing Fig. 17A: all sampled moraines from Tibet show a comparable range in this ratio, regardless of the group that is working there, with our data (closed circles) falling cleanly within this pattern, and a regression analysis shows that the ratio of maximum to mean age is poorly correlated with increasing mean age. This latter point allows us to create a PDF of the maximum to

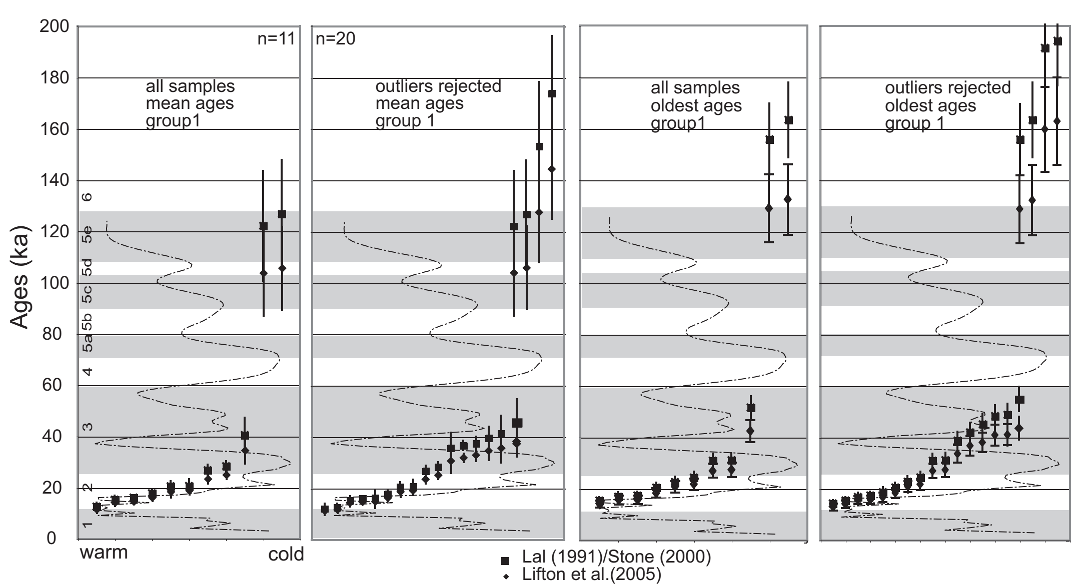

Fig. 18. Moraine ages from group 1 only (1σ uncertainties < 17%), for oldest age and mean age scenario (using both Lal/Stone and Lifton scaling models), before and after rejecting outliers (Table 1), and comparison with the climatic curve (filtered Thompson et al., 1997 curve) and Marine Isotope Stages (Imbrie et al., 1984) (see text for discussion).

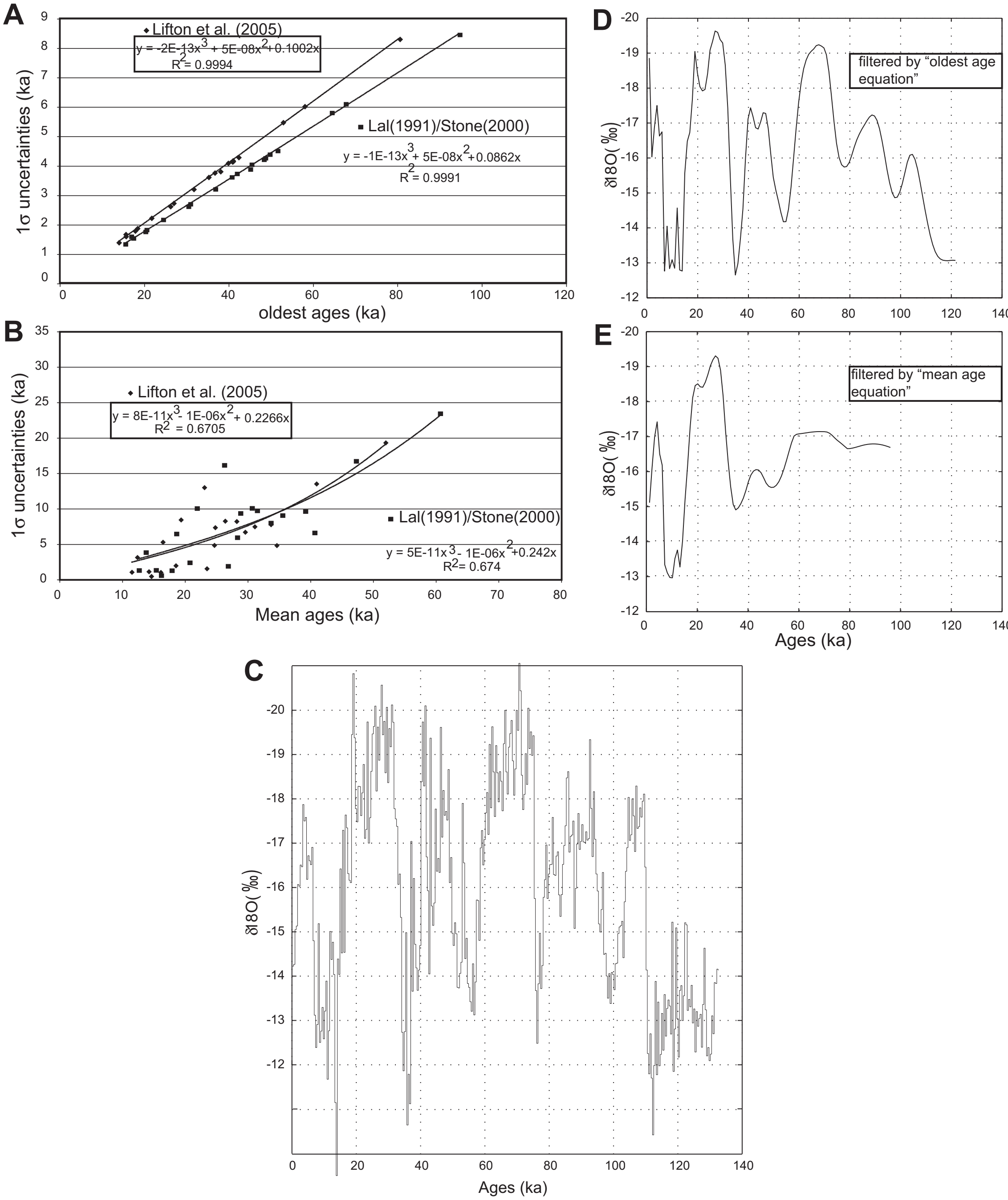

Fig. 19. A and B) 3rd order polynomial (required to pass through the origin) obtained from the 20 oldest (A) or mean (B) moraine ages (<120 ka and with a sufficient number of samples, see text for details) from this study and their 1 σ uncertainties. C) Original $\delta^{18}O$ climate proxy curve from the Guliya ice cap (Thompson et al., 1997). D) Filtered climatic curve with a low-pass filter using the highest uncertainties from oldest ages scaled to model of Lifton. E) Filtered climatic curve with a low-pass filter using the highest uncertainties from mean ages scaled to model of Lifton.

mean age ratio for samples collected by other working groups (dashed line, Fig. 17B) as well as samples collected as part of this work (solid line, Fig. 17B). Both visual inspection, as well as a two-sided Student's *T*-test shows that the means of these populations are indistinguishable at the 95% level. Thus, while on the surface our sample ages appear highly variable and as a result, might lead to the supposition that our sampling was particularly poorly executed, this analysis shows that our data are no more (or no less) variable than all other dated moraines in Tibet. Thus, either sampling has been poorly carried out by all workers from this region (including us), or geological factors such as prior exposure or post-glacial shielding may be important contributors to the observed variation in sample ages from this region.

4.2. Regional climate correlations

The timing of glaciations in Tibet revealed by the exposure age of glacial moraine surfaces has previously been used to infer the spatio-temporal distribution of temperature and precipitation changes in the area (e.g. Finkel et al., 2003; Owen et al., 2005). These types of studies are particularly relevant for testing conceptual models of changes in atmospheric circulation in the vicinity of the high plateau as climate transitions between generally warm and cold periods in Earth's recent (<150 ka) past (e.g. Ruddiman and Kutzbach, 1989; Raymo and Ruddiman, 1992; Benn and Owen, 1998; Lehmkuhl and Haselein, 2000; Aizen et al., 2001; Brown et al., 2003; Abramowski et al., 2006; Harris, 2006). To assess the sensitivity of such interpretations to uncertainties in the scaling model used, or those associated with inferring moraine ages from the distribution of surface sample ages, we compiled all available exposure age sample data from this region and analyzed them in a manner identical to that presented above. These data include a recent compilation of >1000 ^{10}Be moraine ages (Owen et al., 2008b; Heyman et al., 2010) spread out in four climatic zones in the Himalayan-Tibetan orogen (Owen et al., 2008b): 1) the Westernmost orogen (Tibet and Himalaya), 2) the Transhimalaya and Western Tibet region, 3) the monsoon-influenced Himalaya, and 4) the monsoon-influenced Tibet. Following Putkonen and Swanson (2003), we required that a minimum number of samples (at least 5 samples for moraines < 20 ka and at least 6 samples for moraines > 20 ka) be collected and analyzed from each moraine crest to ensure that either the mean or oldest sample age was identified. This criterion eliminates [^{10}Be] reported from samples from moraine surfaces that are presented in a number of studies (e.g. Phillips et al., 2000; Owen et al., 2001, 2002, 2003b,c, 2005, 2006a,b; Brown et al., 2002; Schaefer et al., 2002; Tschudi et al., 2003; Barnard et al., 2004a, 2006; Colgan et al., 2006; Gayer et al., 2006; Heimsath and McGlynn, 2008; Strasky et al., 2009; Zech et al., 2009). The data remaining (Finkel et al., 2003; Owen et al., 2003a, 2009, 2010; Abramowski, 2004, 2006; Barnard et al., 2004b; Meriaux et al., 2004; Chevalier et al., 2005a; Zech et al., 2005a; Seong et al., 2007, 2009; Zhou et al., 2007; Dortch et al., 2010; Hedrick et al., in press) include 51 crests (354 samples) and 20 crests (170 samples) from our study (moraine ages are given in Table 2 and individual sample ages in Tables S1 and S2; locations shown in Fig. 1). Note that four studies have one outlier each and that we took the next oldest age to represent the moraine age (moraine m2 in Barnard et al., 2004b: NDL29; moraine m2i in Seong et al., 2007: K2-83; moraine PM-2 in Hedrick et al., in press: India-13; and moraine T4 in Owen et al., 2009: ron12; italic in Table S2).

The moraine exposure age distribution deduced from the compilation of all moraines <120 ka with a sufficient number of samples is shown as a dashed line in Fig. 15. Overall, the inclusion of additional moraine sites from others gives definition to, but does not change the salient aspects of the PDF determined from our dataset (solid line in Fig. 15). Additionally, when using the oldest sample exposure age to represent the moraine exposure age, inclusion of additional sample sites generally strengthens those peaks in the PDF calculated from only our dataset (solid line in Fig. 15A). Thus, while our data are consistent with those collected by others, the choice of how the exposure age of the moraine is related to the exposure age of samples mantling its surface, plays an important control on determining the first-order structure of the moraine-age PDF from this area.

As with only our data (Fig. 16, solid lines), we subdivided the moraine exposure ages inferred from all samples that have been analyzed in this area according to their geographic region (Fig. 16, dashed lines). As with the moraine exposure age PDF computed from all regions (Fig. 15), the inclusion of additional data strengthens the overall shape and definition of the PDFs determined from our data.

Finally, we consider moraine age distributions that result from a reanalysis of the data after removing additional data outliers as discussed above. Although these results may be less reliable because of the subjective nature of rejecting outliers in the data, it is clear from Fig. 18 (Table 1), that the increase in number of moraines in group 1 ($n = 11$ to $n = 20$) allows identification of moraine age peaks around ~17-25, ~40 and ~100-200 ka, regardless of the scaling model used. These peaks in the moraine age distribution may broadly correspond to the cold periods recognized globally as MIS-2, MIS-3 and MIS-6, respectively (Fig. 18, Marine Isotope Stages of Imbrie et al., 1984).

The δ^{18}O composition of glacial ice varies systematically and inversely with temperature (Yao et al., 1996), and this variation provides a means of assessing the correlation between temperature minima and glacial expansion recorded in the geologic record. Ice core records from Tibet have been collected at the Guliya ice cap in Tibet (Thompson et al., 1997), which contain a record of ~400 year fluctuations in temperature for this region over the last 132 ka (Fig. 19C). Such high frequency features are impossible to resolve given the precision of [^{10}Be] of samples collected from our moraine crests. To provide a rational means of comparing such high-resolution ice cores with our relatively imprecise ages, we considered the two moraine emplacement age scenarios discussed above, and determined how the uncertainties in each moraine exposure age varied with the inferred exposure age of the moraine (Fig. 19). This uncertainty in moraine exposure age sets a lower limit to the wavelength fluctuations in climate that might be inferred using such a chronology. For each scenario, we plot the 1σ uncertainties in the moraine exposure age versus the moraine exposure age (Fig. 19A,B). From this plot, we used a third-order polynomial (that was required to pass through the origin) to determine the uncertainties associated with moraine ages as their age varied. Finally, we applied an adaptive low-pass filter to the δ^{18}O time series (from Thompson et al., 1997) to highlight features of the time-series that

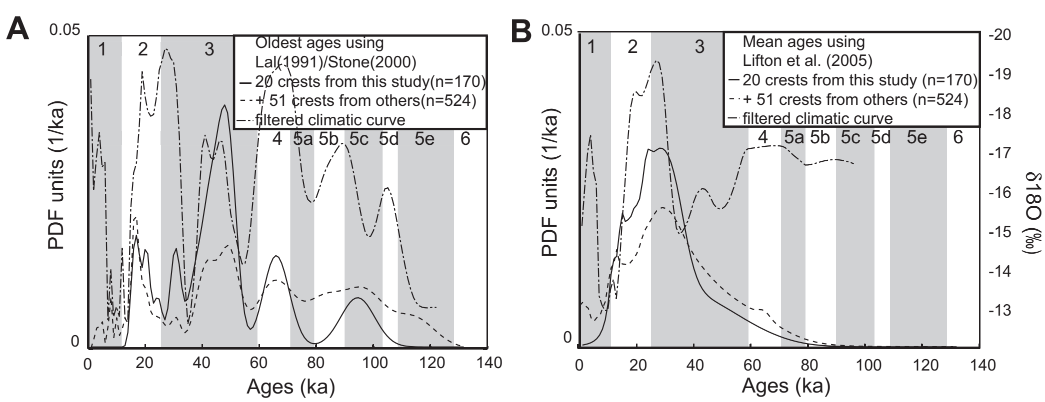

Fig. 20. Same as in Fig. 15 with added filtered climatic curve (dotted-dashed line). Grey-shaded sectors and associated numbers represent Marine Isotope Stages (Imbrie et al., 1984).

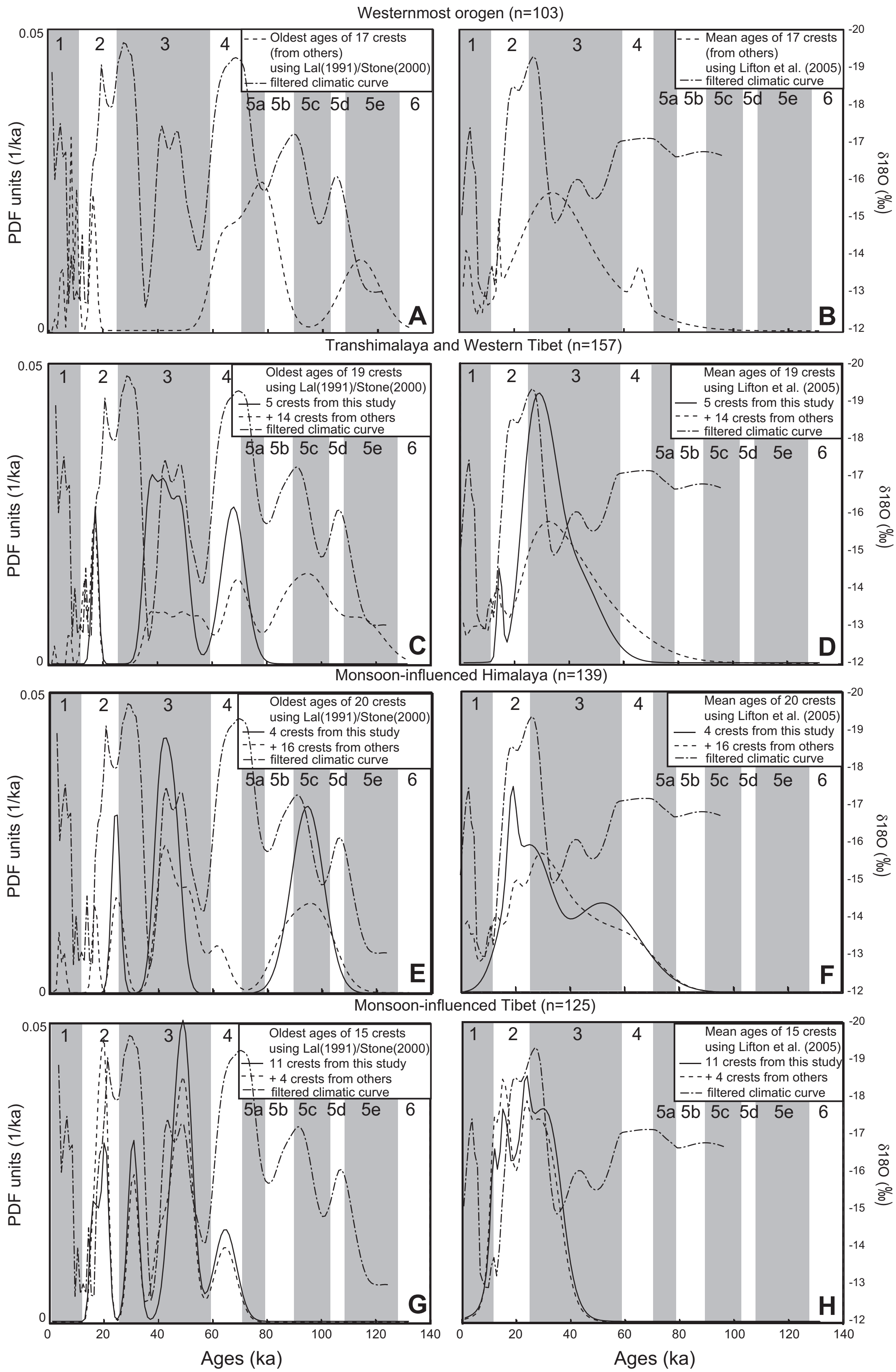

Fig. 21. Same as Fig. 16 with added filtered climatic curve (dotted-dashed line). Grey-shaded sectors and associated numbers represent Marine Isotope Stages (Imbrie et al., 1984).

might be detectable with the cosmogenic moraine ages, supposing that larger amplitude cold periods in climate proxies are associated with increased frequency of moraine emplacements. The cut-off frequency for the low-pass filter was thus allowed to change throughout the time-series such that all frequencies higher than those spanned by the 1σ uncertainties in moraine ages were filtered from the time-series (Fig. 19D,E).

When trying to correlate the moraine emplacement ages with the global climatic curve of Martinson et al. (1987) or with the detailed local climatic curve at the Guliya ice cap of Thompson et al. (1997) (see Fig. S33 for a comparison between the filtered Thompson et al. (1997) and the Martinson et al. (1987) curves), we observe that the correlation of moraine emplacement ages with paleoclimate proxies again changes with both the assumed scaling model, as well as the choice of how to interpret moraine exposure ages in terms of sample exposure ages (Fig. 20). Many peaks in the moraine age PDFs coincide with temperature minima (maximum peaks) recorded by paleoclimate proxies. That is, should the mean age of surface samples represent the moraine emplacement age, moraines in the entire region, and within each sub-region (Fig. 21) may correspond with a broad temperature minimum between ~18-35 ka revealed by the filtered paleoclimate proxy curve (Figs. 20B and 21). However, regarding the oldest sample exposure age as each moraine's age causes ages to approximately align with temperature minima at ~40-50 ka, and to a lesser degree, 18-35 ka (Figs. 20A and 21). Additionally, we find ~ LGM and ~MIS-4 moraines in every region while ~MIS-3 moraines seem to be absent only from the westernmost orogen. This might be due to a sampling bias or to a different climatic system (westerlies or monsoon) occurring in those regions. However, a correlation analysis of these data shows that while these visual trends suggest that such a correlation exists, there are at least as many intervals during which moraine ages are anti-correlated with temperature minima. The net result of this is that both throughout the entire region, as well as within sub-regions of this area, the correlation of moraine exposure ages for the period 15-120 ka and paleoclimate proxies is questionable because it depends on the way in which moraine exposure ages are derived from surface sample ages.

5. Conclusions

We present 249 new ^{10}Be rock sample exposure ages from Tibetan moraines to deduce the timing of moraine emplacement (for information on their extent, see Fig. S34). In interpreting exposure ages of individual rock samples in terms of moraine exposure ages, we considered two main sources of uncertainty: 1) uncertainties within, and variation between, the different scaling models that may be applied to this area, and 2) uncertainties associated with our choice of how to relate these rock sample ages to the emplacement age of the moraine surface. We found that our results were most strongly affected by our choice of whether or not the moraine surface exposure age was best represented by the mean, or oldest sample ages collected from each moraine. In many cases, systematic differences in moraine ages > 50% result from this choice. Secondarily, the choice of the appropriate scaling model (Lifton or Lal/Stone time-dependent) systematically affected moraine surface exposure ages by ~10-20%. When comparing our moraine exposure ages to the timing of temperature minima revealed by independent paleoclimate proxies, we found that the correlation of the timing of moraine emplacement with specific temperature changes depends strongly on these sources of uncertainty. For any given moraine, the choice of the interpretive framework and scaling model can cause the emplacement age to be correlated with a temperature minimum, maximum, or neither of these conditions. On average, moraine emplacement ages revealed by a composite moraine age PDF show some correspondence with temperature mimima, although the changes associated with the different interpretive frameworks suggest that these visual correlations may be coincidental. Furthermore, a correlation analysis suggests that there are at least as many cases in which moraine ages are anti-correlated with temperature minima than are correlated with these paleoclimates, leading to a poor overall correlation.

The consistency of our results with those of others when analyzed in a consistent manner suggests that more samples collected from Tibet may not reveal additional information about the relative importance of temperature mimima versus precipitation maxima (assuming that glacial advances during temperature maxima are driven by increased precipitation) on the emplacement of Tibetan moraines. The large database that we have presented and compiled appears difficult to interpret because of the confounding uncertainties associated with the process of moraine emplacement, degradation and exhumation of rock samples to the moraine surface, as well as uncertainties associated with the appropriate scaling model for this region. To this end, reconstruction of the timing of Tibetan glaciations would foremost benefit from studies that clarify how the exposure age of moraines are related to the ages of rock samples mantling its surface, and secondarily by calibration of ^{10}Be production rates in this area where the age of geomorphic features might be independently determined.

Acknowledgements

This work was performed under the auspices of the European Marie Curie Outgoing International Fellowship, Stanford University, the U.S Department of Energy (University of California, Lawrence Livermore National Laboratory), the Institut National des Sciences et de l'Univers (INSU), Centre National de la Recherche Scientifique (Paris, France), as well as by the China Earthquake Administration and the Ministry of Lands and Resources (Beijing, China). We thank Wen Li and Zhang Pei Quan from the Institute of the Tibetan Plateau, Chinese Academy of Sciences (Beijing, China), for their help in the field. We thank two anonymous reviewers as well as Jakob Heyman for his thorough and constructive comments. The ^{10}Be measurements were performed at the ASTER AMS French national facility (CEREGE, Aix-en-Provence), which is supported by the INSU-CNRS, the French Ministry of Research and Higher Education, IRD and CEA, and at the Center for Accelerator Mass Spectrometry at Lawrence Livermore National Laboratory, USA.

Appendix. Supplementary data

Supplementary data related to this article can be found online at doi:10.1016/j.quascirev.2010.11.005.

References

Abramowski, U., 2004. The use of ^{10}Be surface exposure dating of erratic boulders in the reconstruction of the Late Pleistocene glaciation history of mountainous regions, with examples from Nepal and Central Asia. Dissertation, University of Bayreuth, Bayreuth, 185pp.

Abramowski, U., Bergau, A., Seebach, D., Zech, R., Glaser, B., Sosin, P., Kubik, P.W., Zech, W., 2006. Pleistocene glaciations of Central Asia: results from ^{10}Be surface exposure ages of erratic boulders from the Pamir (Tajikistan) and the Alay-Turkestan range (Kyrgyzstan). Quaternary Science Reviews 25, 1080–1096.

Aizen, E.M., Aizen, V.B., Melack, J.M., Nakamura, T., Ohta, T., 2001. Precipitation and atmospheric circulation patterns at mid-latitudes of Asia. International Journal of Climatology 21, 535–556.

Applegate, P.J., Urban, N.M., Laabs, B.J.C., Keller, K., Alley, R.B., 2010. Modeling the statistical distributions of cosmogenic exposure dates from moraines. Geoscientific Model Development 3, 293–307.

Armijo, R., Tapponnier, P., Mercier, J.L., Han, T., 1986. Quaternary extension in Southern Tibet: field observations and tectonic implications. Journal of Geophysical Research 91, 13803–13872.
Balco, G., Stone, J.O., Lifton, N.A., Dunai, T.J., 2008. A complete and easily accessible means of calculating surface exposure ages or erosion rates from 10Be and 26Al measurements. Quaternary Geochronology. doi:10.1016/j.quageo.2007.12.001.
Barnard, P.L., Owen, L.A., Finkel, R.C., 2004a. Style and timing of glacial and paraglacial sedimentation in a monsoonal influenced high Himalayan environment, the upper Bhagirathi Valley, Garhwal Himalaya. Sedimentary Geology 165, 199–221.
Barnard, P.L., Owen, L.A., Sharma, M.C., Finkel, R.C., 2004b. Late Quaternary landscape evolution of a monsoon-influenced high Himalayan valley, Gori Ganga, Nanda Devi, NE Garhwal. Geomorphology 61, 91–110.
Barnard, P.L., Owen, L.A., Finkel, R.C., Asahi, K., 2006. Landscape response to deglaciation in a high relief, monsoon-influenced alpine environment, Langtang Himal, Nepal. Quaternary Science Reviews 25, 2162–2176.
Barrows, T.T., Lehman, S.J., Fifield, L.K., De Deckker, P., 2007. Absence of Cooling in New Zealand and the adjacent Ocean during the younger Dryas Chronozone. Science 318, 86–89.
Behr, W.M., Rood, D.H., Fletcher, K.E., Guzman, N., Finkel, R.C., Hanks, T.C., Hudnut, K., Kendrick, K.J., Platt, J.P., Sharp, W.D., Weldon, R.J., Yule, J.D., 2009. Uncertainties in slip-rate estimates for the Mission Creek strand of the southern San Andreas fault at Biskra Palms Oasis, southern California. Geological Society of American Bulletin 122 (9/10), 1360–1377. doi:10.1130/B30020.1.
Benn, D., Owen, L.A., 1998. The role of the Indian summer monsoon and the mid-latitude Westerlies in Himalayan glaciation: review and speculative discussion. Geological Society of London Journal 155, 353–363.
Briner, J.P., 2009. Moraine pebbles and boulders yield indistinguishable ^{10}Be ages: a case study from Colorado, USA. Quaternary Geochronology 4. doi:10.1016/j.quageo.2009.02.010.
Briner, J.P., Swanson, T.W., Caffee, M.W., 2001. Late Pleistocene cosmogenic Cl-36 glacial chronology of the southwestern Ahklun mountains, Alaska. Quaternary Research 56, 148–154.
Briner, J.P., Kaufman, D.S., Manley, W.F., Finkel, R.C., 2005. Cosmogenic exposure dating of late Pleistocene moraine stabilization in Alaska. Geological Society of American Bulletin 117, 1108–1120.
Brown, E.T., Edmond, J.M., Raisbeck, G.M., Yiou, F., Kurz, M.D., Brook, E.J., 1991. Examination of surface exposure ages of Antarctic moraines using in situ produced ^{10}Be and ^{26}Al. Geochimica et Cosmochimica Acta 55, 2269–2283.
Brown, E.T., Bendick, R., Bourles, D.L., Gaur, V., Molnar, P., Raisbeck, G.M., Yiou, F., 2002. Slip rates of the Karakorum Fault, Ladakh, India, determined using cosmic ray exposure dating of debris flows and moraines. Journal of Geophysical Research 107 art. no. 2192.
Brown, E.T., Bendick, R., Bourles, D.L., Gaur, V., Molnar, P., Raisbeck, G.M., Yiou, F., 2003. Early Holocene climate recorded in geomorphological features in Western Tibet. Palaeogeography, Palaeoclimatology, Palaeoecology 199, 141–151.
Chevalier, M.-L., Ryerson, F.J., Tapponnier, P., Finkel, R.C., Van Der Woerd, J., Haibing, Li, Qing, Liu, 2005a. Slip-Rate measurements on the Karakorum fault may Imply secular variations in fault Motion. Science 307, 411–414.
Chevalier, M.-L., Ryerson, F.J., Tapponnier, P., Finkel, R.C., Van Der Woerd, J., Haibing, Li, Qing, Liu, 2005b. Response to comment on "Slip-Rate measurements on the Karakorum fault may Imply secular variations in fault Motion". Science 309, 1326c. doi:10.1126/science.1112629.
Colgan, P.M., Munroe, J.S., Zhou, S., 2006. Cosmogenic radionuclide evidence for the limited extent of last glacial maximum glaciers in the Tanggula Shan of the central Tibetan Plateau. Quaternary Research 65, 336–339.
Desilets, D., Zreda, M., 2003. Spatial and temporal distribution of secondary cosmic-ray nucleon intensities and applications to in-situ cosmogenic dating. Earth and Planetary Science Letters 206, 21–42.
Desilets, D., Zreda, M., Prabu, T., 2006. Extended scaling factors for in situ cosmogenic nuclides: new measurements at low latitude. Earth and Planetary Science Letters 246, 265–276.
Dortch, J.M., Owen, L.A., Caffee, M.W., 2010. Quaternary glaciation in the Nubra and Shyok valley confluence, northernmost Ladakh, India. Quaternary Research 74, 132–144.
Dunai, T., 2000. Scaling factors for production rates of in situ produced cosmogenic nuclides: a critical reevaluation. Earth and Planetary Science Letters 176, 157–169.
Dunai, T., 2001. Influence of secular variation of the magnetic field on production rates of in situ produced cosmogenic nuclides. Earth and Planetary Science Letters 193, 197–212.
Finkel, R.C., Owen, L.A., Barnard, P.L., Caffee, M.W., 2003. Beryllium-10 dating of Mount Everest moraines indicates a strong monsoon influence and glacial synchroneity throughout the Himalaya. Geology 31, 561–564.
Gayer, E., Lave, J., Pik, R., France-Lanord, C., 2006. Monsoonal forcing of Holocene glacier fluctuations in Ganesh Himal (Central Nepal) constrained by cosmogenic 3He exposure ages of garnets. Earth and Planetary Science Letters 252, 275–288.
Gillespie, A.R., Molnar, P., 1995. Asynchronous maximum advances of mountain and continental glaciers. Review of Geophysics 33, 311–364.
Gillespie, A.R., Burke, R.M., Komatsu, G., Bayasgalan, A., 2008. Late Pleistocene glaciers in Darhad basin, northern Mongolia. Quaternary Research 69, 169–187.
Gosse, J., Phillips, F., 2001. Terrestrial in situ cosmogenic nuclides: theory and application. Quaternary Science Reviews 20, 1475–1560.
Gosse, J., Klein, J., Evenson, E.B., Lawn, B., Middleton, R., 1995. Beryllium-10 dating of the Duration and retreat of the last Pinedale glacial Sequence. Science 228, 1329–1333.
Hallet, B., Putkonen, J., 1994. Surface dating of dynamic landforms: young boulders on aging moraines. Science 265, 937–940.
Harris, N., 2006. The elevation history of the Tibetan Plateau and its implications for the Asian monsoon. Palaeogeography, Palaeoclimatology. Palaeoecology 241, 4–15.
Hedrick, K. A., Seong, Y. B., Owen, L. A., Caffee, M. W., Dietsch, C. Towards defining the transition in style and timing of Quaternary glaciation between the monsoon-influenced Greater Himalaya and the semi-arid Transhimalaya of Northern India. Quaternary International, in press.
Heimsath, A.M., McGlynn, R., 2008. Quantifying periglacial erosion in the Nepal high Himalaya. Geomorphology 97, 5–23.
Heyman, J., Stroeven, A.P., Harbor, J., Caffee, M.W., 2010. Boulder cosmogenic exposure ages as constraints for glacial chronologies. Geophysical Research Abstracts Vol. 12 EGU2010-14159-1.
Heyman, J., Stroeven, A. P., Harbor, J., Caffee, M. W. Too young or too old: evaluating cosmogenic exposure dating based on an analysis of compiled boulder exposure ages. Earth and Planetary Science letters, in press.
Imbrie, J., Hays, J.D., Martinson, D.G., McIntyre, A., Mix, A.C., Morley, J.J., Pisias, N.G., Prell, W.L., Shackleton, N.J., 1984. The orbital theory of Pleistocene climate: support from a revised chronology of the marine δ^{18} O record. In: Berger, A., Imbrie, J., Hays, J., Kukla, G., Saltzman, B. (Eds.), Milankovitch and Climate: Understanding the Response to Astronomical Forcing. Reidel, Boston, pp. 269–305.
Kohl, C.P., Nishiizumi, K., 1992. Chemical isolation of quartz for measurement of in situ-produced cosmogenic nuclides. Geochimica et Cosmochimica Acta 56, 3583–3587.
Lal, D., 1991. Cosmic ray labeling of erosion surfaces: *in situ* nuclide production rates and erosion models. Earth and Planetary Science Letters 104, 424–439.
Lasserre, C., Gaudemer, Y., Tapponnier, P., Mériaux, A.-S., Van der Woerd, J., Yuan, D., Ryerson, R.J., Caffee, M.W., 2002. Fast late Pleistocene slip rate on the Leng Long Ling segment of the Haiyuan Fault, Qinghai, China. Journal of Geophysical Research 107 (B11), 2276. doi:10.1029/2000JB000060.
Lehmkuhl, F., Haselein, F., 2000. Quaternary paleoenvironmental change on the Tibetan plateau and adjacent areas (Western China and western Mongolia). Quaternary International 65/66, 121–145.
Lifton, N., Bieber, J., Clem, J., Duldig, M., Evenson, P., Humble, J., Pyle, R., 2005. Addressing solar modulation and long-term uncertainties in scaling secondary cosmic rays for in situ cosmogenic nuclide applications. Earth and Planetary Science Letters 239, 140–161.
Liu, Q., 1993. Paleoclimat et contraintes chronologiques sur les mouvements recents dans l'ouest du Tibet: failles du Karakorum et de Longmu Co-Gozha Co, lacs en pull-apart de Longmu Co et de Sumxi Co, Ph.D. thesis Paris 7.
Mahéo, G., Leloup, P.H., Valli, F., Lacassin, R., Arnaud, N., Paquette, J.-L., Fernandez, A., Haibing, Li, Farley, K.A., Tapponnier, P., 2007. Post 4 Ma initiation of normal faulting in southern Tibet. Constraints from the Kung Co half graben. Earth and Planetary Science Letters 256, 233–243.
Martinson, D.G., Pisias, N.G., Hays, J.D., Imbrie, J., Moore, T.C., Shackleton, N.J., 1987. Age dating and the orbital theory of the ice ages: development of a high resolution 0 to 300,000-year chronostratigraphy. Quaternary Research 27, 1–29.
Meriaux, A.-S., Ryerson, F.J., Tapponnier, P., Van der Woerd, J., Finkel, R.C., Xu, Xiwei, Xu, Zhiqin, Caffee, M.W., 2004. Rapid slip along the central Altyn Tagh fault: Morphochronologic evidence from Cherchen He and Sulamu Tagh. Journal of Geophysical Research 109 (B18) art. no. B06,401.
Nishiizumi, K., Winterer, E.L., Kohl, C.P., Lal, D., Arnold, J.R., Klein, J., Middleton, R., 1989. Cosmic ray production rates of ^{10}Be and ^{26}Al in quartz from glacially polished rocks. Journal of Geophysical Research 94 (B12), 17,907–17,915.
Nishiizumi, K., Imamura, M., Caffee, M., Southon, J., Finkel, R., McAnich, J., 2007. Absolute calibration of 10Be AMS standards. Nuclear Instruments and Methods in Physics Research B 258, 403–413.
Owen, L.A., Gualtieri, L., Finkel, R.C., Caffee, M.W., Benn, D.I., Sharma, M.C., 2001. Cosmogenic radionuclide dating of glacial landforms in the Lahul Himalaya, northern India: defining the timing of Late Quaternary glaciation. Journal of Quaternary Science 16, 555–563.
Owen, L.A., Finkel, R.C., Caffee, M.W., Gualtieri, L., 2002. Timing of multiple Late Quaternary glaciations in the Hunza Valley, Karakoram Mountains, northern Pakistan: defined by cosmogenic radionuclide dating of moraines. Geological Society of America Bulletin 114, 593–604.
Owen, L.A., Finkel, R.C., Ma, H., Spencer, J.Q., Derbyshire, E., Barnard, P.L., Caffee, M.W., 2003a. Timing and style of late Quaternary glaciations in NE Tibet. Geological Society of America Bulletin 115, 1356–1364.
Owen, L.A., Ma, H., Derbyshire, E., Spencer, J.Q., Barnard, P.L., Zeng, Y.N., Finkel, R.C., Caffee, M.W., 2003b. The timing and style of Late Quaternary glaciation in the La Ji Mountains, NE Tibet: evidence for restricted glaciation during the latter part of the Last Glacial. Zeitschrift fur Geomorphologie 130, 263–276.
Owen, L.A., Spencer, J.Q., Haizhou, M.A., Barnard, P.L., Derbyshire, E., Finkel, R.C., Caffee, M.W., Zeng, Y.N., 2003c. Timing of late Quaternary glaciation along the southwestern slopes of the Qilian Shan, Tibet. Boreas 32, 281–291.
Owen, L.A., Finkel, R.C., Barnard, P.L., Ma, H., Asahi, K., Caffee, M.W., Derbyshire, E., 2005. Climatic and topographic controls on the style and timing of Late Quaternary glaciation throughout Tibet and the Himalaya defined by ^{10}Be cosmogenic radionuclide surface exposure dating. Quaternary Science Reviews 24 (12–13), 1391–1411.
Owen, L.A., Caffe, M.W., Bovard, K.R., Finkel, R.C., Sharma, M.C., 2006a. Terrestrial cosmogenic nuclide surface exposure dating of the oldest glacial successions in the Himalayan orogen: Ladakh Range, northern India. Geological Society of American Bulletin 118 (3/4), 383–392.

Owen, L.A., Finkel, R.C., Ma, H., Barnard, P.L., 2006b. Late Quaternary landscape evolution in the Kunlun Mountains and Qaidam Basin, Northern Tibet: a framework for examining the links between glaciation, lake level changes and alluvial fan formation. Quaternary International 154/155, 73–86.

Owen, L.A., Caffee, M.W., Finkel, R.C., Seong, Y.B., 2008b. Quaternary glaciation of the Himalayan–Tibetan orogen. Journal of Quaternary Sciences 23, 513–531. ISSN0267-8179.

Owen, L.A., Robinson, R., Benn, D.I., Finkel, R.C., Davis, N.K., Yi, Chaolu, Putkonen, J., Li, Dewen, Murray, A.S., 2009. Quaternary glaciation of Mount Everest. Quaternary Science Reviews 28, 1412–1433. doi:10.1016/j.quascirev.2009.02.010.

Owen, L.A., Yi, Chaolu, Finkel, R.C., Davis, N.K., 2010. Quaternary glaciation of Gurla Mandhata (Naimon'anyi). Quaternary Science Reviews 29, 1817–1830.

Phillips, F.M., Zreda, M.G., Smith, S.S., Elmore, D., Kubik, P.W., Sharma, P., 1990. Cosmogenic Chlorine-36 chronology for glacial deposits at Bloody canyon, eastern Sierra Nevada. Science 248, 1529–1532.

Phillips, F.M., Zreda, M.G., Gosse, J.C., Klein, J., Evenson, E.B., Hall, R.D., Chadwick, O.A., Sharma, P., 1997. Cosmogenic ^{36}Cl and ^{10}Be ages of Quaternary glacial and fluvial deposits of the Wind River range, Wyoming. Geological Society of American Bulletin 109 (11), 1453–1463.

Phillips, W.M., Sloan, V.F., Shroder, J.F., Sharma, P., Clarke, M.L., Rendell, H.M., 2000. Asynchronous glaciation at Nanga Parbat, northwestern Himalaya mountains, Pakistan. Geology 28, 431–434.

Putkonen, J., Swanson, T., 2003. Accuracy of cosmogenic ages for moraines. Quaternary Research 59, 255–261.

Putkonen, J., O'Neal, M.A., 2006. Degradation of unconsolidated Quaternary landforms in the western North America. Geomorphology 75, 408–419.

Raymo, M.E., Ruddiman, W.F., 1992. Tectonic forcing of late Cenozoic climate. Nature 359, 117–124.

Richards, B.W., Owen, L.A., Rhodes, E.J., 2000. Timing of late Quaternary glaciations in the Himalayas of northern Pakistan. Journal of Quaternary Sciences 15, 283–297.

Ruddiman, W.F., Kutzbach, J.E., 1989. Forcing of late Cenozoic northern Hemisphere climate by plateau uplift in southern Asia and the America west. Journal of Geophysical Research 94 (18), 409–427.

Schaefer, J.M., Tschudi, S., Zhao, Z., Wu, X., Ivy-Ochs, S., Wieler, R., Baur, H., Kubik, P.W., Schluchter, C., 2002. The limited influence of glaciations in Tibet on global climate over the past 170000 yr. Earth and Planetary Science Letters 194, 287–297.

Schaefer, J.M., Oberholzer, P., Zhao, Zhizhong, Ivy-Ochs, S., Wieler, R., Baur, H., Kubik, P.W., Schluchter, C., 2008. Cosmogenic beryllium-10 and neon-21 dating of late Pleistocene glaciations in Nyalam, monsoonal Himalayas. Quaternary Science Reviews 27, 295–311.

Schaefer, J.M., Denton, G.H., Kaplan, M., Putnam, A., Finkel, R.C., Barrell, D.J.A., Andersen, B.G., Schwartz, R., Mackintosh, A., Chinn, T., Schluchter, C., 2009. High-Frequency Holocene glacier fluctuations in New Zealand Differ from the northern Signature. Science 324, 622–625.

Seong, Y.B., Owen, L.A., Bishop, M.P., Bush, A., Clendon, P., Copland, P., Finkel, R.C., Kamp, U., Shroder, J.F., 2007. Quaternary glacial history of the Central Karakoram. Quaternary Science Reviews 26, 3384–3405.

Seong, Y.B., Owen, L.A., Yi, C., Finkel, R.C., 2009. Quaternary glaciation of Muztag Ata and Kongur Shan: evidence for glacier response to rapid climate changes throughout the Late-glacial and Holocene in westernmost Tibet. Geological Society of American Bulletin 121, 348–365. doi:10.1130/B26339.1.

Stone, J.O., 2000. Air pressure and cosmogenic isotope production. Journal of Geophysical Research 105, 23,753–23,760.

Strasky, S., Graf, A.A., Zhao, Zhizhong, Kubik, P.W., Baur, H., Schlüchter, C., Wieler, R., 2009. Late Glacial ice advances in southeast Tibet. Journal of Asian Earth Sciences 34, 458–465.

Thompson, L.G., Yao, T., Davis, M.E., Henderson, K.A., Mosley-Thompson, E., Lin, P.-N., Beer, J., Synal, H.-A., Cole-Dai, J., Bolzan, J.F., 1997. Tropical climate Instability: the last glacial Cycle from a Qinghai-Tibetan ice core. Science 276, 1821–1825.

Tschudi, S., Schaefer, J.M., Zhao, Zhizong, Wu, Xihao, Ivy-Ochs, S., Kubik, P.W., Schluchter, C., 2003. Glacial advances in Tibet during the younger Dryas? Evidence from cosmogenic ^{10}Be, ^{26}Al, and ^{21}Ne. Journal of Asian Earth Sciences 22, 301–306.

Van Der Woerd, J., Tapponnier, P., Ryerson, F.J., Mériaux, A.S., Meyer, B., Gaudemer, Y., Finkel, R.C., Caffee, M.W., Guoguang, Z., Zhiqin, Xu, 2002. Uniform postglacial slip-rate along the central 600km of the Kunlun Fault (Tibet), from ^{26}Al, ^{10}Be, and ^{14}C dating of riser offsets, and climatic origin of the regional morphology. Geophysical Journal International 148, 356–388.

Yao, T., Thompson, L.G., Mosley-Thompson, E., Zhihong, Y., Xingping, Z., Lin, P.-N., 1996. Climatological significance of δ^{18}O in north Tibetan ice cores. Journal of Geophysical Research 101 (D23), 29,531–29,537.

Zech, R., Abramowski, U., Glaser, B., Sosin, P., Kubik, P.W., Zech, W., 2005a. Late Quaternary glacier and climate history of the Pamir Mountains derived from cosmogenic ^{10}Be exposure ages. Quaternary Research 64, 212–220.

Zech, R., May, J.H., Kull, C., Ilgner, J., Kubik, P.W., Veit, H., 2008. Timing of the late Quaternary glaciation in the Andes from $\sim$15 to 40S. Journal of Quaternary Sciences 23 (6–7), 635–647.

Zech, R., Zech, M., Kubik, P.W., Kharki, K., Zech, W., 2009. Deglaciation and landscape history around Annapurna, Nepal, based on ^{10}Be surface exposure dating. Quaternary Science Reviews 28, 1106–1118. doi:10.1016/j.quascirev.2008.11.013.

Zhou, ShangZhe, LiuBing, Xu, Colgan, P.M., Mickelson, D.M., XiaoLi, Wang, Jie, Wang, Wei, Zhong, 2007. Cosmogenic ^{10}Be dating of Guxiang and Baiyu glaciations. Chinese Science Bulletin 52, 1387–1393.

Zreda, M.G., Phillips, F.M., 1995. Insights into alpine moraine development from cosmogenic ^{36}Cl buildup dating. Geomorphology 14, 149–156. doi:10.1016/0169-555X(95)00055-9.

Zreda, M.G., Phillips, F.M., Elmore, D., 1994. Cosmogenic ^{36}Cl accumulation in unstable landforms: 2. Simulations and observations on eroding moraines. Water Resources Research 30 (11), 3127–3136. doi:10.1029/94WR00760.

Table S1: Analytical results of ^{10}Be geochronology and surface exposure ages from our study.

	Sample	Lat (N)	Long (E)	Elev (m)	Thick. (cm)	quartz./ granite	boulder/ cobble	shielding factor	^{10}Be [a] (10^6 at/g)	standard used [h]	Lal/Stone time indep Ages (ka) [a]	Desilets Ages (ka) [a]	Dunai Ages (ka) [a]	Lifton Ages (ka) [a]	Lal/Stone time-dep Ages (ka) [a]
1a: Gulu W	T5C-58	30,81	91,56	5003	4	g	b	0,99	1.227±0.024	07KNSTD	15,851±1,418	14,552±1,747	15,041±1,798	14,004±1,413	15,486±1,346
	T5C-59	30,81	91,56	5003	4	g	b	0,99	1.252±0.024	07KNSTD	16,167±1,446	14,809±1,777	15,283±1,826	14,244±1,437	15,768±1,371
	T5C-60	30,81	91,56	4995	4	g	b	1	1.297±0.023	07KNSTD	16,757±1,493	15,285±1,831	15,74±1,877	14,697±1,478	16,292±1,41
	T5C-61	30,81	91,56	4988	4	g	b	1	1.21±0.025	07KNSTD	15,674±1,405	14,419±1,732	14,913±1,784	13,875±1,402	15,328±1,335
	T5C-62	30,81	91,56	4991	4	g	b	1	1.298±0.037	07KNSTD	16,803±1,545	15,325±1,868	15,779±1,916	14,736±1,52	16,333±1,462
	T5C-63	30,81	91,56	4991	4	g	b	1	1.358±0.034	07KNSTD	17,587±1,598	15,941±1,93	16,372±1,974	15,319±1,564	17,026±1,504
	T5C-64	**30,81**	**91,56**	**4987**	**4**	**g**	**b**	**0,99**	**1.393±0.035**	**07KNSTD**	**18,081±1,645**	**16,328±1,979**	**16,747±2,021**	**15,685±1,604**	**17,464±1,546**
1b: Gulu E	**T5C-66**	**30,81**	**91,56**	**4874**	**4**	**g**	**b**	**1**	**1.584±0.04**	**07KNSTD**	**21,603±1,966**	**19,186±2,326**	**19,537±2,358**	**18,355±1,877**	**20,59±1,822**
	T5C-67	30,81	91,56	4874	4	g	b	1	1.364±0.034	07KNSTD	18,586±1,69	16,811±2,036	17,226±2,078	16,148±1,65	17,91±1,584
	T5C-68	30,81	91,57	4858	4	g	b	1	1.32±0.035	07KNSTD	18,124±1,657	16,461±2	16,887±2,043	15,821±1,624	17,499±1,556
	T5C-69	30,81	91,57	4840	4	g	b	1	1.294±0.032	07KNSTD	17,908±1,627	16,307±1,975	16,738±2,018	15,676±1,601	17,308±1,53
	T5C-70	30,81	91,57	4860	4	g	b	1	1.3±0.04	07KNSTD	17,823±1,652	16,225±1,987	16,658±2,032	15,597±1,619	17,233±1,556
	T5C-71	30,81	91,56	4876	4	g	b	1	1.512±0.047	07KNSTD	20,616±1,914	18,404±2,256	18,779±2,293	17,628±1,832	19,717±1,782
	T5C-72	30,81	91,56	4869	4	g	b	1	1.219±0.03	07KNSTD	16,659±1,514	15,297±1,852	15,762±1,9	14,719±1,504	16,203±1,432
	T5C-73	30,81	91,56	4855	4	g	b	1	1.273±0.031	07KNSTD	17,515±1,588	15,987±1,933	16,427±1,978	15,373±1,567	16,96±1,495
2b: ybj inner	T5C-19	30,02	90,24	5305	4	q	b	1	0.947±0.026	07KNSTD	11,044±1,009	10,295±1,25	10,824±1,309	9,991±1,025	10,874±0,967
	T5C-20	30,02	90,24	5302	4	g	b	1	1.135±0.023	07KNSTD	13,252±1,188	12,22±1,468	12,745±1,525	11,763±1,189	13,044±1,137
	T5C-21	30,02	90,24	5302	4	g	b	1	0.904±0.018	07KNSTD	10,558±0,945	9,88±1,186	10,41±1,244	9,607±0,97	10,401±0,905
	T5C-22	**30,02**	**90,24**	**5295**	**4**	**q**	**b**	**1**	**1.821±0.032**	**07KNSTD**	**21,373±1,905**	**18,664±2,236**	**18,999±2,267**	**17,82±1,793**	**20,316±1,759**
	T5C-23	30,02	90,24	5287	4	g	b	1	1.248±0.025	07KNSTD	14,678±1,315	13,445±1,615	13,952±1,668	12,925±1,305	14,384±1,252
2a: ybj outer W	T5C-25	30,02	90,24	5276	4	g	b	0,98	2.881±0.052	07KNSTD	34,463±3,085	28,113±3,378	28,014±3,351	26,742±2,699	31,104±2,703
	T5C-26	30,02	90,24	5258	4	g	b	0,98	2.344±0.042	07KNSTD	28,216±2,523	23,753±2,851	23,874±2,853	22,636±2,282	26,094±2,265
	T5C-27	30,02	90,24	5248	4	q	b	0,98	1.912±0.037	07KNSTD	23,085±2,067	20,021±2,405	20,32±2,43	19,09±1,927	21,797±1,896
	T5C-28	30,02	90,24	5227	4	g	b	0,99	2.711±0.07	07KNSTD	32,977±3,014	27,184±3,304	27,152±3,286	25,838±2,651	29,907±2,657
	T5C-29	30,02	90,24	5221	4	g	b	1	3.202±0.074	07KNSTD	38,979±3,54	31,212±3,781	30,929±3,73	29,618±3,022	34,66±3,057
	T5C-30	**30,02**	**90,24**	**5206**	**4**	**g**	**b**	**1**	**4.812±0.103**	**07KNSTD**	**59,271±5,383**	**43,247±5,24**	**42,211±5,091**	**40,986±4,178**	**49,757±4,383**
	T5C-31	30,02	90,24	5200	4	g	b	1	1.587±0.03	07KNSTD	19,414±1,737	17,235±2,069	17,616±2,105	16,509±1,666	18,585±1,615
	T5C-32	30,02	90,24	5200	4	g	b	1	1.457±0.026	07KNSTD	17,806±1,587	16,003±1,917	16,418±1,958	15,356±1,545	17,165±1,487
	T5C-33	30,02	90,24	5184	4	g	b	1	2.289±0.041	07KNSTD	28,254±2,526	23,862±2,865	23,992±2,867	22,746±2,293	26,123±2,268
	T5C-34	30,02	90,24	5177	4	g	b	1	2.987±0.053	07KNSTD	37,061±3,316	29,977±3,602	29,778±3,562	28,5±2,875	33,168±2,881
2c: ybj outer E	T5C-35	30,02	90,25	5034	4	g	b	1	1.485±0.026	07KNSTD	19,546±1,743	17,468±2,093	17,863±2,131	16,74±1,685	18,698±1,62
	T5C-36	30,02	90,25	5033	4	g	b	1	3.903±0.083	07KNSTD	51,806±4,696	39,326±4,76	38,668±4,659	37,499±3,818	43,556±3,83
	T5C-37	30,02	90,25	5066	4	g	b	0,99	3.624±0.064	07KNSTD	47,221±4,237	36,71±4,418	36,194±4,337	34,991±3,536	40,331±3,51
	T5C-38	30,02	90,25	5026	4	g	b	0,99	4.35±0.075	07KNSTD	57,855±5,198	42,818±5,158	41,9±5,024	40,649±4,109	48,461±4,22
	T5C-39	30,02	90,25	5021	4	g	b	0,99	3.081±0.054	07KNSTD	40,896±3,664	32,83±3,947	32,503±3,891	31,166±3,146	36,056±3,134
	T5C-40	30,02	90,25	5014	4	q	b	0,99	3.504±0.066	07KNSTD	46,725±4,202	36,518±4,401	36,027±4,322	34,795±3,522	39,996±3,489
	T5C-41	30,02	90,25	5010	4	g	b	0,99	3.719±0.065	07KNSTD	49,729±4,462	38,197±4,597	37,623±4,507	36,472±3,685	42,047±3,658
	T5C-42	**30,02**	**90,25**	**4999**	**4**	**g**	**b**	**0,99**	**4.321±0.08**	**07KNSTD**	**58,175±5,243**	**43,078±5,198**	**42,145±5,062**	**40,873±4,142**	**48,748±4,259**
	T5C-43	30,02	90,25	4991	4	g	b	1	2.163±0.031	07KNSTD	29,093±2,581	24,699±2,953	24,829±2,955	23,533±2,359	26,808±2,309
	T5C-44	30,02	90,25	4982	4	g	b	0,99	4.112±0.108	07KNSTD	56,082±5,163	41,861±5,111	41,055±4,99	39,821±4,104	46,921±4,193
2d:** ybj outer N	T5C-44bis	30,02	90,25	5239	4	g	b	0,99	2.105±0.113	07KNSTD	25,417±2,612	21,782±2,837	22,013±2,857	20,755±2,342	23,74±2,386
	T5C-45	30,02	90,24	5261	4	g	b	0,99	1.073±0.032	07KNSTD	12,793±1,182	11,838±1,446	12,375±1,506	11,407±1,18	12,597±1,133
3a:** M4 #1	T7C-7	30,66	88,56	5232	4	q	c	1	5.45±0.064	07KNSTD	64,707±5,765	46,929±5,627	45,391±5,416	44,081±4,425	55,571±4,796
	T7C-11	**30,67**	**88,55**	**5280**	**4**	**g**	**b**	**1**	**11.85±0.09**	**07KNSTD**	**140,405±12,682**	**101,171±12,262**	**97,958±11,809**	**95,497±9,669**	**116,367±10,139**
	T7C-15	30,65	88,56	5096	4	g	b	1	4.252±0.052	07KNSTD	53,466±4,754	40,261±4,821	39,471±4,705	38,349±3,846	45,088±3,884
	T7C-17	30,65	88,56	5101	4	g	c	1	7.523±0.091	07KNSTD	95,379±8,567	71,05±8,573	68,767±8,256	66,538±6,719	81,966±7,124
	T7C-18	30,65	88,56	5102	4	q	b	1	3.449±0.047	07KNSTD	43,15±3,836	34,26±4,102	33,767±4,024	32,532±3,264	37,741±3,253
3b:** M4 #2	T7C-14	30,66	88,55	5231	4	g	b	1	10.217±0.091	07KNSTD	123,137±11,09	90,918±10,999	87,78±10,564	84,716±8,564	103,725±9,023
3c:** M4 #3	T7C-12	30,67	88,55	5283	4	q	b	1	7.089±0.06	07KNSTD	82,66±7,366	61,522±7,386	59,621±7,123	57,244±5,745	70,932±6,117
4c*: M3 old	T7C-19	30,6	88,53	4988	4	g	b	1	19.64±0.25	07KNSTD	274,269±25,806	193,067±24,039	186,541±23,084	182,31±18,969	224,294±20,231
	T7C-20	30,6	88,53	4988	4	g	c	1	30.053±0.29	07KNSTD	436,537±42,633	305,263±39,016	290,614±36,838	282,908±30,095	359,361±33,395
	T7C-21	30,6	88,53	4989	4	g	b	1	27.252±0.244	07KNSTD	391,394±37,748	275,093±34,873	263,881±33,206	255,992±27,027	320,194±29,431
	T7C-22	**30,6**	**88,53**	**4990**	**4**	**g**	**b**	**1**	**44.44±0.304**	**07KNSTD**	**684,136±71,067**	**486,648±65,072**	**463,478±61,325**	**447,554±49,554**	**561,669±54,831**
	T7C-23	30,6	88,53	4993	4	g	b	1	14.691±0.153	07KNSTD	201,077±18,505	142,42±17,473	135,349±16,502	132,033±13,527	167,11±14,801
4a: M3 main	**T7C-24-24bis**	**30,6**	**88,52**	**5036**	**4**	**g**	**c**	**1**	**4.451±0.065 and 4.689±0.083**	**07KNSTD**	**59.157±4.476**	**43.788±4.441**	**42.728±4.311**	**41.488±3.528**	**50.025±3.671**
	T7C-25	30,6	88,52	5041	4	g	b	1	3.206±0.048	07KNSTD	41,295±3,679	33,136±3,972	32,725±3,905	31,472±3,163	36,47±3,152
	T7C-26	30,6	88,52	5042	4	g	b	1	3.238±0.038	07KNSTD	41,69±3,693	33,399±3,991	32,974±3,922	31,72±3,174	36,741±3,156
	T7C-27	30,6	88,52	5051	4	g	b	1	3.487±0.052	07KNSTD	44,749±3,99	35,365±4,242	34,844±4,16	33,626±3,382	38,815±3,356
	T7C-28	30,6	88,52	5056	4	g	b	1	2.963±0.043	07KNSTD	37,872±3,367	30,781±3,685	30,505±3,636	29,262±2,937	33,943±2,928
	T7C-30	30,6	88,52	5086	4	g	b	1	3.458±0.038	07KNSTD	43,667±3,866	34,623±4,136	34,122±4,058	32,885±3,289	38,076±3,268
4b: M3 inner	**T7C-32**	**30,61**	**88,5**	**5254**	**4**	**g**	**b**	**1**	**1.368±0.019**	**07KNSTD**	**15,934±1,408**	**14,526±1,731**	**14,973±1,777**	**13,963±1,395**	**15,55±1,334**
	T7C-33	30,61	88,5	5238	4	g	b	1	0.975±0.021	07KNSTD	11,418±1,026	10,682±1,285	11,198±1,341	10,353±1,049	11,262±0,984
	T7C-34	30,61	88,5	5243	4	g	b	1	0.992±0.016	07KNSTD	11,593±1,028	10,831±1,293	11,345±1,349	10,49±1,051	11,433±0,985
	T7C-35	30,61	88,5	5209	4	g	b	1	1.102±0.018	07KNSTD	13,085±1,161	12,159±1,452	12,675±1,507	11,715±1,174	12,907±1,112
	T7C-36	30,61	88,5	5200	4	g	b	1	1.008±0.023	07KNSTD	12,008±1,083	11,211±1,351	11,738±1,409	10,845±1,101	11,85±1,039
	T7C-37	30,61	88,5	5207	4	g	b	1	1.064±0.024	07KNSTD	12,638±1,14	11,763±1,418	12,29±1,476	11,347±1,153	12,471±1,094
	T7C-39	30,61	88,5	5179	4	g	b	1	1.14±0.022	07KNSTD	13,715±1,225	12,721±1,525	13,231±1,58	12,253±1,235	13,509±1,173
5: M2	T7C-40	30,08	88,43	5337	4	g	b	1	4.279±0.047	07KNSTD	49,52±4,391	37,572±4,492	36,925±4,394	35,84±3,587	41,917±3,601
	T7C-41	30,08	88,43	5337	4	g	b	1	3.848±0.049	07KNSTD	44,478±3,949	34,693±4,151	34,158±4,068	32,903±3,297	38,483±3,313
	T7C-42	30,08	88,42	5334	4	g	b	1	2.942±0.036	07KNSTD	33,957±3,005	27,754±3,314	27,647±3,286	26,391±2,639	30,709±2,636
	T7C-43	30,08	88,42	5337	4	g	b	1	1.34±0.02	07KNSTD	15,381±1,362	14,048±1,676	14,499±1,723	13,489±1,35	15,028±1,293
	T7C-44	30,08	88,42	5341	4	g	b	1	3.713±0.061	07KNSTD	42,822±3,827	33,628±4,038	33,146±3,962	31,879±3,211	37,377±3,24
	T7C-45	30,08	88,42	5340	4	g	b	1	1.911±0.024	07KNSTD	21,942±1,937	19,11±2,277	19,406±2,303	18,234±1,821	20,819±1,784
	T7C-46	**30,08**	**88,42**	**5322**	**4**	**g**	**b**	**1**	**4.622±0.046**	**07KNSTD**	**53,89±4,777**	**40,002±4,782**	**39,187±4,662**	**38,075±3,809**	**45,163±3,877**
	T7C-47	30,08	88,42	5314	4	g	b	1	3.101±0.031	07KNSTD	36,127±3,188	29,208±3,482	29,007±3,442	27,789±2,773	32,443±2,777
	T7C-49	30,08	88,42	5291	4	g	b	1	1.329±0.019	07KNSTD	15,565±1,376	14,223±1,696	14,675±1,742	13,663±1,366	15,19±1,304
	T7C-50	30,08	88,42	5273	4	g	b	1	2.985±0.038	07KNSTD	35,383±3,134	28,772±3,437	28,615±3,403	27,385±2,741	31,849±2,737
	T7C-51	30,08	88,41	5253	4	g	b	1	2.595±0.036	07KNSTD	30,998±2,748	25,816±3,085	25,833±3,073	24,529±2,457	28,346±2,439
6: M1	T7C-63	29,94	88,35	5170	4	g	b	1	2.223±0.028	07KNSTD	27,637±2,443	23,494±2,803	23,636±2,807	22,405±2,239	25,595±2,195
	T7C-64	29,94	88,35	5161	4	g	b	1	2.094±0.028	07KNSTD	26,124±2,312	22,426±2,677	22,622±2,688	21,386±2,139	24,32±2,089
	T7C-65	29,94	88,35	5167	4	g	b	1	2.363±0.033	07KNSTD	29,424±2,608	24,782±2,961	24,869±2,959	23,59±2,363	27,075±2,33
	T7C-66	29,94	88,35	5161	4	g	b	1	2.276±0.054	07KNSTD	28,414±2,577	24,057±2,911	24,176±2,913	22,932±2,339	26,246±2,314
	T7C-68	29,94	88,35	5140	4	g	b	1	2.402±0.03	07KNSTD	30,283±2,678	25,442±3,036	25,508±3,031	24,193±2,419	27,759±2,382
	T7C-69	29,94	88,35	5130	4	g	b	1	2.398±0.067	07KNSTD	30,36±2,793	25,511±3,112	25,576±3,107	24,259±2,501	27,821±2,489
	T7C-70	29,94	88,35	5120	4	g	b	1	2.045±0.025	07KNSTD	25,982±2,295	22,366±2,667	22,572±2,68	21,333±2,131	24,199±2,075
	T7C-71	29,94	88,35	5110	4	g	b	1	2.368±0.061	07KNSTD	30,248±2,764	25,454±3,094	25,525±3,089	24,208±2,483	27,73±2,464
	T7C-72	**29,94**	**88,36**	**5070**	**4**	**g**	**b**	**1**	**2.634±0.052**	**07KNSTD**	**34,287±3,081**	**28,324±3,411**	**28,251±3,387**	**26,98±2,731**	**30,945±2,7**
7: M	T7C-55	29,82	88,19	5340	4	g	b	1	1.052±0.017	07KNSTD	12,125±1,075	11,258±1,344	11,773±1,4	10,882±1,09	11,943±1,029
	T7C-56	29,82	88,19	5345	4	g	b	1	2.279±0.043	07KNSTD	26,287±2,353	22,36±2,686	22,533±2,695	21,301±2,15	24,457±2,126
	T7C-57	29,82	88,19	5350	4	g	b	1	1.404±0.024	07KNSTD	16,126±1,435	14,645±1,752	15,082±1,797	14,065±1,413	15,687±1,356
	T7C-58	29,82	88,19	5355	4	g	b	1	1.307±0.03	07KNSTD	14,97±1,352	13,704±1,653	14,174±1,703	13,165±1,338	14,651±1,286
	T7C-59	**29,82**	**88,19**	**5360**	**4**	**g**	**b**	**1**	**2.938±0.033**	**07KNSTD**	**33,739±2,98**	**27,583±3,29**	**27,5±3,265**	**26,214±2,618**	**30,502±2,614**
	T7C-60	29,82	88,19	5355	4	g	b	1	1.295±0.04	07KNSTD	14,837±1,373	13,592±1,663	14,069±1,714	13,061±1,354	14,529±1,309
	T7C-61	29,82	88,19	5350	4	g	b	1	1.717±0.025	07KNSTD	19,736±1,748	17,421±2,079	17,767±2,112	16,67±1,669	18,869±1,623
	T7C-62	*29,83*	*88,2*	*5320*	*4*	*g*	b	*1*	*6.199±0.068*	*07KNSTD*	*73,115±6,521*	*53,395±6,409*	*51,204±6,115*	*49,1±4,93*	*62,709±5,415*
8*: Dingye N	T5C-141	28,32	87,72	5071	5	q	c	0,99	1.363±0.033	07KNSTD	18,332±1,664	16,553±2,003	16,992±2,047	15,881±1,62	17,628±1,556
	T5C-142	28,32	87,72	5061	3	q	c	0,99	3.566±0.115	07KNSTD	47,707±4,474	36,933±4,557	36,546±4,49	35,197±3,683	40,365±3,681
	T5C-143	28,32	87,72	5043	2	q	c	0,99	2.664±0.067	07KNSTD	35,514±3,241	29,145±3,54	29,155±3,526	27,733±2,841	31,785±2,819
	T5C-144	28,32	87,72	5018	2	q	c	0,99	2.42±0.059	07KNSTD	32,595±2,965	27,229±3,301	27,351±3,302	25,884±2,645	29,482±2,606
	T5C-146	28,32	87,73	4960	3	g	c	0,99	5.225±0.134	07KNSTD	73,558±6,786	54,975±6,726	53,303±6,491	50,458±5,204	62,652±5,607
	T5C-147	28,32	87,73	4937	5	q	c	0,99	3.454±0.162	07KNSTD	49,657±4,969	38,2±4,898	37,776±4,824	36,477±4,022	41,681±4,067
	T5C-148	28,32	87,73	4907	6	q	c	0,99	4.468±0.112	07KNSTD	65,91±6,061	48,438±5,912	47,079±5,719	45,23±4,654	55,84±4,982
	T5C-149	28,32	87,73	4864	4	q	c	0,99	10.871±0.266	07KNSTD	164,784±15,502	117,624±14,591	114,117±14,082	110,479±11,537	132,877±12,06
	T5C-150	28,32	87,73	4835	3	q	c	0,99	9.223±0.267	07KNSTD	139,598±13,238	102,596±12,782	100,234±12,427	96,846±10,194	114,055±10,46
	T5C-151	28,32	87,73	4812	4	q	c	0,99	8.489±0.227	07KNSTD	130,631±12,268	97,506±12,081	95,465±11,772	91,675±9,58	107,674±9,782
	T5C-152	28,32	87,73	4773	3	q	c	0,99	13.439±0.423	07KNSTD	213,03±20,768	152,799±19,379	146,719±18,501	140,495±15,059	174,421±16,397
	T5C-153	**28,32**	**87,73**	**4741**	**4**	**q**	**b**	**0,99**	**21.24±0.295**	**07KNSTD**	**356,795±34,36**	**254,68±32,248**	**245,03±30,812**	**234,071±24,718**	**287,44±26,406**
	T5C-154	28,32	87,73	4727	3	q	b	0,99	6.736±0.118	07KNSTD	106,214±9,667	80,702±9,818	78,739±9,532	75,07±7,659	90,024±7,928
	T5C-155	28,32	87,74	4696	5	q	c	0,99	3.475±0.088	07KNSTD	55,814±5,125	42,181±5,143	41,548±5,043	40,135±4,128	46,291±4,124
9b:** Dingye S main #1	**T5C-115**	**28,15**	**87,65**	**5254**	**4**	**g**	**b**	**0,96**	**2.192±0.056**	**07KNSTD**	**27,855±2,54**	**23,545±2,857**	**23,773±2,873**	**22,42±2,296**	**25,7±2,278**
	T5C-116	28,15	87,65	5247	4	q	c	0,96	1.393±0.035	07KNSTD	17,746±1,614	15,973±1,935	16,404±1,978	15,32±1,566	17,111±1,513
	T5C-118	28,15	87,65	5250	4	q	b	0,96	0.928±0.028	07KNSTD	11,793±1,09	10,994±1,343	11,509±1,401	10,647±1,102	11,617±1,045
	T5C-119	28,15	87,65	5254	4	q	c	0,96	1.295±0.036	07KNSTD	16,445±1,508	14,958±1,82	15,411±1,868	14,357±1,477	15,977±1,426
9c: Dingye S main #2	T5C-121	28,15	87,65	5223	4	q	c	0,99	1.576±0.065	07KNSTD	19,697±1,905	17,484±2,195	17,894±2,237	16,729±1,796	18,824±1,776
	T5C-122	28,15	87,65	5225	4	q	c	0,99	2.194±0.055	07KNSTD	27,45±2,501	23,291±2,825	23,535±2,843	22,186±2,27	25,362±2,246
	T5C-123	28,15	87,65	5220	4	q	b	0,99	1.295±0.032	07KNSTD	16,199±1,469	14,782±1,788	15,248±1,836	14,197±1,448	15,76±1,39
	T5C-124	28,15	87,65	5216	5	q	c	0,99	1.02±0.03	07KNSTD	12,879±1,187	11,979±1,462	12,503±1,519	11,541±1,192	12,694±1,139
	T5C-125	28,15	87,65	5215	4	q	b	0,99	1.514±0.038	07KNSTD	18,988±1,726	16,946±2,052	17,365±2,094	16,233±1,658	18,199±1,608
	T5C-126	**28,15**	**87,65**	**5220**	**4**	**q**	**c**	**0,99**	**3.841±0.093**	**07KNSTD**	**48,421±4,422**	**37,034±4,501**	**36,613±4,43**	**35,279±3,614**	**40,784±3,615**

9d:** Dingye S main #3	T5C-127	28,15	87,65	5151	4	q	b	0,99	1.155±0.028	07KNSTD	14,799±1,342	13,677±1,654	14,185±1,708	13,153±1,342	14,51±1,28
	T5C-129	28,15	87,65	5146	4	q	c	0,99	2.454±0.065	07KNSTD	31,642±2,9	26,388±3,212	26,543±3,217	25,047±2,575	28,716±2,559
	T5C-130	**28,15**	**87,66**	**5140**	**4**	**g**	**b**	**0,99**	**3.612±0.085**	**07KNSTD**	**46,867±4,269**	**36,32±4,408**	**35,967±4,346**	**34,545±3,532**	**39,768±3,516**
	T5C-131	28,15	87,66	5142	4	q	c	0,99	2.136±0.055	07KNSTD	27,563±2,515	23,46±2,849	23,712±2,867	22,354±2,291	25,461±2,259
	T5C-132	28,15	87,66	5143	4	g	b	0,99	1.359±0.034	07KNSTD	17,482±1,588	15,84±1,917	16,288±1,963	15,206±1,552	16,883±1,491
9a: Dingye S frontal	**T5C-133**	**28,13**	**87,67**	**5006**	**4**	**g**	**b**	**1**	**1.939±0.048**	**07KNSTD**	**26,413±2,403**	**22,789±2,763**	**23,091±2,788**	**21,734±2,222**	**24,509±2,168**
	T5C-134	28,13	87,67	5012	4	q	c	1	1.283±0.032	07KNSTD	17,399±1,58	15,868±1,921	16,329±1,968	15,243±1,556	16,814±1,485
	T5C-135	28,13	87,67	5012	4	q	c	1	1.435±0.035	07KNSTD	19,46±1,765	17,469±2,113	17,906±2,157	16,736±1,707	18,621±1,642
	T5C-137	28,13	87,67	5011	4	q	c	1	1.538±0.038	07KNSTD	20,883±1,899	18,583±2,251	19,011±2,294	17,762±1,815	19,87±1,757
	T5C-138	28,13	87,67	5007	4	q	c	1	1.753±0.045	07KNSTD	23,856±2,177	20,901±2,538	21,278±2,573	19,922±2,042	22,409±1,989
	T5C-139	28,13	87,67	5012	4	q	b	1	1.721±0.051	07KNSTD	23,367±2,158	20,517±2,508	20,911±2,546	19,564±2,024	22,007±1,978
	T5C-140	28,13	87,67	5004	4	g	c	1	1.642±0.064	07KNSTD	22,362±2,144	19,746±2,467	20,155±2,508	18,844±2,009	21,155±1,978
10:** cho oyu	KC2-A	28,35	86,63	4948	5	q	b	1	2.368±0.06	KNSTD	30,091±2,745	25,552±3,103	25,755±3,114	24,295±2,489	27,533±2,442
	KC2-B	28,35	86,63	4948	5	q	b	1	2.371±0.062	KNSTD	30,13±2,757	25,581±3,111	25,784±3,123	24,321±2,497	27,564±2,452
	KC2-D	**28,35**	**86,63**	**4948**	**4**	**q**	**b**	**1**	**2.751±0.073**	**KNSTD**	**34,706±3,18**	**28,756±3,501**	**28,794±3,49**	**27,382±2,814**	**31,158±2,775**
	KC2-E	28,35	86,63	4948	4	q	b	1	2.393±0.062	KNSTD	30,16±2,757	25,603±3,113	25,805±3,124	24,341±2,498	27,588±2,452
11: KungCo	KC2-266	28,78	86,47	4882	4	q	c	1	1.42±0.036	KNSTD	18,506±1,684	16,861±2,043	17,291±2,086	16,189±1,655	17,78±1,573
	KC2-267	28,78	86,47	4874	4	q	c	1	3.356±0.083	KNSTD	44,166±4,034	35,27±4,287	34,958±4,231	33,51±3,434	38,095±3,379
	KC2-268	**28,78**	**86,46**	**4866**	**7**	**q**	**c**	**1**	**5.55±0.148**	**KNSTD**	**75,735±7,014**	**57,561±7,06**	**55,945±6,83**	**52,954±5,48**	**64,545±5,8**
	KC2-269	28,78	86,46	4858	5	q	c	1	4.363±0.069	KNSTD	58,529±5,245	43,562±5,24	42,694±5,112	41,283±4,164	48,715±4,23
	KC2-270	28,78	86,46	4849	3	q	c	1	1.724±0.041	KNSTD	22,636±2,051	20,148±2,437	20,526±2,472	19,243±1,961	21,397±1,885
	KC2-271	28,78	86,46	4847	2	q	c	1	1.621±0.038	KNSTD	21,123±1,913	18,958±2,292	19,359±2,33	18,129±1,847	20,085±1,769
	KC2-272	28,78	86,46	4843	5	q	c	1	1.508±0.036	KNSTD	20,176±1,828	18,208±2,201	18,625±2,242	17,44±1,777	19,254±1,696
	KC2-273	28,78	86,46	4840	6	q	c	1	1.356±0.047	KNSTD	18,314±1,722	16,744±2,068	17,179±2,113	16,083±1,688	17,612±1,614
	KC2-274	28,78	86,46	4835	3	q	c	1	4.249±0.073	KNSTD	56,617±5,087	42,441±5,113	41,694±5	40,338±4,078	47,051±4,097
	KC2-275	28,78	86,46	4831	4	q	c	1	1.094±0.026	KNSTD	14,579±1,32	13,728±1,658	14,24±1,713	13,228±1,347	14,301±1,259
	KC2-276	28,78	86,46	4827	5	q	c	1	2.425±0.041	KNSTD	32,783±2,925	27,652±3,317	27,738±3,313	26,332±2,651	29,669±2,57
	KC2-277	28,78	86,46	4821	3	q	c	1	0.625±0.016	KNSTD	8,285±0,752	8,048±0,973	8,595±1,035	7,938±0,81	8,109±0,716
	KC2-278	28,78	86,46	4817	7	q	c	1	1.083±0.026	KNSTD	14,888±1,348	14,005±1,692	14,504±1,745	13,487±1,374	14,584±1,284
	KC2-279	28,78	86,46	4795	5	q	c	1	0.844±0.02	KNSTD	11,522±1,044	11,025±1,332	11,559±1,391	10,705±1,091	11,339±0,999
	KC2-280	28,78	86,46	4777	5	q	c	1	1.674±0.039	KNSTD	23,1±2,092	20,585±2,489	20,963±2,524	19,66±2,003	21,794±1,919
12a:** Pulan M1W	KC2-39	30,38	81,18	4504	4	g	c	1	1.334±0.039	KNSTD	19,746±1,822	18,199±2,223	18,52±2,253	17,481±1,808	18,887±1,696
	KC2-40	**30,38**	**81,18**	**4506**	**7**	**g**	**c**	**1**	**1.595±0.055**	**KNSTD**	**24,193±2,279**	**21,743±2,689**	**21,959±2,704**	**20,817±2,189**	**22,743±2,087**
	KC2-44	30,38	81,18	4515	4	g	b	1	1.449±0.05	KNSTD	21,337±2,005	19,474±2,404	19,763±2,43	18,669±1,959	20,293±1,858
12c: Pulan M1E	**KC2-45**	**30,38**	**81,18**	**4530**	**3**	**g**	**b**	**1**	**3.702±0.091**	**KNSTD**	**54,11±4,952**	**41,823±5,091**	**41,06±4,976**	**39,861±4,09**	**45,499±4,041**
	KC2-46	30,38	81,18	4533	6	g	b	1	3.12±0.115	KNSTD	46,588±4,451	37,373±4,663	36,856±4,579	35,744±3,798	40,02±3,722
	KC2-47	30,38	81,18	4532	5	g	b	1	1.413±0.036	KNSTD	20,808±1,897	19,032±2,31	19,331±2,336	18,252±1,87	19,827±1,758
	KC2-48	30,38	81,18	4530	10	g	c	1	2.251±0.055	KNSTD	34,69±3,159	29,421±3,57	29,27±3,536	28,094±2,874	31,338±2,773
	KC2-49	30,38	81,18	4530	5	g	c	1	1.667±0.043	KNSTD	24,596±2,244	22,028±2,675	22,223±2,687	21,086±2,161	23,08±2,048
	KC2-50	30,38	81,18	4526	5	g	b	1	2.163±0.054	KNSTD	32,033±2,921	27,567±3,347	27,524±3,327	26,323±2,696	29,196±2,587
12b: Pulan M2	**KC2-51**	**30,38**	**81,17**	**4476**	**5**	**g**	**b**	**1**	**7.172±0.157**	**KNSTD**	**110,894±10,217**	**86,204±10,566**	**83,719±10,21**	**80,542±8,3**	**94,724±8,45**
	KC2-52	30,38	81,17	4477	5	g	b	1	3.595±0.088	KNSTD	54,794±5,014	42,374±5,158	41,579±5,038	40,356±4,141	46,049±4,089
	KC2-53	30,38	81,17	4471	5	g	c	1	6.238±0.213	KNSTD	96,351±9,213	74,823±9,359	72,793±9,063	70,021±7,433	82,615±7,67
	KC2-54	30,38	81,17	4470	5	g	b	1	5.957±0.131	KNSTD	91,946±8,431	71,428±8,722	69,48±8,443	67,033±6,884	78,753±6,997
	KC2-55	30,38	81,17	4470	5	g	c	1	4.59±0.084	KNSTD	70,477±6,37	54,86±6,638	53,16±6,402	50,755±5,155	60,818±5,328
	KC2-56	30,38	81,17	4467	5	g	b	1	5.349±0.229	KNSTD	82,486±8,161	64,544±8,232	63,091±8,012	60,719±6,629	70,618±6,8
	KC2-57	30,38	81,17	4466	5	g	c	1	2.022±0.052	KNSTD	30,799±2,814	26,766±3,254	26,77±3,24	25,546±2,621	28,219±2,507
	KC2-58	30,38	81,17	4465	5	g	c	1	4.116±0.088	KNSTD	63,237±5,748	48,371±5,868	46,971±5,671	45,381±4,63	53,941±4,755
	KC2-59	30,38	81,17	4466	5	g	c	1	2.111±0.054	KNSTD	32,164±2,938	27,745±3,372	27,699±3,352	26,503±2,718	29,3±2,602
13: EXS	KC2-66	30,99	81,26	4801	4	q	b	1	1.12±0.05	LLNL3000	13,443±1,318	12,82±1,622	13,269±1,672	12,383±1,344	13,251±1,268
	KC2-67	**30,99**	**81,26**	**4799**	**4**	**g**	**b**	**1**	**1.458±0.06**	**LLNL3000**	**17,533±1,692**	**16,201±2,031**	**16,54±2,066**	**15,594±1,672**	**16,974±1,599**
	KC2-69	30,99	81,26	4796	4	q	b	1	1.443±0.041	LLNL3000	17,373±1,595	16,077±1,958	16,42±1,992	15,478±1,595	16,832±1,504
	KC2-70	30,99	81,26	4794	4	q	b	1	1.211±0.031	LLNL3000	14,581±1,327	13,808±1,673	14,233±1,718	13,318±1,362	14,324±1,268
	KC2-71	30,99	81,26	4795	4	q	b	1	1.156±0.032	LLNL3000	13,915±1,274	13,235±1,609	13,676±1,656	12,776±1,313	13,701±1,22
	KC2-72	30,99	81,26	4793	4	g	b	1	1.42±0.042	LLNL3000	17,116±1,58	15,876±1,94	16,227±1,975	15,289±1,582	16,605±1,493
	KC2-73	30,99	81,26	4797	4	q	b	1	1.425±0.03	LLNL3000	17,149±1,541	15,899±1,913	16,249±1,947	15,311±1,55	16,634±1,453
	KC2-74	30,99	81,26	4798	4	q	b	1	1.29±0.04	LLNL3000	15,504±1,438	14,574±1,786	14,976±1,827	14,055±1,46	15,168±1,37
14: WXS	Zi-85	31,01	81,24	4800	4	g	b	1	3.725±0.064	LLNL3000	45,035±4,035	36,055±4,336	35,471±4,247	34,374±3,47	39,124±3,4
	Zi-86	31,01	81,24	4800	4	g	b	1	3.537±0.061	LLNL3000	42,744±3,828	34,604±4,161	34,081±4,079	32,927±3,323	37,55±3,262
	Zi-87	31,01	81,24	4800	4	g	b	1	3.239±0.102	LLNL3000	39,102±3,651	32,123±3,954	31,731±3,889	30,572±3,189	34,977±3,177
	Zi-88	**31,01**	**81,24**	**4800**	**4**	**g**	**b**	**1**	**4.712±0.081**	**LLNL3000**	**57,138±5,134**	**43,188±5,203**	**42,19±5,059**	**41,026±4,148**	**48,354±4,212**
	Zi-89	31,01	81,24	4800	4	g	b	1	3.659±0.077	LLNL3000	44,229±3,998	35,554±4,297	34,999±4,211	33,873±3,434	38,566±3,384
	zi-90	31,01	81,24	4800	4	g	b	1	3.123±0.107	LLNL3000	37,689±3,553	31,142±3,854	30,805±3,796	29,649±3,117	33,88±3,109
	Zi91	31,01	81,24	4800	4	g	b	1	3.593±0.078	LLNL3000	43,42±3,933	35,048±4,241	34,499±4,156	33,358±3,397	38,007±3,342
	zi-92	31,01	81,24	4800	4	g	b	1	3.355±0.144	LLNL3000	40,523±3,967	33,104±4,189	32,654±4,115	31,496±3,413	36,022±3,439
	zi-93	31,01	81,24	4800	4	g	b	1	1.794±0.037	KNSTD	22,56±2,027	20,168±2,428	20,392±2,444	19,302±1,954	21,431±1,871
	zi-94	31,01	81,24	4800	4	g	b	1	3.942±0.194	LLNL3000	47,692±4,821	37,595±4,85	36,972±4,751	35,951±3,998	40,965±4,041
	zi95	31,01	81,24	4800	4	g	b	1	4.237±0.077	KNSTD	53,703±4,831	41,097±4,954	40,277±4,833	39,172±3,965	45,438±3,964
	zi-96	31,01	81,24	4800	4	g	b	1	4.177±0.211	LLNL3000	50,565±5,148	39,262±5,088	38,541±4,974	37,495±4,194	43,019±4,275
	zi-98	31,01	81,24	4800	4	g	b	1	1.987±0.095	LLNL3000	23,897±2,388	21,21±2,716	21,393±2,729	20,285±2,237	22,573±2,204
	zi-99	31,01	81,24	4800	4	g	b	1	1.407±0.032	KNSTD	17,672±1,594	16,309±1,967	16,645±1,999	15,698±1,594	17,099±1,5
15: A Qu	KC2-75	31,03	81,17	5093	4	q	b	1	3.119±0.069	KNSTD	34,712±3,14	28,632±3,46	28,388±3,416	27,304±2,778	31,501±2,768
	KC2-76	**31,04**	**81,18**	**5091**	**4**	**q**	**b**	**1**	**3.949±0.069**	**LLNL3000**	**41,771±3,742**	**33,429±4,019**	**32,88±3,935**	**31,764±3,206**	**36,895±3,207**
	KC2-77	31,04	81,18	5103	4	q	b	1	2.265±0.064	LLNL3000	23,728±2,183	20,764±2,533	20,925±2,542	19,83±2,046	22,437±2,009
	KC2-78	*31,04*	*81,18*	*5106*	*4*	*q*	b	*1*	*22.385±0.261*	*LLNL3000*	*247,422±23,082*	*176,054±21,806*	*167,549±20,615*	*162,967±16,852*	*203,159±18,195*
	KC2-80	31,04	81,18	5117	4	q	b	1	3.408±0.06	LLNL3000	35,581±3,183	29,18±3,505	28,889±3,455	27,818±2,805	32,203±2,796
	KC2-82	31,03	81,17	5131	4	q	b	1	2.457±0.06	KNSTD	26,835±2,439	23,018±2,788	23,06±2,782	21,991±2,246	25,06±2,214
	KC2-83	31,04	81,18	5132	4	g	b	1	2.246±0.08	LLNL3000	23,223±2,195	20,347±2,521	20,518±2,531	19,436±2,049	22,012±2,027
16b*: Manikala M2E	WG1-1	32,04	80,02	4490	3	q	c	1	13.341±0.226	LLNL3000	187,045±17,352	138,353±17,065	132,503±16,247	129,472±13,377	157,349±14,074
	WG1-2	32,04	80,02	4492	3	q	c	1	15.473±0.114	KNSTD	229,053±21,156	171,709±21,183	164,147±20,12	159,837±16,447	191,361±16,99
	WG1-3	32,04	80,02	4494	3	q	c	1	23.292±0.255	LLNL3000	338,193±32,259	249,701±31,495	238,808±29,903	231,783±24,371	282,252±25,764
	WG1-4	32,04	80,02	4496	3	q	c	1	19.057±0.321	LLNL3000	272,019±25,782	199,602±25,002	192,189±23,922	188,304±19,744	226,433±20,608
	WG1-5	32,04	80,02	4498	3	q	c	1	13.722±0.186	LLNL3000	191,875±17,705	142,108±17,481	135,651±16,585	132,555±13,635	161,721±14,38
	WG1-6	32,04	80,02	4500	3	q	c	1	11.18±0.291	LLNL3000	154,771±14,593	115,879±14,407	112,012±13,853	109,454±11,47	129,242±11,778
	WG1-7	**32,04**	**80,02**	**4520**	**3**	**q**	**c**	**1**	**22.911±0.172**	**KNSTD**	**344,185±32,743**	**254,004±31,999**	**242,584±30,335**	**235,758±24,733**	**287,017±26,115**
	WG1-8	32,04	80,02	4540	3	q	c	1	11.776±0.194	LLNL3000	160,142±14,741	119,01±14,599	114,906±14,019	112,354±11,549	133,586±11,864
	WG1-9	32,04	80,02	4550	3	q	c	1	10.637±0.094	KNSTD	150,217±13,621	112,562±13,692	108,842±13,168	106,334±10,808	125,492±10,976
	WG1-10	32,04	80,01	4555	3	q	c	1	14.438±0.123	KNSTD	206,24±18,96	152,925±18,788	145,897±17,812	141,968±14,555	174,262±15,424
16a: Manikala M1	WG1-11	32,05	80	4760	3	q	c	1	3.468±0.06	LLNL3000	41,273±3,696	33,745±4,057	33,19±3,972	32,159±3,246	36,774±3,195
	WG1-12	32,05	80	4760	3	q	c	1	3.357±0.059	LLNL3000	39,945±3,577	32,825±3,947	32,323±3,869	31,291±3,159	35,824±3,114
	WG1-13	32,05	80	4760	3	q	c	1	3.813±0.095	LLNL3000	45,43±4,155	36,431±4,433	35,782±4,334	34,82±3,573	39,686±3,526
	WG1-14	32,05	80	4760	3	q	c	1	1.763±0.044	LLNL3000	20,879±1,897	18,874±2,286	19,096±2,303	18,116±1,851	20,037±1,77
	WG1-15	**32,04**	**80**	**4760**	**3**	**q**	**c**	**1**	**4.085±0.1**	**LLNL3000**	**48,702±4,452**	**38,36±4,666**	**37,641±4,558**	**36,713±3,765**	**42,005±3,728**
	WG1-16	32,05	80	4760	3	q	c	1	1.748±0.044	LLNL3000	20,695±1,883	18,728±2,27	18,955±2,287	17,979±1,838	19,873±1,758
	WG1-17	32,05	80	4760	3	q	c	1	3.454±0.103	LLNL3000	41,109±3,818	33,631±4,127	33,084±4,042	32,052±3,33	36,657±3,311
	WG1-18	32,04	80	4760	3	q	c	1	3.62±0.095	LLNL3000	43,102±3,954	34,978±4,263	34,363±4,169	33,347±3,43	38,042±3,391
	WG1-19	32,05	80	4760	3	q	c	1	3.156±0.069	LLNL3000	37,533±3,396	31,138±3,765	30,734±3,699	29,699±3,022	33,974±2,986
16c*: Manikala M2W	WG1-20	32,04	80,01	4645	3	q	c	1	13.225±0.167	LLNL3000	171,544±15,722	125,668±15,381	120,796±14,701	118,245±12,104	143,477±12,677
	WG1-21	32,05	80,01	4645	3	q	c	1	11.802±0.233	LLNL3000	152,36±14,103	113,219±13,927	109,366±13,381	106,91±11,04	127,225±11,372
	WG1-22	32,05	80,01	4645	3	q	c	1	8.657±0.152	LLNL3000	110,612±10,079	85,543±10,42	82,726±10,025	80,169±8,19	95,803±8,449
	WG1-23	32,05	80,01	4645	3	q	c	1	11.569±0.1	KNSTD	156,383±14,199	115,784±14,093	111,772±13,53	109,301±11,116	130,513±11,427
	WG1-24	**32,05**	**80,01**	**4640**	**3**	**q**	**c**	**1**	**14.825±0.202**	**LLNL3000**	**193,812±17,893**	**141,921±17,458**	**135,258±16,536**	**132,302±13,609**	**163,341±14,53**
	WG1-25	32,05	80,01	4640	3	q	c	1	11.647±0.147	LLNL3000	150,649±13,735	112,174±13,683	108,383±13,149	105,932±10,811	125,825±11,069
	WG1-26	32,05	80,01	4640	3	q	c	1	9.582±0.128	LLNL3000	123,1±11,158	94,704±11,509	91,816±11,1	89,21±9,074	104,996±9,199
	WG1-27	32,05	80,01	4640	3	q	c	1	11.358±0.21	LLNL3000	146,773±13,526	109,695±13,459	106,056±12,943	103,637±10,668	122,745±10,924
16d*: Manikala M3	WG1-28	32,04	80,03	4393	3	q	c	1	4.959±0.118	LLNL3000	70,822±6,493	56,154±6,851	54,392±6,604	52,22±5,365	61,989±5,515
	WG1-29	32,04	80,03	4445	3	q	c	1	3.016±0.053	LLNL3000	41,698±3,735	34,648±4,167	34,127±4,086	33,074±3,339	37,08±3,223
	WG1-30	32,04	80,033	4445	3	q	c	1	7.653±0.227	LLNL3000	107,537±10,142	84,389±10,481	81,799±10,11	79,17±8,314	93,453±8,55
	WG1-31	32,04	80,032	4445	3	q	c	1	7.062±0.131	LLNL3000	99,032±9,02	77,669±9,455	75,293±9,12	72,987±7,457	86,263±7,61
	WG1-32	32,04	80,03	4467	3	q	c	1	12.613±0.172	LLNL3000	178,452±16,411	132,287±16,233	127,015±15,496	124,021±12,731	149,893±13,289
	WG1-33	32,04	80,03	4467	3	q	c	1	14.702±0.157	LLNL3000	209,613±19,339	156,595±19,285	149,934±18,351	145,764±14,99	177,202±15,741
	WG1-34	**32,04**	**80,03**	**4467**	**3**	**q**	**c**	**1**	**16.249±0.205**	**LLNL3000**	**233±21,69**	**174,969±21,684**	**167,675±20,649**	**163,013±16,877**	**194,086±17,37**
17a*: CK M3	CK-40	32,49	79,67	4320	7	q	b	1	8.174±0.157	KNSTD	130,941±12,039	101,797±12,477	98,948±12,066	96,703±9,95	111,382±9,903
	CK-43	32,48	79,66	4390	2	q	b	1	8.065±0.186	KNSTD	119,411±11,061	93,856±11,547	91,078±11,149	88,537±9,165	102,645±9,206
	CK-44	32,48	79,66	4400	4	q	b	1	11.297±0.238	KNSTD	171,431±16	128,244±15,866	123,323±15,171	120,639±12,535	144,172±12,989
	CK-45	32,48	79,66	4410	9	q	b	1	9.201±0.18	KNSTD	143,812±13,278	109,639±13,471	106,173±12,977	103,766±10,703	121,048±10,798
	CK-46	**32,48**	**79,66**	**4425**	**7**	**q**	**b**	**1**	**11.972±0.144**	**KNSTD**	**184,574±16,956**	**137,508±16,872**	**131,865±16,084**	**128,931±13,224**	**155,882±13,803**
	CK-47	32,48	79,66	4435	8	q	b	1	7.373±0.107	KNSTD	112,035±10,15	88,136±10,706	85,288±10,307	82,801±8,423	97,225±8,522
	CK-48	32,48	79,66	4440	6	q	b	1	9.765±0.277	KNSTD	146,856±13,924	111,406±13,894	107,811±13,377	105,391±11,099	123,386±11,318
17b:** CK M2 inner	CK-50	32,49	79,65	4440	10	q	b	1	1.041±0.028	KNSTD	15,664±1,431	14,957±1,816	15,317±1,852	14,462±1,483	15,376±1,366
	CK-52	**32,49**	**79,65**	**4460**	**7**	**q**	**b**	**1**	**6.286±0.11**	**KNSTD**	**93,139±8,45**	**73,144±8,882**	**70,879±8,564**	**68,794±7,008**	**81,387±7,152**

	CK-53	32,49	79,65	4470	7	q	b	1	4.655±0.092	KNSTD	68,224±6,184	53,482±6,482	51,682±6,233	49,807±5,071	59,96±5,271
17c: CK M2 outer	CK-54	32,49	79,65	4490	7	q	b	1	3.841±0.091	KNSTD	55,584±5,077	43,29±5,264	42,338±5,125	41,226±4,224	47,71±4,229
	CK-55	32,49	79,65	4485	6	q	b	1	2.706±0.054	KNSTD	38,775±3,489	32,526±3,922	32,075±3,85	31,073±3,149	35,041±3,062
	CK-56	32,49	79,65	4480	5	q	b	1	3.352±0.08	KNSTD	47,85±4,364	38,466±4,674	37,791±4,571	36,863±3,774	41,55±3,679
	CK-57	32,49	79,65	4475	5	q	b	1	5.209±0.106	KNSTD	75,045±6,824	59,522±7,23	57,861±6,995	55,644±5,68	65,681±5,791
	CK-58	32,49	79,65	4470	8	q	b	1	1.655±0.045	KNSTD	24,191±2,216	21,799±2,653	21,913±2,655	20,934±2,152	22,972±2,047
	CK-60	32,49	79,65	4440	6	q	b	1	2.567±0.094	KNSTD	37,571±3,579	31,748±3,954	31,349±3,888	30,341±3,217	34,095±3,164
	CK-61	**32,49**	**79,65**	**4425**	**6**	**q**	**b**	**1**	**5.214±0.14**	**KNSTD**	**77,647±7,199**	**61,763±7,586**	**60,225±7,363**	**58,091±6,022**	**67,824±6,103**
	CK-63	32,49	79,66	4390	7	q	b	1	4.709±0.183	KNSTD	71,819±6,964	57,178±7,205	55,439±6,954	53,277±5,724	63,049±5,95

Sample density is 2.7 g/cm³; No erosion rate was applied.

We used Cronus 2.2 with constant file 2.2.1.

[a] Uncertainties are reported at the 1ς confidence level.

[h] ^{10}Be isotope ratios for 07KNSTD=2.85x10^{-12}; for KNSTD=3.11x10^{-12}; for LLNL3000=3x10^{-12}

* Moraines not taken into account because >120 ka.

** Moraines not taken into account because their number of samples is too small, according to our criterion.

Samples T7C-62 on M and KC2-78 on AQu are outliers because twice as old as the next odest age.